AD-A068 548 ILLINOIS UNIV AT URBANA-CHAMPAIGN ELECTROMAGNETICS LAB F/G 20/14
ANALYSIS OF ARBITRARILY SHAPED WIRE ANTENNAS RADIATING OVER A L--ETC(U)
MAR 79 P PARHAMI, R MITTRA DAAG29-77-G-0111
UNCLASSIFIED UIEM79-6 ARO-14686.4-EL NL

1 OF 2
AD
A068548

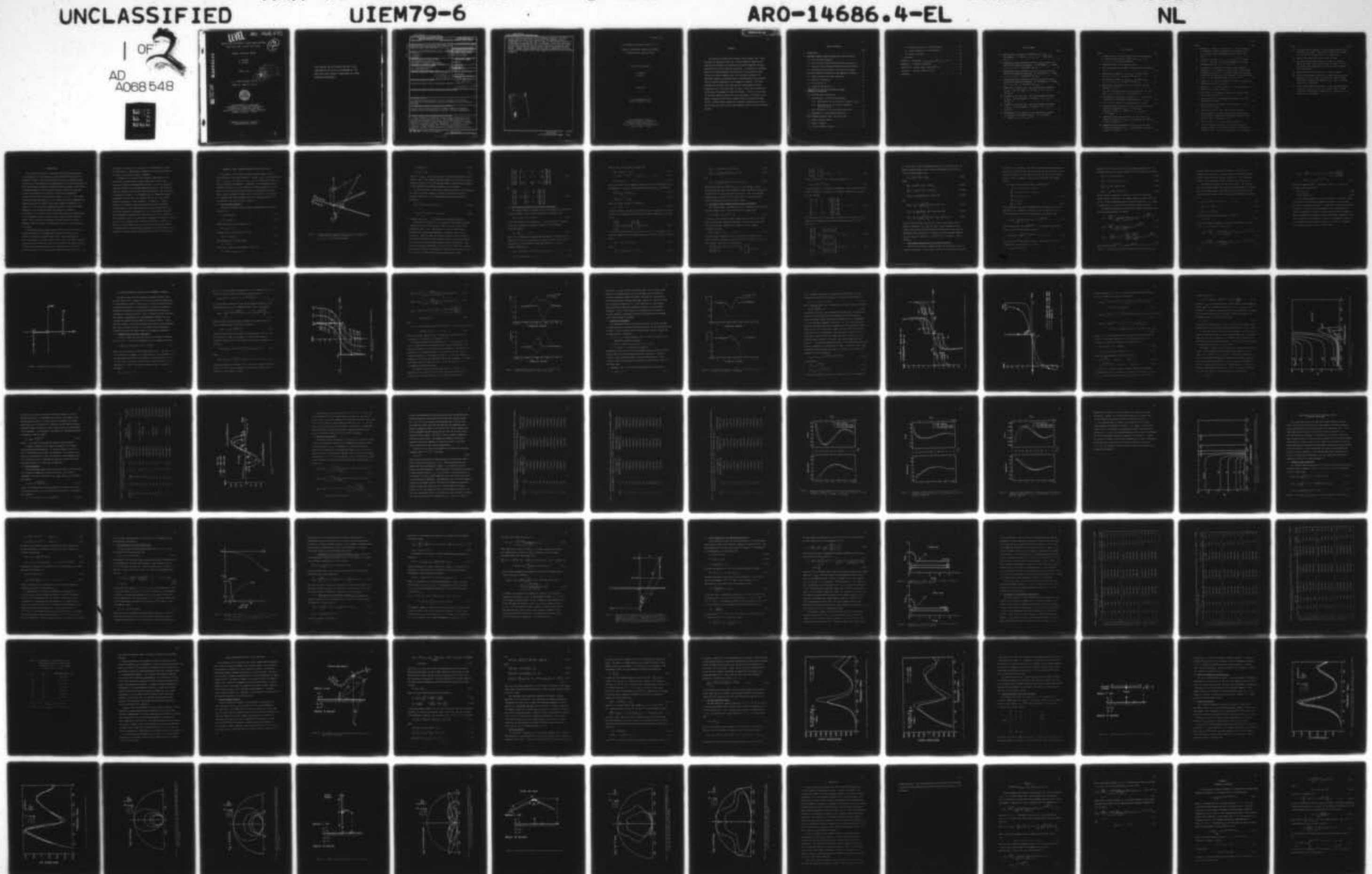

LEVEL II

ARO 14686.4-EL

ANALYSIS OF ARBITRARILY SHAPED WIRE ANTENNAS RADIATING OVER A LOSSY HALF-SPACE

12 NW

INTERIM TECHNICAL REPORT

P. PARHAMI
R. MITTRA

MARCH 1979

U. S. ARMY RESEARCH OFFICE
GRANT NO. DAAG29-77-G0111

ELECTROMAGNETICS LABORATORY
DEPARTMENT OF ELECTRICAL ENGINEERING
ENGINEERING EXPERIMENT STATION
UNIVERSITY OF ILLINOIS AT URBANA-CHAMPAIGN
URBANA, ILLINOIS 61801

THE FINDINGS IN THIS REPORT ARE NOT TO BE CONSTRUED AS AN OFFICIAL DEPARTMENT OF THE ARMY POSITION, UNLESS SO DESIGNATED BY OTHER AUTHORIZED DOCUMENTS.

UNCLASSIFIED

SECURITY CLASSIFICATION OF THIS PAGE (When Data Entered)

REPORT DOCUMENTATION PAGE		READ INSTRUCTIONS BEFORE COMPLETING FORM
1. REPORT NUMBER	2. GOVT ACCESSION NO.	3. RECIPIENT'S CATALOG NUMBER
4. TITLE (and Subtitle) 6 ANALYSIS OF ARBITRARILY SHAPED WIRE ANTENNAS RADIATING OVER A LOSSY HALF-SPACE.		5. TYPE OF REPORT & PERIOD COVERED 9 Interim Technical Report
		6. PERFORMING ORG. REPORT NUMBER 14 UI EM79-6, UILU-ENG-79-2546
7. AUTHOR(s) 10 P. Parhami, R. Mittra		8. CONTRACT OR GRANT NUMBER(s) 15 DAAG29-77-G-0111
9. PERFORMING ORGANIZATION NAME AND ADDRESS Electromagnetics Laboratory, Department of Electrical Engineering, University of Illinois, Urbana, Illinois		10. PROGRAM ELEMENT, PROJECT, TASK AREA & WORK UNIT NUMBERS P-14686-EL
11. CONTROLLING OFFICE NAME AND ADDRESS U. S. Army Research Office, Post Office Box 12211, Research Triangle Park, NC 27709		12. REPORT DATE 11 March, 1979
		13. NUMBER OF PAGES 135
14. MONITORING AGENCY NAME & ADDRESS (if different from Controlling Office) 12 137p.		15. SECURITY CLASS. (of this report) UNCLASSIFIED
		15a. DECLASSIFICATION/DOWNGRADING SCHEDULE NA

16. DISTRIBUTION STATEMENT (of this Report)

Approved for public release; distribution unlimited.

18 ARO

19 14686.4-EL

17. DISTRIBUTION STATEMENT (of the abstract entered in Block 20, if different from Report)

18. SUPPLEMENTARY NOTES

The findings in this report are not to be construed as an official Department of the Army position, unless so designated by other authorized documents.

19. KEY WORDS (Continue on reverse side if necessary and identify by block number)

antennas over lossy ground; method of moments; Sommerfeld integrals; steepest descent path integration; reflection coefficient approximation.

20. ABSTRACT (Continue on reverse side if necessary and identify by block number)

The problem of an arbitrarily oriented current element over a lossy half-space is analyzed in this work. Various numerical approaches are developed and discussed for evaluating the infinite Sommerfeld integrals appearing in the vector potential expressions. In particular, a technique based on the steepest descent path integration is introduced for exact evaluation of these integrals, and, as an efficient alternative, an additional technique is developed based on approximating the well-behaved (cont.)

DD FORM 1 JAN 73 1473 EDITION OF 1 NOV 65 IS OBSOLETE

UNCLASSIFIED

SECURITY CLASSIFICATION OF THIS PAGE (When Data Entered)

408 102

1B

cont.

Fourier transform expressions of the Sommerfeld integrals. The latter technique has the merit of not requiring any time-consuming infinite integrations and, at the same time, is shown to yield accurate results for a wide range of parameters of practical interest. Finally, in this paper, the thin-wire antenna problem over a lossy half-space is analyzed via the method of moments and the current element solution techniques discussed earlier. Several antenna examples are included to demonstrate the effect of the lossy half-space on their input impedance and the far-field radiation patterns.

UILU-ENG-79-2546

Electromagnetics Laboratory Report No. 79-6

ANALYSIS OF ARBITRARILY SHAPED WIRE ANTENNAS RADIATING OVER A LOSSY HALF-SPACE

Interim Technical Report

P. Parhami

R. Mittra

March 1979

U. S. Army Research Office
Grant No. DAAG29-77-G-0111

Electromagnetics Laboratory
Department of Electrical Engineering
Engineering Experiment Station
University of Illinois at Urbana-Champaign
Urbana, Illinois 61801

ABSTRACT

The problem of an arbitrarily oriented current element over a lossy half-space is analyzed in this work. Various numerical approaches are developed and discussed for evaluating the infinite Sommerfeld integrals appearing in the vector potential expressions. In particular, a technique based on the steepest descent path integration is introduced for exact evaluation of these integrals, and, as an efficient alternative, an additional technique is developed based on approximating the well-behaved Fourier transform expressions of the Sommerfeld integrals. The latter technique has the merit of not requiring any time-consuming infinite integrations and, at the same time, is shown to yield accurate results for a wide range of parameters of practical interest. Finally, in this paper, the thin-wire antenna problem over a lossy half-space is analyzed via the method of moments and the current element solution techniques discussed earlier. Several antenna examples are included to demonstrate the effect of the lossy half-space on their input impedance and the far-field radiation patterns.

TABLE OF CONTENTS

	Page
1. INTRODUCTION	1
2. ARBITRARY CURRENT ELEMENT RADIATING OVER LOSSY HALF-SPACE	3
2.1 Vector Potential Approach	3
2.2 Vertical Current Element-Transform Domain Expressions	6
2.3 Horizontal Current Element-Transform Domain Expressions	8
2.4 Space-Domain Representation of the Vector Potentials	10
3. EXACT AND ASYMPTOTIC EVALUATION OF THE SOMMERFELD INTEGRALS	16
3.1 Steepest Descent Path (SDP) Integration	16
3.2 Branch-Cut Contribution	21
3.3 Pole Contribution	29
3.4 Asymptotic Approximation	32
4. COMPUTATIONS OF THE VECTOR POTENTIALS WITHOUT SOMMERFELD INTEGRATIONS	42
4.1 Transform Domain Expressions	42
4.2 Approximating γ_2 and Space-Domain Results	44
4.2.1 Approximation for the horizontal component $({}_0\bar{\Pi}_{h1x})$	46
4.2.2 Approximation for the vertical components $({}_0\bar{\Pi}_{h1z}$ and ${}_0\bar{\Pi}_{v1z})$	46
4.3 Error Estimation for the Approximate Expressions	50
4.4 Advantages of the Approximate Expressions	53
5. WIRE ANTENNAS RADIATING OVER A LOSSY HALF-SPACE	59
5.1 Antenna Integral Equation	59
5.2 Method of Moments	62
5.3 Far-Field Radiation Pattern	64

5.4 Horizontal Antenna over Lossy Half-Space 67

5.5 Vertical Antenna over Lossy Half-Space 69

5.6 Inverted Vee-Dipole 69

6. CONCLUSION 79

APPENDIX I: EVALUATION OF ${}_0\Pi_{h1x}$, ${}_0\Pi_{h1z}$, AND ${}_0\Pi_{v1z}$ AT $\theta_2 = 0$ 81

APPENDIX II: ASYMPTOTIC EVALUATION 83

APPENDIX III: VARIOUS PARTIAL DERIVATIVES OF g 88

APPENDIX IV: COMPLETE COMPUTER LISTING 91

REFERENCES 124

LIST OF TABLES

Page

3.1 Demonstrating the branch cut contributions for ${}_0\Pi_{v1z}$. In this example: F = 30 MHz, $\phi_2 = 0$, $\varepsilon_g = 10$, $\sigma = .001$ mhos/m, and $I_{v0} = 1$ 30

3.2 Comparing the exact integration values for ${}_0\Pi_{v1z}$ with its one- and two-term asymptotic expansions. In this example, f = 30 MHz, $\phi_2 = 0$, $\varepsilon_g = 10$, $\sigma = .001$ mhos/m, and $I_{v0} = 1$ 34

3.3 Comparing the exact integration values for ${}_0\Pi_{h1x}$ with its one- and two-term asymptotic expansions. In this example, f = 30 MHz, $\phi_2 = 0$, $\varepsilon_g = 10$, $\sigma = .001$ mhos/m, and $I_{h0} = 1$ 35

3.4 Comparing the exact integration values for ${}_0\Pi_{h1z}$ with its one- and two-term asymptotic expansions. In this example, f = 30 MHz, $\phi_2 = 0$, $\varepsilon_g = 10$, $\sigma = .001$ mhos/m, and $I_{h0} = 1$ 36

4.1 Comparison of the RCM, exact, and the approximate evaluations of ${}_0\Pi_{v1z}$. For this example, f = 30 MHz, $\theta_2 = 45^o$, $\phi_2 = 0^o$, and $I_{v0} = 1$ 54

4.2 Comparison of the RCM, exact, and the approximate evaluations of ${}_0\Pi_{h1x}$. For this example, f = 30 MHz, $\theta_2 = 45^o$, $\phi_2 = 0^o$, and $I_{h0} = 0$ 55

4.3 Comparison of the RCM, exact, and the approximate evaluations of ${}_0\Pi_{h1z}$. For this example, f = 30 MHz, $\theta_2 = 45^o$, $\phi_2 = 0^o$, and $I_{v0} = 0$ 56

4.4 Demonstration of the stability of the approximate technique as a function of secondary height z_2'. In this example. f = 18 MHz, $r_2/\lambda = .6$, and $\theta_2 = 45^o$ 57

LIST OF FIGURES

Figure | Page

1. Geometry and the coordinate systems for the current element P_1 radiating over imperfect ground, where $\varepsilon_{1r} = 1$ and $\varepsilon_{2r} = \varepsilon_g - j\sigma/(\omega\varepsilon_0)$ have been assumed 4
2. Integration path Γ in the complex ξ-plane 15
3. The steepest descent path (SDP) of integration as a function of θ_2 18
4. High-frequency examples of the ${}_0\Pi_{h1x}$. For these cases, $\theta_2 = 5^o$, $h = 5m$, $\varepsilon_g = 10$, and $\sigma = .01$ mhos/m 20
5. Low-frequency examples of the ${}_0\Pi_{h1x}$. For these cases, $\theta_2 = 5^o$, $h = 5m$, $\varepsilon_g = 10$, and $\sigma = .01$ mhos/m 22
6. Branch-point and branch-cut loci as a function of ground parameters ε_g and σ/f 24
7. The correct SDP when branch cuts are intercepted. For this case, $\varepsilon_g = 10$, and $\sigma/f = 2 \times 10^{-11}$ mhos/m/Hz 25
8. The minimum θ_2 contours as a function of κ. A branch point is captured by the SDP path deformation when $\theta_2 > \theta_{min}$ . . . 28
9. Pole loci as a function of ground parameters ε_g and σ/f . . . 31
10. Comparing the SDP integration with the one- and the two-term asymptotic expansions of ${}_0\Pi_{v1z}$. For this case, frequency = 30 MHz, $\theta_2 = 10^o$, $\phi_2 = 0$, $\varepsilon_g = 10$, and $\sigma = .01$ mhos/m 37
11. Comparing the SDP integration with the one- and two-term asymptotic expansions of ${}_0\Pi_{h1x}$. The parameters are identical to those in Figure 10 38
12. Comparing the SDP integration with the one- and two-term asymptotic expansions of ${}_0\Pi_{h1z}$. The parameters are identical to those in Figure 10 39

Figure | Page

13. Minimum k_1r_2 contours as a function of κ. Once a branch cut is captured, a branch-cut integration is negligible if the k_1r_2 is greater than the minimum values depicted in this graph 41

14. The plot of the functions $|\bar{\gamma}_2|$, $|\gamma_2|$, and $|e^{-j\gamma_1 z_2}|$ versus $\sqrt{\alpha^2 + \beta^2}$. Note that for $|\kappa|$ large enough, the following approximation holds: $\gamma_2 e^{-j\gamma_1 z_2} \approx \bar{\gamma}_2 e^{-j\gamma_1 z_2}$ 45

15. The geometry for computing the vertical vector potential components. r_2' is chosen to be large enough so that the RCM expressions are valid at 0'. Therefore, the vector potential values along the interval 0'0 are obtained by using the initial value at 0' and integrating down along the z-axis 49

16. Examples of $|\kappa|$ contours for which < 10% error is ensured for observation points on or above it 52

17. Examples of $|\kappa|$ contours for which < 5% error is ensured for observation points on or above it 52

18. The geometry of an arbitrarily shaped wire antenna located over a lossy half-space 60

19. Input resistance of an unloaded dipole antenna (2L = 10m) radiating in free space 65

20. Input reactance of an unloaded dipole antenna (2L = 10m) radiating in free space 66

21. Center-fed horizontal dipole over a lossy half-space 68

22. Input resistance of a center-fed horizontal dipole antenna as a function of frequency and the ground parameters. Note that 2L = 10m, 2a = 0.1m, and h = 3m 70

23. Input reactance of the antenna defined in Figure 22 71

24. Far-field radiation pattern for the horizontal antenna defined in Figure 22 at 15 MHz. Note that the patterns are computed at k_1r = 500, and in this plane, $|E_\phi|$ is negligible . 72

Figure Page

25. Far-field radiation pattern for the horizontal antenna defined in Figure 22 at 15 MHz. Note that the patterns are computed at $k_1r = 500$, and in this plane, $|E_\theta|$ is negligible 73

26. Center-fed vertical dipole over a lossy half-space 74

27. The far-field radiation pattern for a center-fed vertical dipole (2L = 10m, h = 8m, and 2a = 0.1m) at 15 MHz. Note that the patterns are computed at $k_1r = 500$, and in this example, $|E_\phi|$ is negligible 75

28. Center-fed inverted Vee-dipole over a lossy half-space . . . 76

29. The far-field radiation pattern for a center-fed inverted Vee-dipole (L = 7.5m, h = 10m, $\psi = 90^\circ$, and 2a = 0.1m) at 10 MHz. Note that the patterns are computed at $k_1r = 500$, and in this plane, $|E_\phi|$ is negligible 77

30. The far-field radiation pattern for a center-fed inverted Vee-dipole (L = 7.5m, h = 10m, $\psi = 90^\circ$, and 2a = 0.1m) at 10 MHz. Note that the patterns are computed at $k_1r = 500$, and in this plane, $|E_\theta|$ is negligible 78

1. INTRODUCTION

The conventional approach to analyzing antenna structures radiating in the presence of a lossy half-space involves repeated evaluation of the Sommerfeld integrals, which were originally introduced by Sommerfeld about 70 years ago [1] and appeared in the expressions for the vector potentials [2]. Since these infinite integrals are generally highly oscillatory and difficult to evaluate numerically, much attention has been focused in recent years on developing techniques for efficiently evaluating the Sommerfeld integrals without unduly sacrificing the accuracy [3] - [14]. Even though the latest reported procedures [7] - [12] require an order of magnitude less computing time than the earlier "brute-force" numerical integration techniques [3] - [5], the overall computing time severely limits the physical dimensions of the antenna structures being numerically analyzed. Brittingham et al. [10] have used an interpolation scheme on a precalculated grid of Sommerfeld integral values in order to analyze larger structures. However, this technique is only useful for fixed frequency and ground parameters, since a new grid is required each time any of these parameters are changed.

Considerable computing time is saved if one uses the first term in the asymptotic expansion of the Sommerfeld integrals, better known as the Fresnel's Reflection Coefficient Method (RCM). These approximations, which are expressed in a simple closed form, are valid only when the antenna structures and the observation points are sufficiently high above the ground. As expected, the RCM expressions have only been employed for analyzing antenna structures at the high end of the frequency spectrum [10], [12], [13].

An important contribution of this paper is the development of a novel technique which is computationally comparable to the RCM approximation, yet valid for a much wider range of parameters.

In Chapter 2, the complex vector potential expressions for an arbitrarily oriented electric-current element source over a lossy half-space are derived demonstrating that three of the vector potential components contain the troublesome Sommerfeld integrals. An efficient numerical technique, based on the Steepest Descent Path (SDP) integration, is presented in Chapter 3 for evaluating the exact Sommerfeld integral expressions, and the results are compared with the one- and two-term asymptotic expansions of these integrals. In Chapter 4, a unique procedure is developed in which the well-behaved Fourier transform representations of the Sommerfeld integrals are approximated such that the inverse transform is performed via a set of known exact identities. These approximate expressions are shown not only to closely follow the SDP integration results for a wide range of parameters of practical interest, but to be in a convenient form for numerical evaluation. Finally, in Chapter 5, several examples, which are solved via the method of moments in conjunction with the approximate expressions derived in Chapter 4, are presented of various antenna structures radiating over a lossy half-space.

2. ARBITRARY CURRENT ELEMENT RADIATING OVER LOSSY HALF-SPACE

The geometry of an arbitrarily oriented current element P_1 over a lossy half-space is depicted in Figure 1. Regions 1 and 2 are characterized by ($\varepsilon_1 = \varepsilon_{1r}\varepsilon_0$, $\mu_1 = \mu_0$) and ($\varepsilon_2 = \varepsilon_{2r}\varepsilon_0$, $\mu_2 = \mu_0$), respectively, where ε_0 and μ_0 are free-space parameters. In addition to the standard Cartesian coordinate system (x, y, z), two spherical coordinate systems (r, θ_1, ϕ_1) and (r_2, θ_2, ϕ_2) are also defined in Figure 1 centered about the source point P_1 and its geometrical image point P_2, respectively. Our objective is to determine the field radiated by P_1 at the observation point 0, in the presence of the lossy half-space (region 2).

2.1 Vector Potential Approach

Starting with Maxwell's equation and the suppressed time convention $\exp(j\omega t)$, viz.,

$$\nabla \times \vec{H} = j\omega\varepsilon_0\varepsilon_r\vec{E} + \vec{J} \tag{2.1a}$$

$$\nabla \times \vec{E} = -j\omega\mu_0\vec{H} \quad , \tag{2.1b}$$

one may define the vector potential $\vec{\Pi}$ as

$$\vec{H} = j\omega\varepsilon_0\varepsilon_r\nabla \times \vec{\Pi} \quad . \tag{2.2}$$

Introduction of a scalar potential Φ from

$$\nabla\Phi = \vec{E} - \omega^2\mu_0\varepsilon_0\varepsilon_r\vec{\Pi} \tag{2.3}$$

and application of the Lorentz gauge

$$\nabla \cdot \vec{\Pi} - \Phi = 0 \quad , \tag{2.4}$$

allows one to finally express Maxwell's equation as

$$(\nabla^2 + k^2)\vec{\Pi} = -(j\omega\varepsilon_0\varepsilon_r)^{-1}\,\vec{J} \tag{2.5}$$

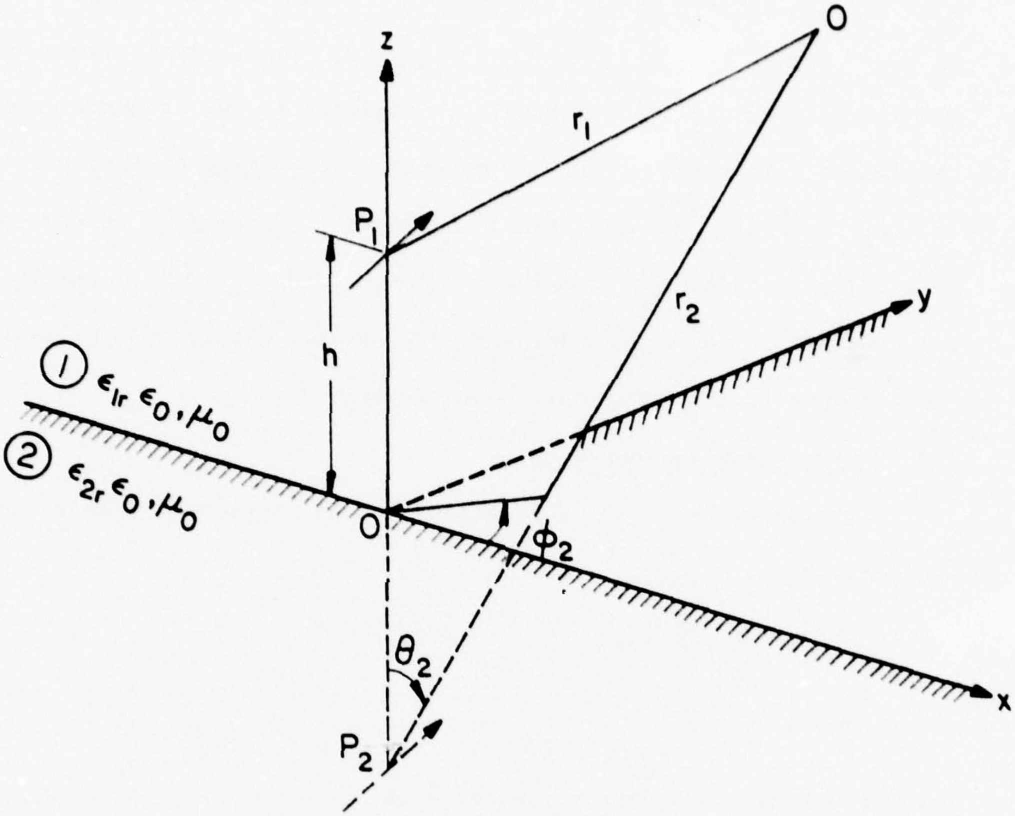

Figure 1. Geometry and the coordinate systems for the current element P_1 radiating over imperfect ground, where $\varepsilon_{1r} = 1$ and $\varepsilon_{2r} = \varepsilon_g - j\sigma/(\omega\varepsilon_0)$ have been assumed.

$$\vec{H} = j\omega\varepsilon_0\varepsilon_r\nabla \times \vec{\Pi} \tag{2.6}$$

$$\vec{E} = (\nabla\nabla\cdot + k^2)\vec{\Pi} \tag{2.7}$$

where $k^2 = \omega^2\mu_0\varepsilon_0\varepsilon_r$. The preceding results are general and valid for both regions 1 and 2. The boundary conditions needed to solve the vector differential Equation (2.5) can be obtained simply by enforcing the continuity of the tangential $\vec{E}$- and $\vec{H}$-field components at the interface.

As in most infinite-interface-type problems reported in the literature, the Fourier transform technique is employed for deriving the vector potential expressions. The two-dimensional Fourier transform pair is defined as

$$\tilde{\vec{\Pi}} = \iint_{-\infty}^{\infty} \vec{\Pi} \exp[-j(\alpha x + \beta y)]\, dx\, dy \tag{2.8a}$$

$$\vec{\Pi} = \frac{1}{4\pi^2} \iint_{-\infty}^{\infty} \tilde{\vec{\Pi}} \exp[j(\alpha x + \beta y)]\, d\alpha\, d\beta \quad . \tag{2.8b}$$

Throughout this paper, ~ on top denotes the transformed quantity.

Without loss of generality, the problem of an arbitrarily oriented current source over lossy half-space (Figure 1) can be treated as two independent cases: first, the problem of a vertical current source oriented in the z-direction and, second, a horizontal source in the x-direction. These two cases are analyzed in detail in the following sections with subscripts v and h denoting the field quantities belonging to the vertical and the horizontal current sources, respectively. Once the vector potential expressions are derived, the $\vec{E}$- and $\vec{H}$-field components are directly obtained by transforming the general vector equations given in (2.6) and (2.7) into the following convenient matrix forms:

$$\begin{bmatrix} \tilde{E}_x \\ \tilde{E}_y \\ \tilde{E}_z \end{bmatrix} = \begin{bmatrix} k^2 - \alpha^2 & -\alpha\beta & j\alpha \frac{\partial}{\partial z} \\ -\alpha\beta & k^2 - \beta^2 & j\beta\frac{\partial}{\partial z} \\ j\alpha \frac{\partial}{\partial z} & j\beta\frac{\partial}{\partial z} & (k^2 + \frac{\partial^2}{\partial z^2}) \end{bmatrix} \begin{bmatrix} \tilde{\Pi}_x \\ \tilde{\Pi}_y \\ \tilde{\Pi}_z \end{bmatrix} \tag{2.9}$$

and

$$\begin{bmatrix} \tilde{H}_x \\ \tilde{H}_y \\ \tilde{H}_z \end{bmatrix} = j\omega\varepsilon_0\varepsilon_r \begin{bmatrix} 0 & -\frac{\partial}{\partial z} & j\beta \\ \frac{\partial}{\partial z} & 0 & -j\alpha \\ -j\beta & j\alpha & 0 \end{bmatrix} \begin{bmatrix} \tilde{\Pi}_x \\ \tilde{\Pi}_y \\ \tilde{\Pi}_z \end{bmatrix} . \tag{2.10}$$

2.2 Vertical Current Element-Transform Domain Expressions

The current element is assumed to be in the z-direction (see Figure 1), located at height h over the lossy ground, and with a moment $I_v dz'$:

$$\vec{J}_v = \hat{z}\, I_v\, dz'\, \delta(x)\, \delta(y)\, \delta(z) \quad . \tag{2.11}$$

As has been verified in the literature [2], only the vertical component of the vector potential is needed to satisfy all of the boundary conditions, namely

$$\vec{\Pi}_{vi} = \hat{z}\Pi_{viz} \quad ; \quad i = 1,2 \tag{2.12}$$

where i = 1,2 indicates the region under consideration. Using the source condition in (2.11), one can express the general solution for the vector potential $\tilde{\Pi}_{viz}$ by satisfying both the wave Equation (2.5) and the radiation conditions as

$$\tilde{\Pi}_{v1z} = I_{v0} \exp[-j\gamma_1|z-h|]/2j\gamma_1 + A_1 \exp(-j\gamma_1 z) \quad ; \quad z \geq 0 \tag{2.13a}$$

$$\tilde{\Pi}_{v2z} = A_2 \exp(j\gamma_2 z) \quad ; \quad z \leq 0 \tag{2.13b}$$

where A_1 and A_2 are arbitrary constants and

$$I_{v0} = (j\omega\varepsilon_0\varepsilon_{1r})^{-1}\, I_v\, dz' \tag{2.14}$$

$$\gamma_i = [k_i^2 - \alpha^2 - \beta^2]^{1/2} \quad ; \quad I_m(\gamma_i) \leq 0 \quad ; \quad i = 1,2 \tag{2.15}$$

$$k_i^2 = \omega^2\mu_0\varepsilon_{1r}\varepsilon_0 \quad ; \quad i = 1,2 \quad . \tag{2.16}$$

If the continuity of the tangential components of the E- and H-fields across the boundary is enforced, the following constraints on $\tilde{\Pi}_{viz}$ are obtained

$$\frac{\partial}{\partial z}\tilde{\Pi}_{v1z}\Big|_{z=0} = \frac{\partial}{\partial z}\tilde{\Pi}_{v2z}\Big|_{z=0} \tag{2.17a}$$

$$\tilde{\Pi}_{v1z}\Big|_{z=0} = \kappa\,\tilde{\Pi}_{v2z}\Big|_{z=0} \tag{2.17b}$$

where the complex constant κ is defined as

$$\kappa = \varepsilon_{2r}/\varepsilon_{1r} \quad . \tag{2.18}$$

Constants A_1 and A_2, present in the vector potential expressions (2.13a) and (2.13b) can be determined by satisfying the boundary conditions (2.17a) and (2.17b):

$$\begin{bmatrix} A_1 \\ \\ A_2 \end{bmatrix} = I_{v0}\,\frac{1}{j(\kappa\gamma_1+\gamma_2)}\begin{bmatrix} \dfrac{\kappa\gamma_1 - \gamma_2}{2\gamma_1} \\ \\ 1 \end{bmatrix} \exp\,(-j\gamma_1 h) \quad . \tag{2.19}$$

If (2.19) is substituted back into (2.13a) and (2.13b), the complete vector potential expression in the transform domain can be written in the following form:

$$\tilde{\Pi}_{v1z} = \tilde{\Pi}^{i}_{v1z} + \tilde{\Pi}^{r}_{v1z} + {}_0\tilde{\Pi}_{v1z} \tag{2.20}$$

where

$$\tilde{\Pi}^{i}_{v1z} = I_{v0}\,\exp[-j\gamma_1|z - h|]/2j\gamma_1 \tag{2.21a}$$

$$\tilde{\Pi}^r_{v1z} = - I_{v0} \exp[-j\gamma_1(z + h)]/2j\gamma_1 \qquad (2.21b)$$

$$_0\tilde{\Pi}_{v1z} = I_{v0} \frac{\kappa}{j(\kappa\gamma_1 + \gamma_2)} \exp[-j\gamma_1(z + h)] \qquad (2.21c)$$

and

$$\tilde{\Pi}_{v2z} = I_{v0} \frac{1}{j(\kappa\gamma_1 + \gamma_2)} \exp(-j\gamma_1 h) \exp(j\gamma_2 z) \quad . \qquad (2.22)$$

Note that the first two terms of $\tilde{\Pi}_{v1z}$, viz., $\tilde{\Pi}^i_{v1z}$ and $\tilde{\Pi}^r_{v1z}$, can be interpreted as the direct and the perfect ground reflection contributions to the fields for observation points in region 1. Thus, the remaining component $_0\tilde{\Pi}_{v1z}$ is simply the correction term to the perfect ground solution in the general lossy half-space problem.

2.3 Horizontal Current Element-Transform Domain Expressions

The current element is assumed to be in the x-direction (see Figure 1), located at height h over lossy ground and with a moment $I_h dx'$:

$$\vec{J}_h = \hat{x} I_h dx' \delta(x) \delta(y) \delta(z - h) \quad . \qquad (2.23)$$

As expected, the horizontal current element solution above a lossy half-space is indeed more complicated than that for the vertical case, and two vector potential components are needed to obtain a complete solution [2], namely,

$$\vec{\Pi}_{hi} = \hat{x} \Pi_{hix} + \hat{z} \Pi_{hiz} \quad ; \quad i = 1,2 \quad . \qquad (2.24)$$

Using the source condition in (2.23), the general solutions for the vector potential components satisfying both the wave Equation (2.5) and the radiation condition can be expressed as

$$\begin{bmatrix} \tilde{\Pi}_{h1x} \\ \tilde{\Pi}_{h1z} \end{bmatrix} = \begin{bmatrix} I_{h0} \exp[-j\gamma_1|z - h|]/2j\gamma_1 \\ 0 \end{bmatrix} + \begin{bmatrix} B_{1x} \\ B_{1z} \end{bmatrix} \exp(-j\gamma_1 z) \quad ; \quad z \geq 0$$

(2.25)

$$\begin{bmatrix} \tilde{\Pi}_{h2x} \\ \tilde{\Pi}_{h2z} \end{bmatrix} = \begin{bmatrix} B_{2x} \\ B_{2z} \end{bmatrix} \exp\,(j\gamma_2 z) \quad ; \quad z \le 0 \tag{2.26}$$

where γ_i is defined in (2.15) and I_{h0} is assumed to be

$$I_{h0} = (j\omega\varepsilon_0\varepsilon_{1r})^{-1}\, I_h\, dx' \quad . \tag{2.27}$$

If the continuity of the tangential components of the E- and the H-fields across the boundary is enforced, the following constraints on $\tilde{\Pi}_{hix}$ and $\tilde{\Pi}_{hiz}$ are obtained:

$$\begin{bmatrix} j\alpha & \frac{\partial}{\partial z} & -j\alpha & -\frac{\partial}{\partial z} \\ 1 & 0 & -\kappa & 0 \\ 0 & 1 & 0 & -\kappa \\ \frac{\partial}{\partial z} & 0 & -\kappa\frac{\partial}{\partial z} & 0 \end{bmatrix} \begin{bmatrix} \tilde{\Pi}_{h1x} \\ \tilde{\Pi}_{h1z} \\ \tilde{\Pi}_{h2x} \\ \tilde{\Pi}_{h2z} \end{bmatrix} = 0 \quad ; \quad z = 0 \quad . \tag{2.28}$$

The conditions in (2.28) are used to determine the constants B_{ix} and B_{iz} present in the general vector potential expressions given in (2.25) and (2.26):

$$\begin{bmatrix} B_{1x} \\ B_{1z} \end{bmatrix} = I_{h0} \begin{bmatrix} \dfrac{\gamma_1 - \gamma_2}{2j\gamma_1(\gamma_1 + \gamma_2)} \\ \dfrac{j\alpha\,(\gamma_1 - \gamma_2)}{k_1^2(\kappa\gamma_1 + \gamma_2)} \end{bmatrix} \exp\,(-j\gamma_1 h) \quad ; \quad z \ge 0 \tag{2.29a}$$

$$\begin{bmatrix} B_{2x} \\ B_{2z} \end{bmatrix} = I_{h0} \begin{bmatrix} \dfrac{1}{j\kappa\,(\gamma_1 + \gamma_2)} \\ \dfrac{j\alpha\,(\gamma_1 - \gamma_2)}{k_1^2\kappa(\kappa\gamma_1 + \gamma_2)} \end{bmatrix} \exp\,(-j\gamma_1 h) \quad ; \quad z \le 0 \tag{2.29b}$$

If (2.29a) and (2.29b) are substituted back into (2.25) and (2.26), the complete transform domain vector potential expressions can be put into the following convenient form:

$$\tilde{\Pi}_{h1x} = \tilde{\Pi}^{i}_{h1x} + \tilde{\Pi}^{r}_{h1x} + {}_0\tilde{\Pi}_{h1x} \tag{2.30}$$

where

$$\tilde{\Pi}^{i}_{h1x} = I_{h0} \exp\left[-j\gamma_1|z - h|\right]/2j\gamma_1 \tag{2.31a}$$

$$\tilde{\Pi}^{r}_{h1x} = - I_{h0} \exp\left[-j\gamma_1(z + h)\right]/2j\gamma_1 \tag{2.31b}$$

$${}_0\tilde{\Pi}_{h1x} = I_{h0} \frac{1}{j(\gamma_1 + \gamma_2)} \exp\left[-j\gamma_1(z + h)\right] \tag{2.31c}$$

and

$${}_0\tilde{\Pi}_{h1z} = I_{h0}\, j\alpha \frac{\gamma_1 - \gamma_2}{k_1^2(\kappa\gamma_1 + \gamma_2)} \exp\left[-j\gamma_1(z + h)\right] \tag{2.32}$$

$$\tilde{\Pi}_{h2x} = I_{h0} \frac{1}{j\kappa(\gamma_1 + \gamma_2)} \exp(-j\gamma_1 h) \exp(j\gamma_2 z) \tag{2.33}$$

$$\tilde{\Pi}_{h2z} = I_{h0}\, j\alpha \frac{\gamma_1 - \gamma_2}{k_1^2\kappa(\kappa\gamma_1 + \gamma_2)} \exp(-j\gamma_1 h) \exp(j\gamma_2 z) \quad . \tag{2.34}$$

As in the vertical case, the first two terms of the dominant vector potential component, viz., $\tilde{\Pi}^{i}_{h1x}$ and $\tilde{\Pi}^{r}_{h1x}$, can be interpreted as the direct and the perfect ground reflection contributions to the fields for observation points in region 1. Therefore, the two remaining components ${}_0\tilde{\Pi}_{h1x}$ and ${}_0\tilde{\Pi}_{h1z}$ are simply the correction terms to the perfect ground solution.

2.4 Space-Domain Representation of the Vector Potentials

Since for most practical antenna problems the observation points are located above ground, in this section, only the vector potential components

in region 1 are considered. The complete transform domain expressions for these vector potentials, both for the vertical and the horizontal current elements, are derived in the previous sections, and the inverse transform relation (2.8b) is employed to obtain the corresponding space-domain results.

By using a spherical-type change of variables, viz.,

$$\begin{cases} x = r_2 \sin\theta_2 \cos\phi_2 = \rho_2 \cos\phi_2 \\ y = r_2 \sin\theta_2 \sin\phi_2 = \rho_2 \sin\phi_2 \\ z + h = r_2 \cos\theta_2 = z_2 \end{cases} \tag{2.35}$$

$$\begin{cases} \alpha = -\lambda \cos\zeta \\ \beta = -\lambda \sin\zeta \end{cases} , \tag{2.36}$$

the incident and the perfect ground-reflection components of the vector potentials, viz., Equations (2.21a),(2.21b) and (2.31a),(2.31b) can be inverse transformed into the following general space-domain form:

$$W = \frac{I_0}{4\pi j} \int_0^\infty \frac{\lambda}{\sqrt{k_1^2 - \lambda^2}} J_0(\rho_2\lambda) \exp\,[-j|z|\sqrt{k_1^2 - \lambda^2}]\, d\lambda \tag{2.37}$$

with the requirement that $\mathrm{Im}\sqrt{k_1^2 - \lambda^2} \leq 0$. In deriving the preceding equation, the following identity was used

$$\cos(n\tau)J_n(z) = \frac{(-j)^{-n}}{2\pi} \int_{-\pi}^{\pi} e^{-jz\cos(\tau'-\tau)} \cos\,(n\tau')\, d\tau' \tag{2.38}$$

where J_n is the n^{th}-order Bessel function. Expression (2.37) can be integrated in a closed form [15] to yield:

$$W = I_0 \exp\,(-jk_1 r)/4\pi r \quad . \tag{2.39}$$

Equation (2.39) is used to write the space-domain expressions for the aforementioned vector potential components in the following closed forms:

$$\Pi^i_{v1z} = I_{v0} \exp(-jk_1 r_1)/4\pi r_1 \tag{2.40a}$$

$$\Pi^r_{v1z} = -I_{v0} \exp(-jk_1 r_2)/4\pi r_2 \tag{2.40b}$$

$$\Pi^i_{h1x} = I_{h0} \exp(-jk_1 r_1)/4\pi r_1 \tag{2.41a}$$

$$\Pi^r_{h1x} = -I_{h0} \exp(-jk_1 r_2)/4\pi r_2 \quad . \tag{2.41b}$$

One may recognize Equations (2.40a) and (2.41a) as the free-space Green's function solution for the current element P_1, while (2.40b) and (2.41b) are the corresponding perfect ground contributions, i.e., source at image point P_2, to the fields at observation points in region 1.

Inverting the remaining vector potential components in region 1 and after some manipulations, one obtains:

$$_0\Pi_{v1z} = \frac{2I_{v0}\kappa}{4\pi j} \int_0^\infty \frac{\lambda}{\kappa\sqrt{k_1^2 - \lambda^2} + \sqrt{\kappa k_1^2 - \lambda^2}} J_0(\rho_2\lambda) \quad e^{-jz_2\sqrt{k_1^2-\lambda^2}} \, d\lambda \tag{2.42}$$

$$_0\Pi_{h1x} = \frac{2I_{h0}}{4\pi j} \int_0^\infty \frac{\lambda}{\sqrt{k_1^2-\lambda^2} + \sqrt{\kappa k_1^2-\lambda^2}} J_0(\rho_2\lambda) e^{-jz_2\sqrt{k_1^2-\lambda^2}} \, d\lambda \tag{2.43}$$

$$_0\Pi_{h1z} = -\frac{2I_{h0}}{4\pi k_1^2} \cos\phi_2 \int_0^\infty \lambda^2 \frac{\sqrt{k_1^2-\lambda^2} - \sqrt{\kappa k_1^2-\lambda^2}}{\kappa\sqrt{k_1^2-\lambda^2} + \sqrt{\kappa k_1^2-\lambda^2}} J_1(\rho_2\lambda) e^{-jz_2\sqrt{k_1^2-\lambda^2}} \, d\lambda \tag{2.44}$$

where relations $\mathrm{Im}\sqrt{k_1^2 - \lambda^2} \leq 0$ and $\mathrm{Im}\sqrt{\kappa k_1^2 - \lambda^2} \leq 0$ in (2.42) - (2.44) must hold. The infinite integrals present in the above equations are

popularly known as the Sommerfeld integrals [1] and cannot be expressed in a closed form. Efficient numerical evaluation of these integrals, which have been recently verified [3] - [14], represents the major task in analyzing antenna structures over lossy ground.

The Sommerfeld integral can take several forms. For this work, the forms containing Hankel functions in their integrands are preferred, since the integrals appear to be numerically more tractable. Incorporating the well-known identities between Bessel and Hankel functions, viz.,

$$J_i(x) = \frac{1}{2}\,[H_i^{(1)}(x) + H_i^{(2)}(x)] \quad ; \quad i = 0,1 \tag{2.45a}$$

$$H_0^{(1)}(x) = -\,H_0^{(2)}(-x) \tag{2.45b}$$

$$H_1^{(1)}(x) = H_1^{(2)}(-x) \quad , \tag{2.45c}$$

and introducing the following change of variable

$$\lambda = k_1 \sin \xi \quad , \tag{2.46}$$

the vector potential components containing the Sommerfeld integrals (2.42) - (2.44) take the following form

$$_0\Pi_{v1z} = \frac{I_{v0}k_1\kappa}{4\pi j}\int_\Gamma \frac{\sin \xi \cos \xi}{\kappa\cos \xi + \sqrt{\kappa-\sin^2\xi}}\, H_0^{(2)}(k_1\rho_2 \sin \xi)e^{-jk_1 z_2 \cos\xi}\, d\xi \tag{2.47}$$

$$_0\Pi_{h1x} = \frac{I_{h0}k_1}{4\pi j}\int_\Gamma \frac{\sin \xi \cos \xi}{\cos \xi + \sqrt{\kappa-\sin^2\xi}}\, H_0^{(2)}(k_1\rho_2 \sin \xi)\, e^{-jk_1 z_2 \cos\xi}\, d\xi \tag{2.48}$$

and

$$ {}_0\Pi_{h1z} = -\frac{I_{h0}k_1}{4\pi}\cos\phi_2 \int_\Gamma \sin^2\xi\cos\xi\,\frac{\cos\xi - \sqrt{\kappa-\sin^2\xi}}{\kappa\cos\xi + \sqrt{\kappa-\sin^2\xi}} $$

$$ \cdot\, H_1^{(2)}(k_1\rho_2\sin\xi)e^{-jk_1z_2\cos\xi}\,d\xi \tag{2.49} $$

where the integration path Γ is depicted in Figure 2, on which the following conditions must hold

$$ \mathrm{Im}(\cos\xi) \leq 0 \tag{2.50a} $$

$$ \mathrm{Im}(\sqrt{\kappa - \sin^2\xi}) \leq 0 \quad . \tag{2.50b} $$

In the following chapter, an efficient numerical integration scheme is discussed for evaluating the Sommerfeld integrals via the steepest descent path integration technique. An additional approach is introduced in Chapter 4 in which the transform domain of the troublesome vector potential components are initially approximated such that the Sommerfeld infinite integrals do not appear in their space-domain expressions. These two techniques plus the asymptotic solution to the Sommerfeld integrals are compared, and several numerical results are included to demonstrate the efficiency and the accuracy of each procedure.

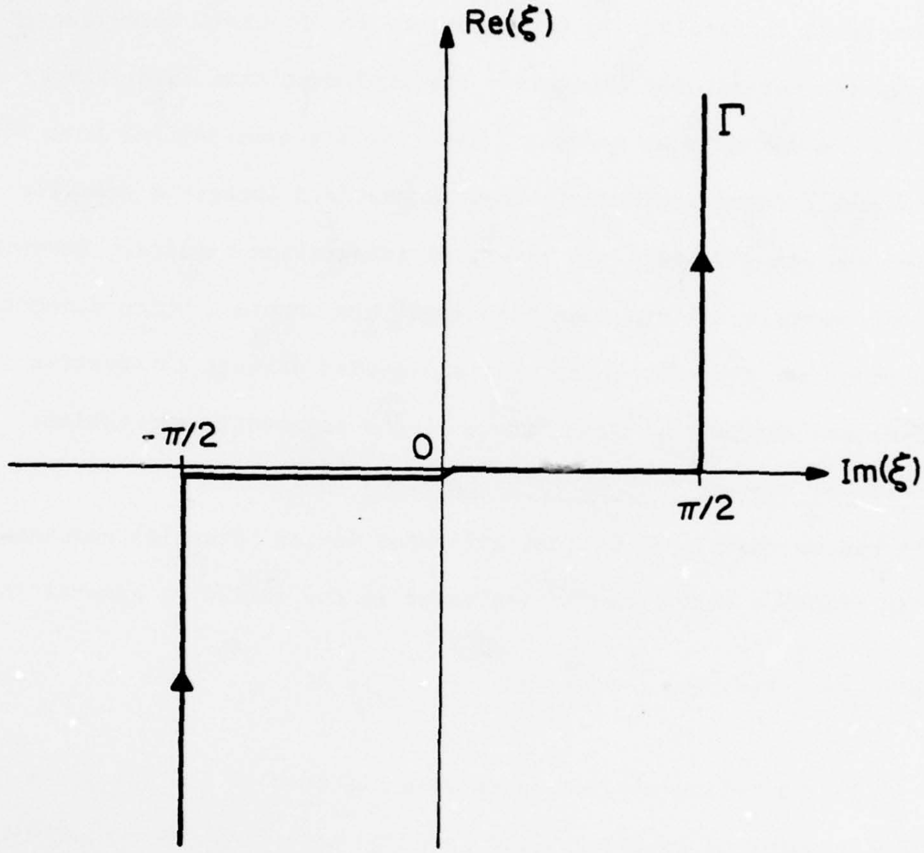

Figure 2. Integration path Γ in the complex ξ-plane.

3. EXACT AND ASYMPTOTIC EVALUATION OF THE SOMMERFELD INTEGRALS

The three correction vector potential components derived in the previous chapter, viz., Equations (2.47)-(2.49), cannot be expressed in a closed form and contain a certain class of infinite integrals known as the Sommerfeld integrals. In this chapter, an efficient technique is presented for numerically evaluating the aforementioned integrals by deforming the integration contour Γ into the steepest descent path (SDP). The asymptotic approximations to these Sommerfeld integrals are also obtained and compared with the numerical integration results. Several numerical examples are included throughout the chapter, which demonstrate the accuracy and the efficiency of the steepest descent integration technique and define the useful range of the asymptotic expressions.

3.1 Steepest Descent Path (SDP) Integration

It can be readily shown that all three vector potential components given in (2.47) - (2.49) can be expressed in the following general form:

$$u = \frac{1}{4\pi j} \int_{\Gamma} P(\xi) \exp \left[-jk_1 r_2 \cos (\xi - \theta_2)\right] d\xi \tag{3.1}$$

where $P(\xi)$ is a relatively slowly varying function of ξ. The point $\xi = \theta_2$ is a saddle point of Equation (3.1), and the path Γ can be deformed to a steepest descent path (SDP) by enforcing the condition $\text{Re}[\cos(\xi - \theta_2)] = 1$. (At this point it is assumed that no poles or branch points of $P(\xi)$ are intercepted.) On SDP, the following convenient change of variable is introduced:

$$\cos (\xi - \theta_2) = 1 - jt^2 \tag{3.2}$$

where t is a real parameter ranging from $-\infty$ to $+\infty$. Equation (3.2) can be used to explicitly define the steepest descent path as:

$$\xi_{SDP} = \pm\left[\pi/2 + j\ \mathrm{Ln}\ (t^2 + j + |t|\ \sqrt{t^2 + 2j})\right] + \theta_2 \quad ; \quad t \gtrless 0\ , \tag{3.3}$$

or if one needs to separate the real and the imaginary behaviors of the steepest descent path, the following equivalent form can be derived

$$\xi_{SDP} = \pm \left\{ \cos^{-1}\left[\frac{-t^2 + \sqrt{t^4 + 4}}{2}\right] + j\ \cosh^{-1}\left[\frac{t^2 + \sqrt{t^4 + 4}}{2}\right]\right\} + \theta_2\ . \quad t \gtrless 0 \tag{3.4}$$

where the inverse cosine function is assumed to be between 0 and $\pi/2$ and the inverse hyperbolic function is defined as

$$\cosh^{-1} \Psi = \mathrm{Ln}\left[\Psi + \sqrt{\Psi^2 - 1}\right]\ . \tag{3.5}$$

The SDP can be traced in the ξ-plane, by using Equations (3.3) or (3.4) as a function of t and θ_2 (see Figure 3). Applying the change of variable in Equation (3.2) to the integral expression in Equation (3.1), we obtain

$$u = \exp(-jk_1 r_2 - j\pi/4)/(2\sqrt{2}\ \pi) \int_{-\infty}^{\infty} Q(t)\ \exp\ (-k_1 r_2 t^2)\ dt \tag{3.6}$$

where

$$Q(t) = \left[P(\xi)\ \sec \frac{\xi - \theta_2}{2}\right]_t = \sqrt{2}\ e^{j\pi/4}\ (t^2 + 2j)^{-1/2}\ P(\xi)\Big|_t\ . \tag{3.7}$$

Using the general form obtained in (3.6), the vector potential expressions in (2-47) - (2.49) can be formulated on the steepest descent path as a function of real variable t, namely,

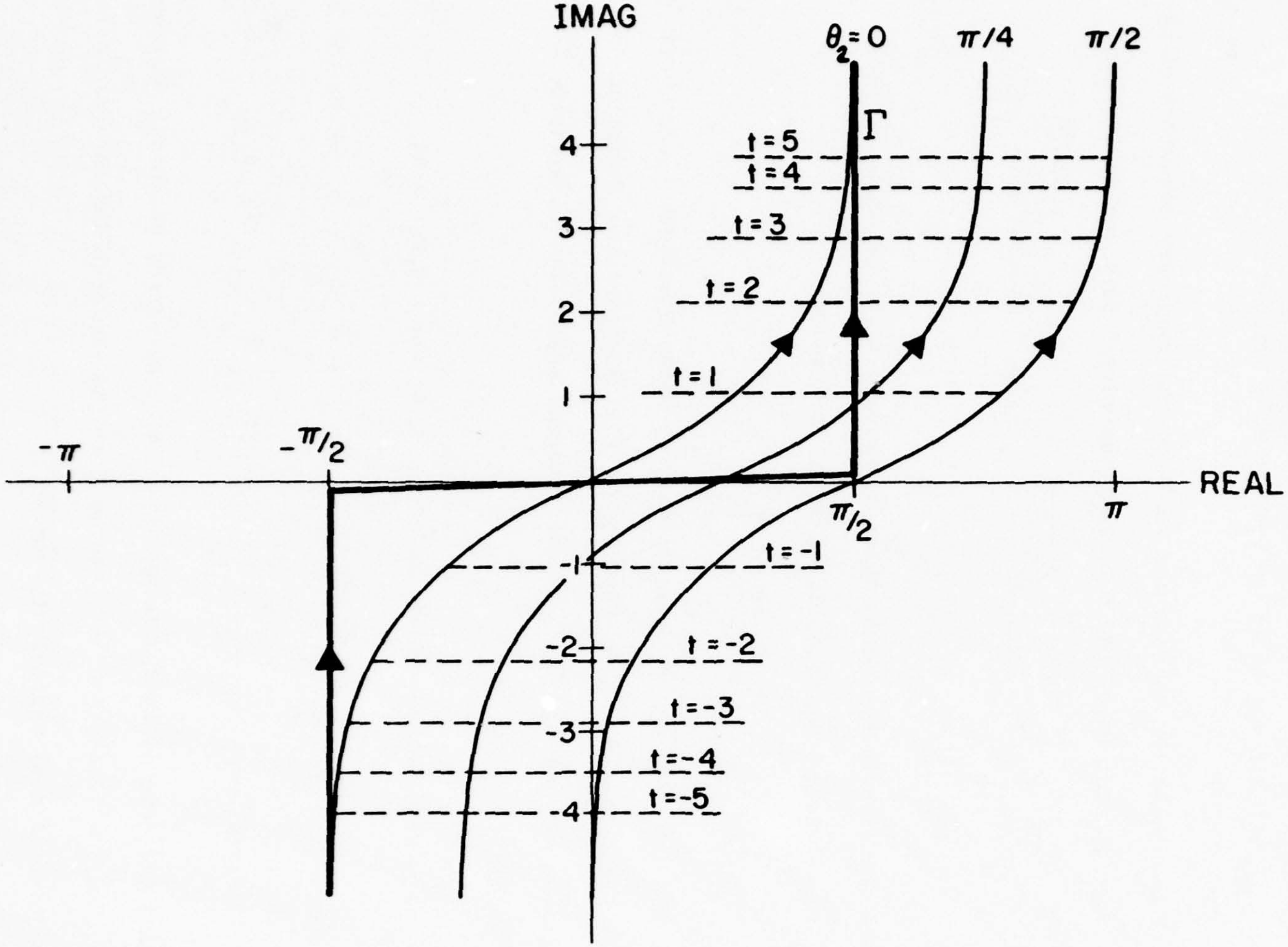

Figure 3. The steepest descent path (SDP) of integration as a function of θ_2.

$$ {}_0\Pi_{v1z} = I_{v0} \int_{-\infty}^{\infty} \frac{\kappa R_0(t)}{\left[\kappa \cos \xi + \sqrt{\kappa - \sin^2 \xi}\right]_t} \exp(-k_1 r_2 t^2)\, dt \tag{3.8} $$

$$ {}_0\Pi_{h1x} = I_{h0} \int_{\infty}^{\infty} \frac{R_0(t)}{\left[\cos \xi + \sqrt{\kappa - \sin^2 \xi}\right]_t} \exp(-k_1 r_2 t^2)\, dt \tag{3.9} $$

$$ {}_0\Pi_{h1z} = -jI_{h0} \cos \phi_2 \int_{-\infty}^{\infty} R_1(t) \left[\sin \xi \, \frac{\cos \xi - \sqrt{\kappa - \sin^2 \xi}}{\kappa \cos \xi + \sqrt{\kappa - \sin^2 \xi}}\right]_t $$

$$ \cdot \exp(-k_1 r_2 t^2)\, dt \tag{3.10} $$

where

$$ R_i(t) = (2\pi)^{-1} k_1 \exp(-jk_1 r_2)(t^2 + 2j)^{-1/2} [\sin \xi \cos \xi \exp(jk_1 \rho_2 \sin \xi)]_t $$

$$ \cdot H_i^{(2)}(k_1 \rho_2 \sin \xi)\big|_t \quad ; \quad i = 0,1 \quad , \tag{3.11} $$

$H_i^{(2)}$ is the Hankel function of the i^{th} order and of second kind, and ξ is expressed as a function of t in Equation (3.3).

The relations expressed in Equations (3.8) - (3.10) are exact if no poles or branch points are intercepted under the path deformation. The detailed discussions of the possible pole and branch-cut contributions are presented in the following sections. It should also be noted that the apparent singularity of the Hankel functions at $\theta_2 = 0$ in the Sommerfeld integrals is overcome by the remaining terms in the integrands. In Appendix I, equivalent versions of Equations (3.8) - (3.10) are derived for $\theta_2 = 0$ for numerical integration purposes.

By observing the integral expressions in (3.8) - (3.10), it is apparent that for large $k_1 r_2$ the effective integration interval will be quite small and contain relatively few oscillations (see Figure 4).

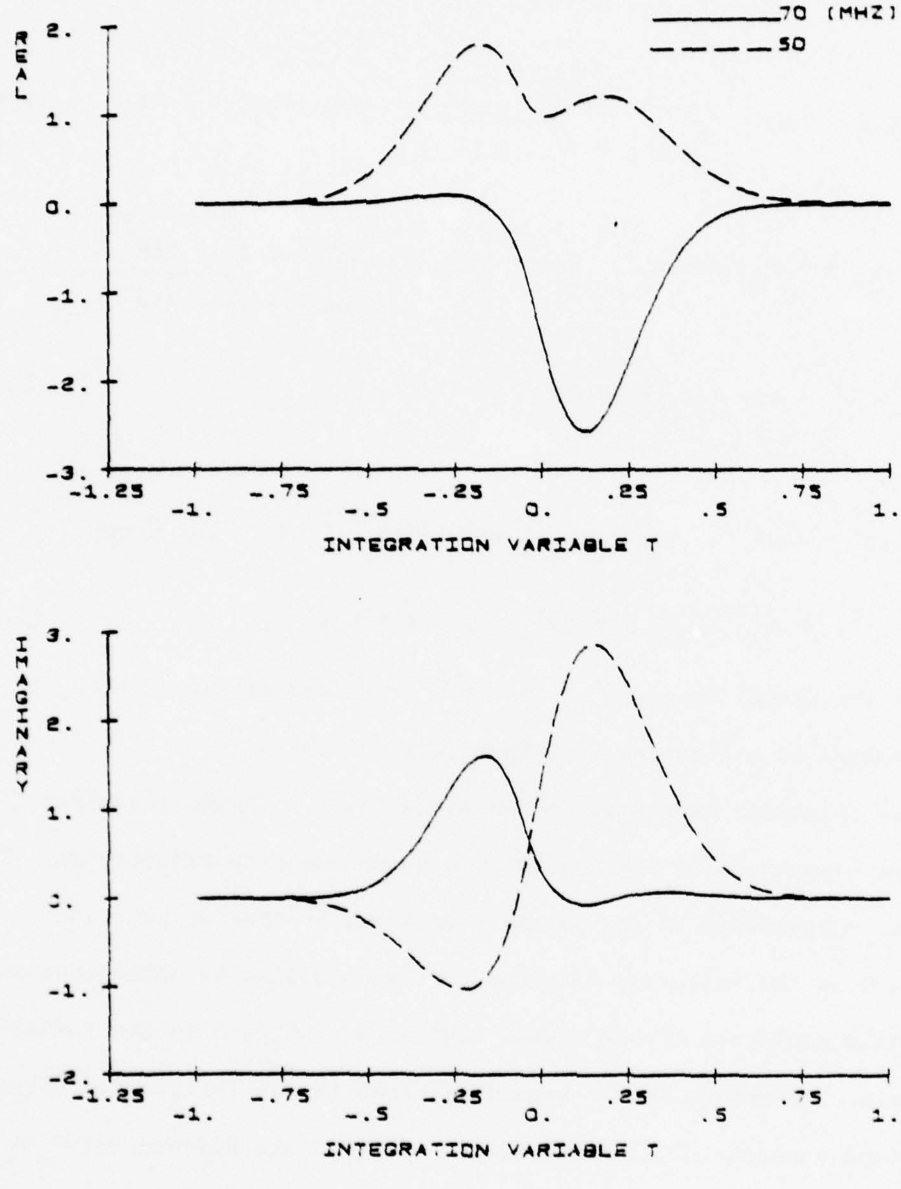

Figure 4. High-frequency examples of the ${}_0\Pi_{h1x}$. For these cases, $\theta_2 = 5°$, $h = 5m$, $\varepsilon_g = 10$, and $\sigma^0 = .01$ mhos/m.

Fortunately, at lower frequencies (smaller k_1r_2), the oscillatory terms present in the integrands are scaled accordingly and, even though the effective integration interval increases, the number of oscillations in the integrand does not increase appreciably (Figure 5). This fact allows one to integrate Equations (3.8) - (3.10) numerically by employing an efficient Gaussian quadrature integration routine for a wide range of parameters. Later in this chapter, the efficiency and the accuracy of the above numerical integration procedure are demonstrated and compared to the other available techniques.

3.2 Branch-Cut Contribution

The expressions derived in the previous section are valid only when no singularities are intercepted during the steepest descent path deformation. In order to locate the poles and the branch points, one must consider the following physical constraints:

a) $0 \leq \theta_2 < \pi/2$, since Equations (3.8) - (3.10) are valid only for observation points above ground;

b) $\mathrm{Re}(\kappa) \geq 1$ and $\mathrm{Im}(\kappa) \leq 0$, since $\kappa = \varepsilon_g - j\sigma/(\omega\varepsilon_0)$;

c) $-\frac{\pi}{2} < \mathrm{Re}(\xi) < \pi$ on the SDP (see Figure 3).

Furthermore, since $\cos(\xi)$ is a single-valued function, condition (2.50a) does not have to be satisfied during the path deformation. Condition (2.50b) is used to define an upper- and a lower-Riemann sheet in the ξ-plane in which this condition is satisfied in the upper and violated in the lower sheet.

Equations (3.8) - (3.10) have the same branch points satisfying

$$\kappa - \sin^2 \xi_b = 0 \quad . \tag{3.12}$$

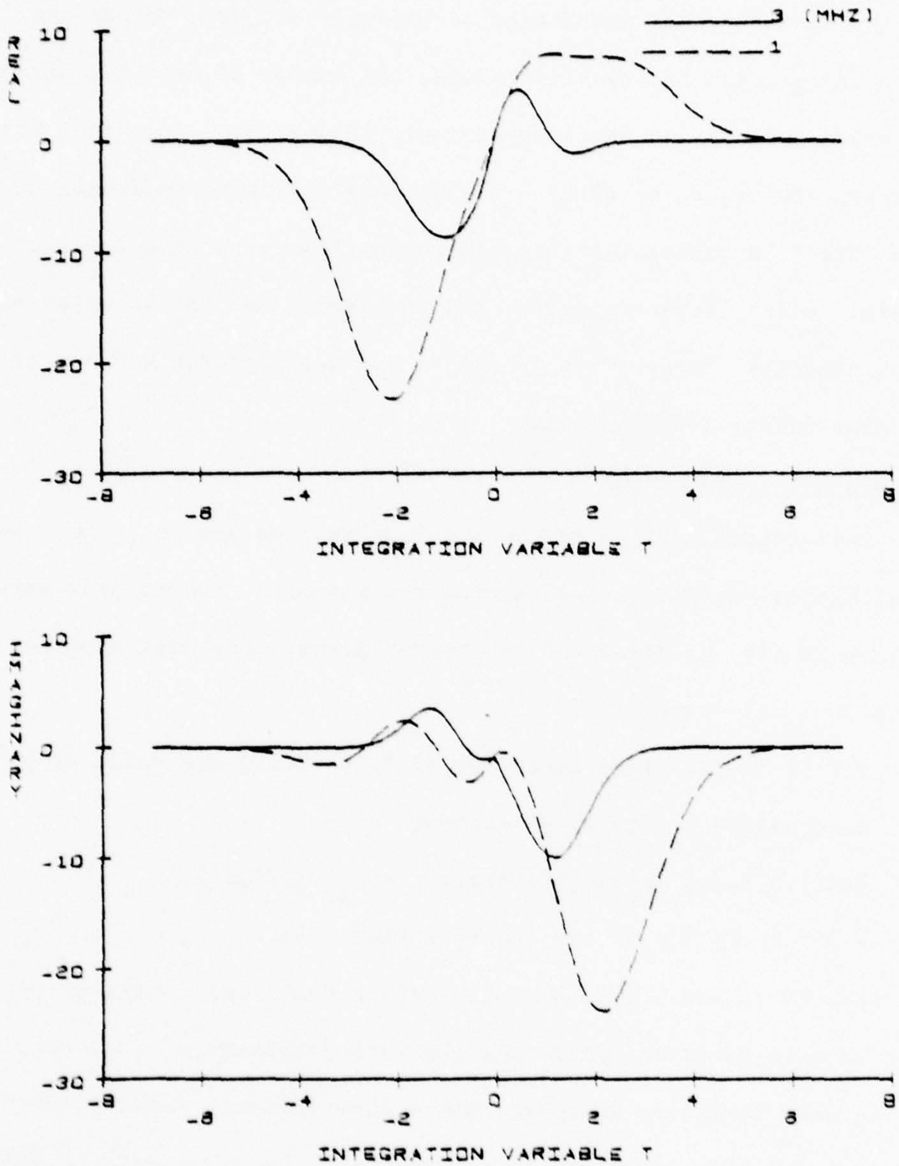

Figure 5. Low-frequency examples of the $_{\rho}\Pi_{h1x}$. For these cases, $\theta_2 = 5°$, $h = 5m$, $\epsilon_g = 10$, and $\sigma = .01$ mhos/m.

If one considers the physical constraints discussed earlier, only the following two branch point solutions are of importance (see Figure 6):

$$\xi_b = \pi/2 \pm j \,\mathrm{Ln}\, (\sqrt{\kappa} + \sqrt{\kappa - 1}) \quad . \tag{3.13}$$

The corresponding branch cuts of Equation (3.13) which satisfy the relation

$$\mathrm{Im}\, (\sqrt{\kappa - \sin^2 \xi}) = 0 \quad , \tag{3.14}$$

as depicted in Figure 6, are the boundaries through which the integration path will travel to and from the two Riemann sheets defined earlier. Since the steepest descent path defined in Equation (3.3) is independent of κ, one can easily demonstrate that for $0 \leq \theta_2 < 90°$ only the branch point with the upper sign can be captured by the SDP deformation (Figure 7). Therefore, one can allow the SDP to enter the lower sheet only when the lower branch cut, corresponding to the lower sign of Equation (3.13), is intercepted, since the path will always intercept the lower cut at an additional point forcing it to return to the upper Riemann sheet (see Figure 7). A branch-cut integration, however, is performed around the upper branch cut whenever it is intercepted in order to remain the proper sheet. The branch cut in the upper-half plane as a function of a positive real parameter β can be expressed as

$$\xi_{bc} = \pi/2 + j \,\mathrm{Ln}\, (\sqrt{\kappa - \beta^2} + \sqrt{\kappa - 1 - \beta^2}) \quad , \tag{3.15a}$$

or, equivalently,

$$\sin \xi_{bc} = \sqrt{\kappa - \beta^2} \tag{3.15b}$$

$$\cos \xi_{bc} = -j \sqrt{\kappa - 1 - \beta^2} \quad . \tag{3.15c}$$

By applying the change of variable in Equation (3.15) to the Sommerfeld

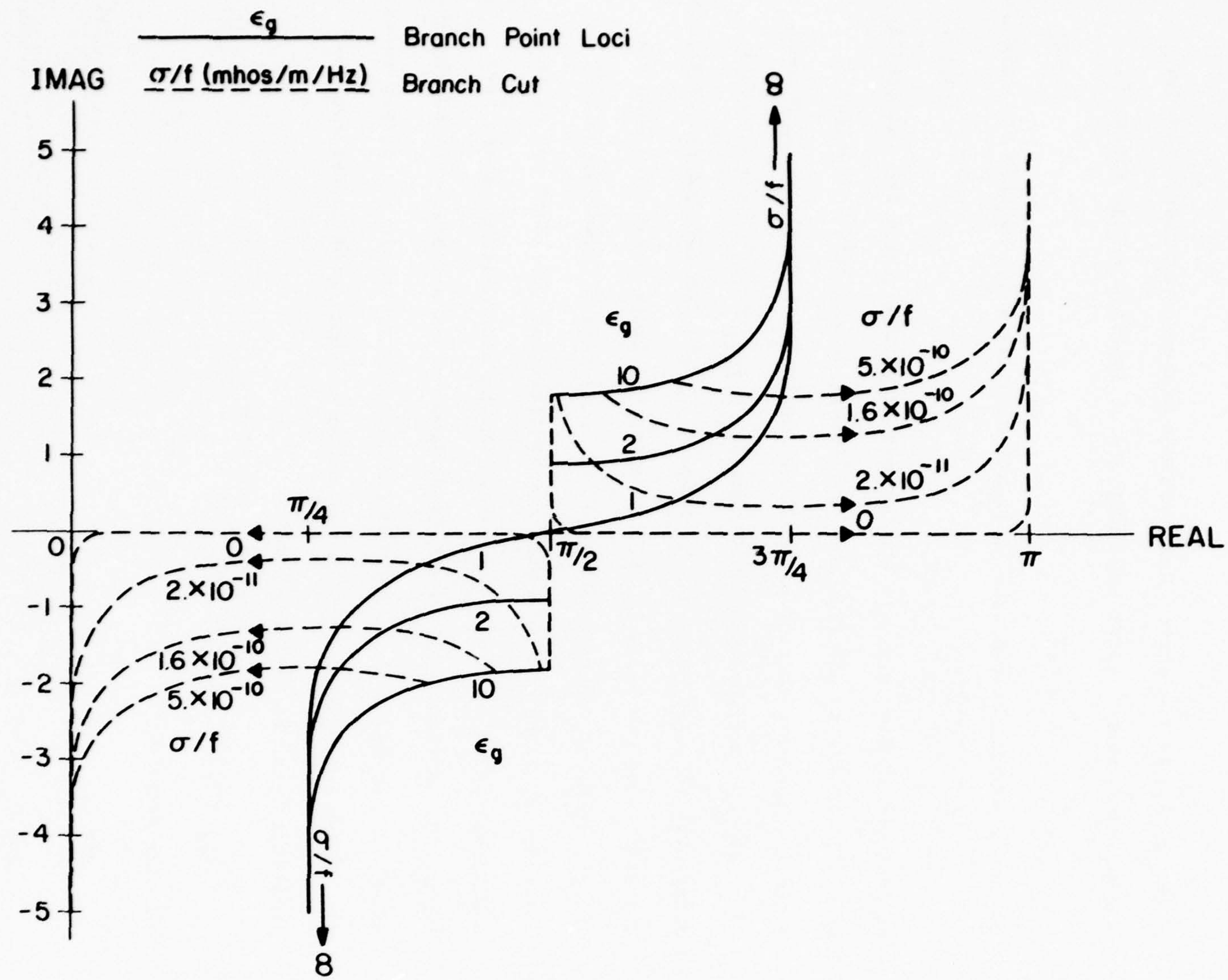

Figure 6. Branch-point and branch-cut loci as a function of ground parameters ϵ_g and σ/f.

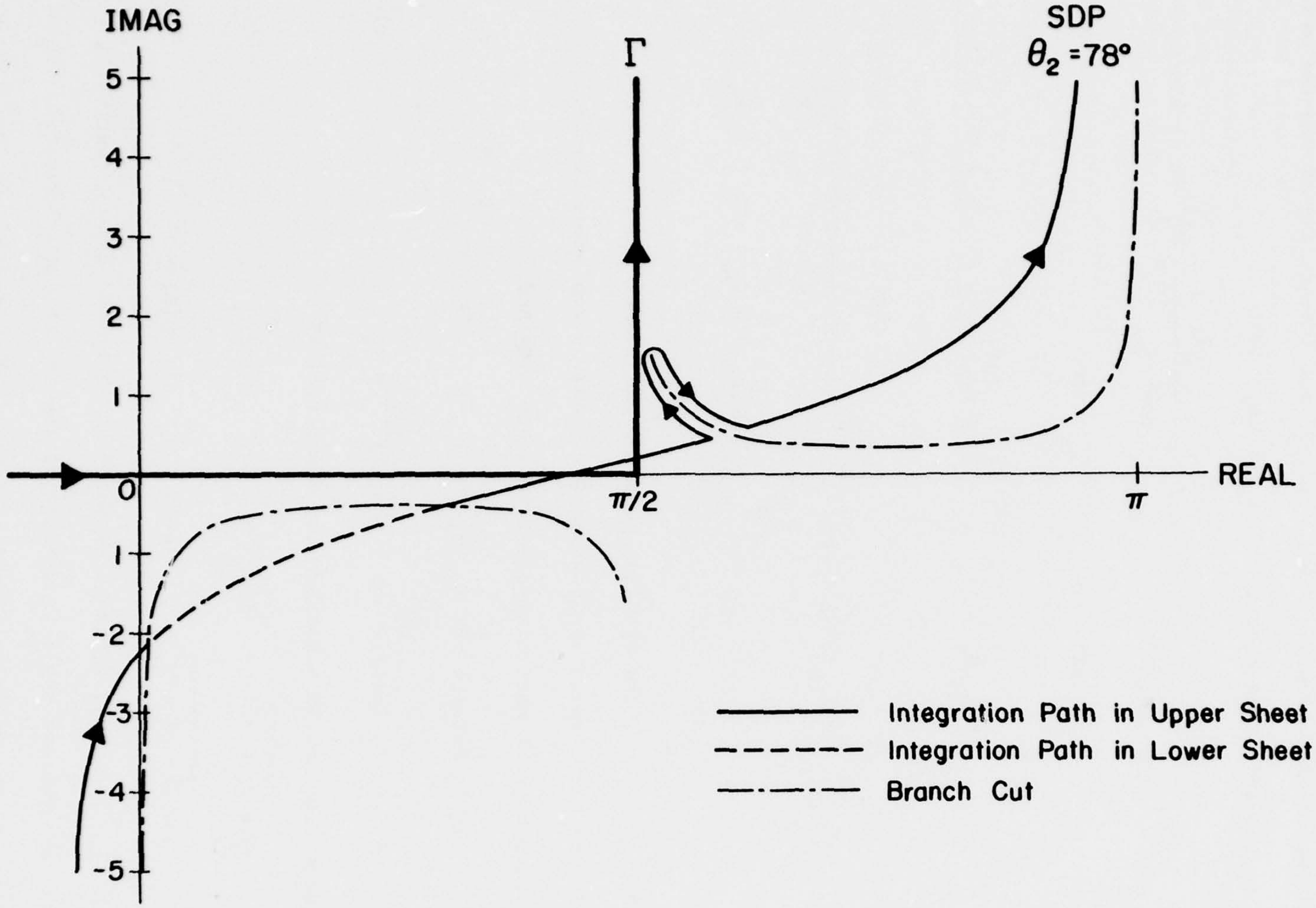

Figure 7. The correct SDP when branch cuts are intercepted. For this case, $\varepsilon_g = 10$, and $\sigma/f = 2 \times 10^{-11}$ mhos/m/Hz.

integrals expressed in (2.47) - (2.49) and integrating around the branch cut, the following contributions are obtained:

$$ {}_0\Pi_{v1z}\Big|_{bc} = I_{v0} k_1 \kappa (2\pi j)^{-1} \int_0^{\beta_1} \frac{\beta^2}{\kappa^2 \cos^2 \xi_{bc} - \beta^2} H_0^{(2)}(k_1 \rho_2 \sin \xi_{bc}) $$

$$ \cdot \exp(-jk_1 z_2 \cos \xi_{bc})\, d\beta \tag{3.16} $$

$$ {}_0\Pi_{h1x}\Big|_{bc} = I_{h0} k_1 (2\pi j)^{-1} \int_0^{\beta_1} \frac{\beta^2}{\kappa - 1} H_0^{(2)}(k_1 \rho_2 \sin \xi_{bc}) \exp(-jk_1 z_2 \cos \xi_{bc})\, d\beta \tag{3.17} $$

$$ {}_0\Pi_{h1z}\Big|_{bc} = I_{h0} k_1 (2\pi)^{-1} \cos \phi_2 \int_0^{\beta_1} (1 + \kappa) \frac{\beta^2}{\kappa^2 \cos^2 \xi_{bc} - \beta^2} $$

$$ \cdot \sin \xi_{bc} \cos \xi_{bc} H_1^{(2)}(k_1 \rho_2 \sin \xi_{bc}) \exp(-jk_1 z_2 \cos \xi_{bc})\, d\beta, \tag{3.18} $$

where $\beta = \beta_1$ is the crossing point of the branch cut and the SDP in the ξ-place. By expanding Equation (3.2) and by employing the (3.15) relations, the following conditions are obtained for β_1

$$ \sin \theta_2 \,\mathrm{Re}(A) + \cos \theta_2 \,\mathrm{Im}(B) = 1 \tag{3.19a} $$

$$ [-\sin \theta_2 \,\mathrm{Im}(A) + \cos \theta_2 \,\mathrm{Re}(B)]^{1/2} = t_1 \tag{3.19b} $$

where the complex numbers A and B are defined as

$$ A = \sqrt{\kappa - \beta_1^2} \quad ; \quad \mathrm{Re}(A) \geq 0 \quad , \quad \mathrm{Im}(A) \leq 0 \tag{3.20a} $$

$$ B = \sqrt{\kappa - 1 - \beta_1^2} \quad ; \quad \mathrm{Re}(B) \geq 0 \quad , \quad \mathrm{Im}(B) \leq 0 \quad . \tag{3.20b} $$

In (3.19), $t = t_1$ defines the point at which the SDP, corresponding to the observation angle θ_2, intercepts the branch cut of Equation (3.15) at $\beta = \beta_1$. After some algebraic manipulations, Equation (3.19a) can be

further simplified to

$$\theta_2 = \sin^{-1}\left([Re^2(A) + Im^2(B)]^{-1/2}\right) - \tan^{-1}\left(\frac{Im(B)}{Re(A)}\right) \tag{3.21}$$

from which θ_{min}, the observation angle at which *SDP* will pass through the branch point, can be computed by setting $\beta_1 = 0$. Since θ_{min} is only a function of κ, Figure 8 is constructed to show its variations as a function of the ground parameters and the frequency. Therefore, whenever the observation angle θ_2 satisfies the condition

$$\theta_2 > \theta_{min} \quad , \tag{3.22}$$

the branch-cut contributions in (3.16) - (3.18) are to be added to their respective SDP vector potential formulations expressed in (3.8) - (3.10).

It should be pointed out that once the condition (3.22) is met, the branch-cut integration limit β_1 can be computed numerically by iterating on Equation (3.21). Also, because of the branch-cut interception, the SDP integrand will be discontinuous at point $t = t_1$, which is readily computed by substituting the value of β_1 into (3.19b).

Fortunately, in many cases, the branch-cut contributions are several orders of magnitude smaller than the SDP integral value and can be ignored [16]. Therefore, it is necessary to introduce a condition for which one can ignore the branch-cut integration and thereby compute the vector potentials more efficiently. This task can be accomplished by initially considering the exp $(-k_1 r_2 t^2)$ term present in all three vector potential integrands shown in (3.8) - (3.10). If no poles are present on or near the contour, a finite integration in the interval

$$|t| \leq \left(\frac{9}{k_1 r_2}\right)^{1/2} \tag{3.23}$$

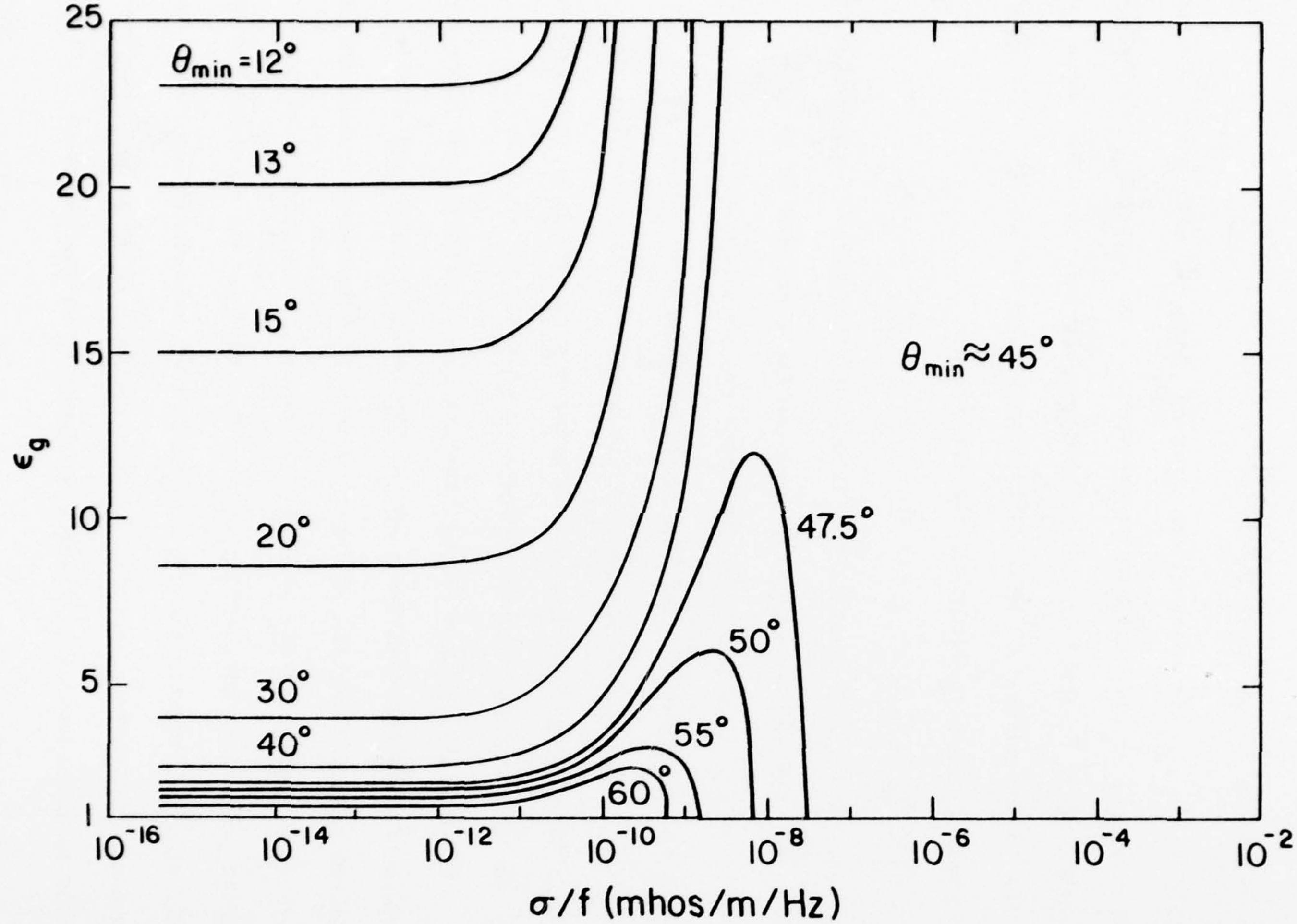

Figure 8. The minimum θ_2 contours as a function of κ. A branch point is captured by the SDP path deformation when $\theta_2 > \theta_{min}$.

will result in an error on the order of 0.01% as compared to the full infinite integration. By examining the branch-cut loci (Figure 6) and the SDP behavior (Figure 3) in the ξ-plane, an assumption can be made which states that if the branch cut intercepts the SDP inside the finite integration interval defined in (3.23), then the branch-cut contribution is not negligible. Or equivalently, the branch-cut contribution requires an additional condition, namely,

$$t_1 \leq t_{max} = 3(k_1 r_2)^{-1/2} \qquad (3.24)$$

where $t = t_1$ is the SDP and branch-cut intercept defined earlier.

In summary, condition (3.22) signals the capture of the branch point during the path deformation. If captured, condition (3.24) is used to decide whether the branch-cut integration can be ignored or not. Table 3.1 is constructed to verify the validity of the assumptions which led to Equation (3.24) by comparing the branch-cut values with the SDP integration results for a wide range of parameters.

3.3 Pole Contribution

Unlike the branch points, which exist in all three of the correction vector potential components, the poles only exist in the vertical components of the vector potentials, viz., ${}_0\Pi_{h1z}$ and ${}_0\Pi_{v1z}$, and satisfy the relation

$$\kappa \cos \xi_p + \sqrt{\kappa - \sin^2 \xi_p} = 0 \quad . \qquad (3.25)$$

Again, by considering the physical constraints discussed at the start of the previous section, only the following two poles need to be considered (see Figure 9):

$$\xi_p = \pi/2 \pm j \left[\mathrm{Ln}\,(\sqrt{\kappa} - j) - \mathrm{Ln}\,(\sqrt{\kappa + 1})\right] \quad . \qquad (3.26)$$

Table 3.1 Demonstrating the branch-cut contribution for ${}_0\Pi_{v1z}$. In this example: f = 30 MHz, $\phi_2 = 0$, $\epsilon_g = 10$, $\sigma = .001$ mhos/m, and $I_{v0} = 1$.

r_2(meters)	θ_2	t_{max}	t_1	β_1	SDP integration result × 10^4	Branch-cut contribution × 10^4	Total value × 10^4
20.	0.	.85	---	---	55.2-j2.07	---	55.2-j2.07
20.	30.	.85	---	---	53.2-j2.47	---	53.2-j2.46
20.	60.	.85	.81	1.8	44.6-j4.74	$-7.3 \times 10^{-4}+j1.3 \times 10^{-3}$	44.6-j4.74
20.	90.	.85	.55	2.0	14.5-j20.9	-.223+j.308	14.3-j20.6
10.	0.	1.2	---	---	111.6-j6.02	---	111.1-j6.02
10.	30.	1.2	---	---	107.6-j7.38	---	107.6-j7.38
10.	60.	1.2	.81	1.8	93.0-j14.4	-.128+j.204	92.9-j14.2
10.	90.	1.2	.55	2.0	50.2-j47.1	-3.85+j2.45	46.3-j44.7
5.	0.	1.7	---	---	-226.5+j17.5	---	-226.5+j17.5
5.	30.	1.7	---	---	-221.3+j21.3	---	-221.3+j21.3
5.	60.	1.7	.81	1.8	-199.1+j36.0	3.17-j3.61	-195.9+j32.4
5.	90.	1.7	.55	2.0	-140.3+j86.6	16.5-j22.7	-123.8+j63.9

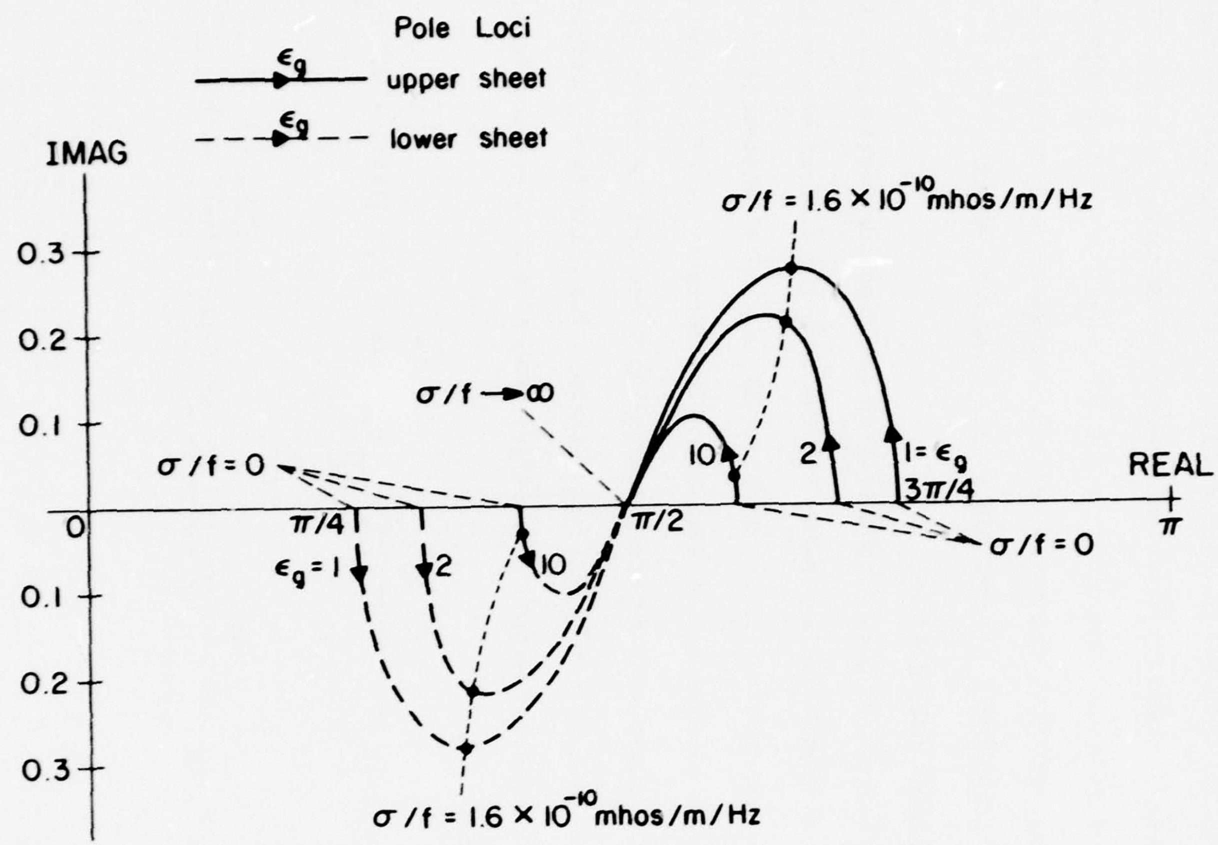

Figure 9. Pole loci as a function of ground parameters ϵ_g and σ/f.

Fortunately, one can verify that for $0 \leq \sigma/f < \infty$, $0 \leq \theta_2 < 90°$, and by considering the correct Riemann sheets (see Figure 7), the poles in Equation (3.26) will not be captured by the SDP and the residue contribution is not needed. However, under extreme circumstances, i.e., $\theta_2 \approx 90°$ and small ε_g, a pole can come close to the SDP. In this case, a higher-order Gaussian quadrature integration routine is required and possibly the effective integration interval in (3.23) should be expanded.

3.4 Asymptotic Approximation

The steepest descent formulation of the previous sections can be used to derive an asymptotic expansion for the Sommerfeld integrals in terms of inverse powers of $k_1 r_2$. In Appendix II, a general discussion is presented for asymptotically evaluating the integral in (3.1), and as an example, the first two asymptotic expansion terms for the vector potential expressions in (2.47) - (2.49) are derived. The first terms, better known as the Fresnel's reflection coefficient method (RCM) approximations, are shown to be:

$$ {}_0\Pi_{v1z} = I_{v0} \frac{2\kappa \cos \theta_2}{\kappa \cos \theta_2 + \sqrt{\kappa - \sin^2 \theta_2}} \exp(-jk_1 r_2)/4\pi r_2 + O(k_1 r_2)^{-2} \tag{3.27} $$

$$ {}_0\Pi_{h1x} = I_{h0} \frac{2 \cos \theta_2}{\cos \theta_2 + \sqrt{\kappa - \sin^2 \theta_2}} \exp(-jk_1 r_2)/4\pi r_2 + O(k_1 r_2)^{-2} \tag{3.28} $$

$$ {}_0\Pi_{h1z} = I_{h0}\, 2 \cos \phi_2 \sin \theta_2 \cos \theta_2 \frac{\cos \theta_2 - \sqrt{\kappa - \sin^2 \theta_2}}{\kappa \cos \theta_2 + \sqrt{\kappa - \sin^2 \theta_2}} \cdot \exp(-jk_1 r_2)/4\pi r_2 + O(k_1 r_2)^{-2} \quad . \tag{3.29} $$

The above RCM expressions have been extensively used for high-frequency antenna applications (k_1r_2 large) with surprisingly accurate results, e.g., [13], [14]. This success has been mainly due to the fact that for observation points away from the interface, the remaining vector potential components present in (2.20) and (2.30) tend to dominate over the RCM components thereby reducing the net error in the total vector potential values computed. Therefore, little is gained by adding the complicated second terms in the asymptotic expansion of the vector potentials, derived in Appendix II, since the accuracy of the total vector potential will not be affected appreciably.

An error of 5% or less can be expected in the RCM vector potential components shown in (3.27) - (3.29) when

$$k_1r_2 \geq 10 \quad , \tag{3.30}$$

and as long as the branch-cut conditions given in the previous section are not violated (see Tables 3.2 - 3.4). These conditions are more general than the one proposed by Sarkar [7] in defining the useful range of the RCM expressions. The second terms in the asymptotic expansion, as demonstrated in Tables 3.2 - 3.4, only offer a slight improvement in the accuracy of the ${}_0\Pi_{h1x}$ RCM expression in the region where the branch-cut contribution is negligible. The remaining vector potential components, however, do not benefit from the 2^{nd} term in the asymptotic expansions, possibly because they contain a pole in their Sommerfeld integrals. Figures 10 - 12 also compare the RCM, two-term asymptotic expansion and the exact integration values of the correction vector potential components for a typical half-space as a function of k_1r_2. Finally, in order to

Table 3.2 Comparing the exact integration values for ${}_0\Pi_{v1z}$ with its one- and two-term asymptotic expansions. In this example, f = 30 MHz, $\phi_2 = 0$, $\varepsilon_g = 10$, $\sigma = .001$ mhos/m, and $I_{v0} = 1$.

k_1r_2	θ_2	1-term asymptotic expansion (RCM) × 10^3	2-term asymptotic expansion × 10^3	SDP integration result × 10^3
1.	20.	35.7-j58.0	57.3-j51.8	34.6-j68.2
4.	20.	-10.9+j13.1	-12.2+j12.5	-10.4+j14.1
8.	20.	-1.40-j8.40	-1.08-j8.55	-1.69-j8.41
12.	20.	4.85+j2.96	4.80+j3.11	4.93+j2.85
1.	60.	28.6-j46.8	64.4-j55.2	29.1-j59.0
4.	60.	-8.73+j10.6	-11.0+j10.8	-7.97+j1.31
8.	60.	-1.15-j6.76	-.813-j7.23	-2.02-j6.96
12.	60.	3.91+j2.37	3.97+j2.62	4.23+j2.08
1.	80.	15.5-j26.0	-192.9-j169.2	19.8-j48.6
4.	80.	-4.76+j5.87	6.87+j16.6	-4.54+j11.5
8.	80.	-.668-j3.72	-4.59-j3.27	-2.82-j4.69
12.	80.	2.17+j1.28	3.16-j.168	3.24+j.619

Table 3.3 Comparing the exact integration values for ${}_0\Pi_{h1x}$ with its one- and two-term asymptotic expansions. In this example, f = 30 MHz, $\phi_2 = 0$, $\varepsilon_g = 10$, $\sigma = .001$ mhos/m, and $I_{h0} = 1$.

$k_1 r_2$	θ_2	1-term asymptotic expansion (RCM) × 10^3	2-term asymptotic expansion × 10^3	SDP integration result × 10^3
1.	20.	17.1-j24.3	17.2-j34.3	14.1-j36.0
4.	20.	-5.10+j5.42	-4.24+j6.17	-4.48+j6.32
8.	20.	-.383-j3.70	-.667-j3.66	-.665-j3.70
12.	20.	2.03+j1.42	2.10+j1.31	2.11+j1.32
1.	60.	11.4-j15.8	-10.0-j31.7	7.76-j36.9
4.	60.	-3.38+j3.50	-2.19+j4.67	-2.26+j4.84
8.	60.	-.217-j2.42	-.634-j2.40	-.635-j2.41
12.	60.	1.32+j.946	1.43+j.796	1.43+j.799
1.	80.	4.72-j6.36	-17.0-j24.2	.329-j39.8
4.	80.	-1.39+j1.41	-.208+j2.71	.405+j2.31
8.	80.	-.077-j.987	-.516-j.975	-.537-j.953
12.	80.	.532+j.391	.655+j.240	.651+j.236

Table 3.4 Comparing the exact integration values for ${}_0\Pi_{h1z}$ with its one- and two-term asymptotic expansions. In this example, f = 30 MHz, $\phi_2 = 0$, $\varepsilon_g = 10$, $\sigma = .001$ mhos/m, and $I_{h0} = 1$.

$k_1 r_2$	θ_2	1-term asymptotic expansion (RCM) × 10^3	2-term asymptotic expansion × 10^3	SDP integration result × 10^3
1.	20.	-3.18+j5.00	-7.88+j3.04	-3.84+j6.20
4.	20.	.963-j1.13	1.24-j.963	.895-j1.33
8.	20.	.112+j.733	.036+j.758	.172+j.739
12.	20.	-.418-j.263	-.405-j.296	-.437-j.242
1.	60.	-8.08+j12.5	-17.7+j16.5	-12.9+j21.9
4.	60.	2.44-j2.80	3.07-j2.97	1.97-j4.50
8.	60.	.261+j1.84	.190+j1.98	.739+j1.93
12.	60.	3.91+j2.37	3.97+j2.62	4.23+j2.08
1.	80.	-5.96+j9.14	84.9+j79.0	-20.6+j34.1
4.	80.	1.80-j2.05	-3.21-j7.17	.419-j6.80
8.	80.	.189+j1.35	1.98+j1.24	1.48+j1.84
12.	80.	-.764-j.493	-1.25+j.140	-1.32-j.111

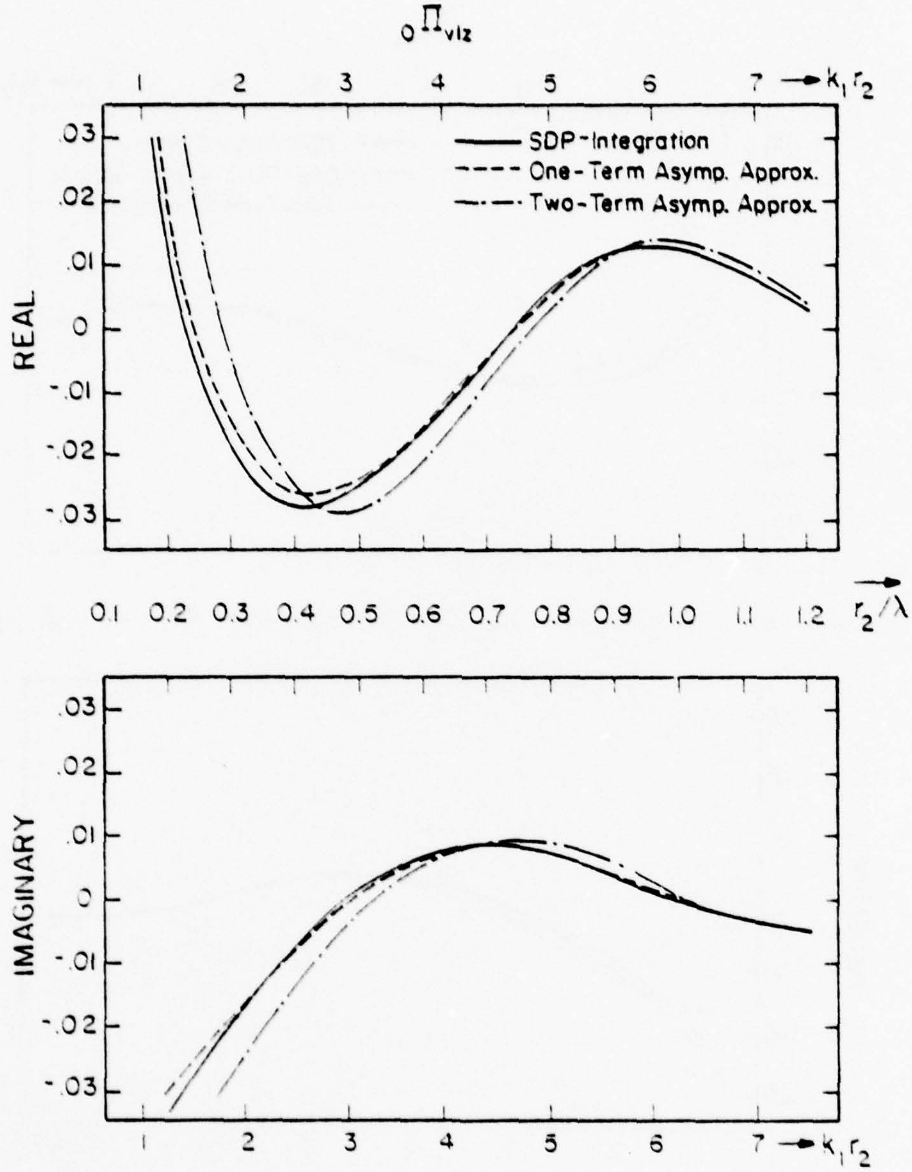

Figure 10. Comparing the SDP integration with the one- and the two-term asymptotic expansions of $_0\Pi_{v1z}$. For this case, frequency = 30 MHz $\theta_2 = 10°$, $\phi_2 = 0$, $\varepsilon_g = 10$, and $\sigma = .01$ mhos/m.

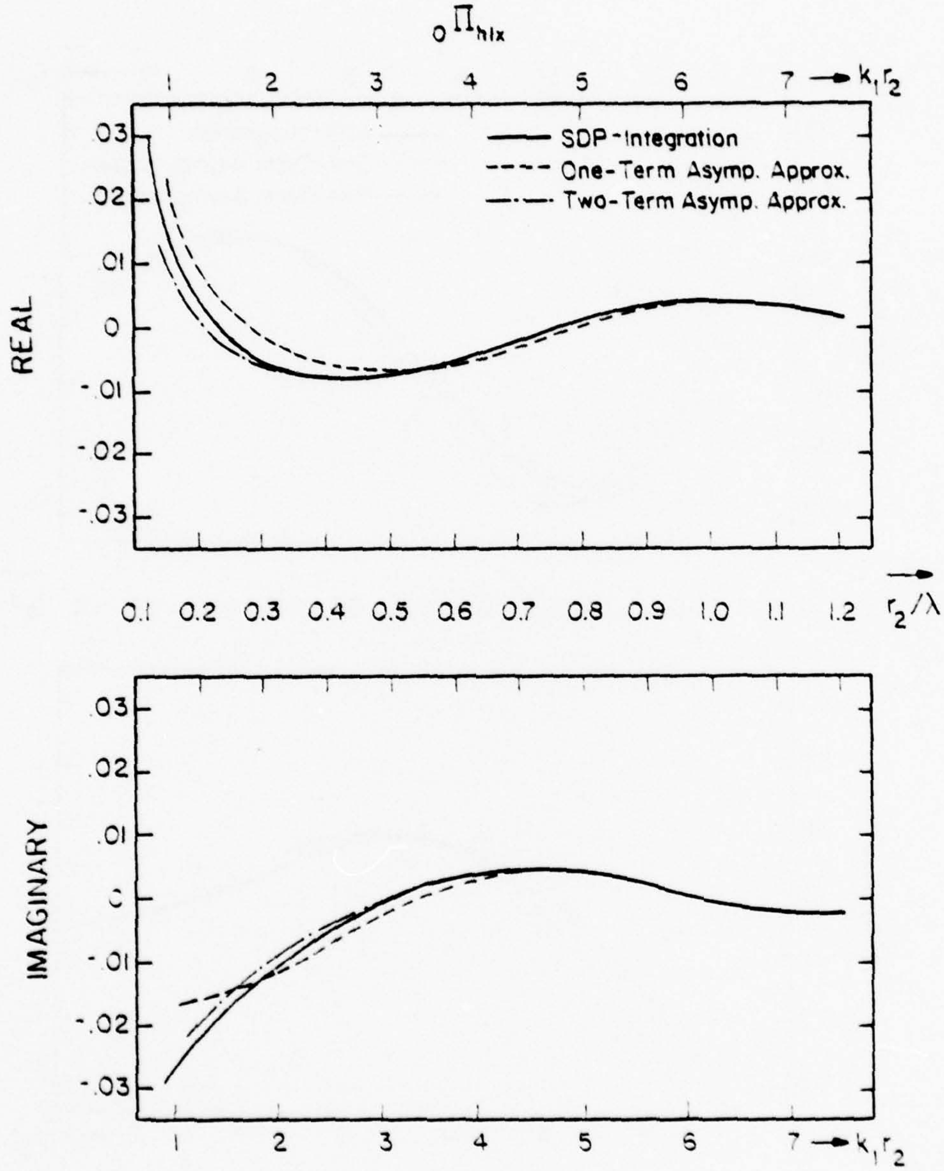

Figure 11. Comparing the SDP integration with the one- and two-term asymptotic expansions of $_0\Pi_{h1x}$. The parameters are identical to those in Figure 10.

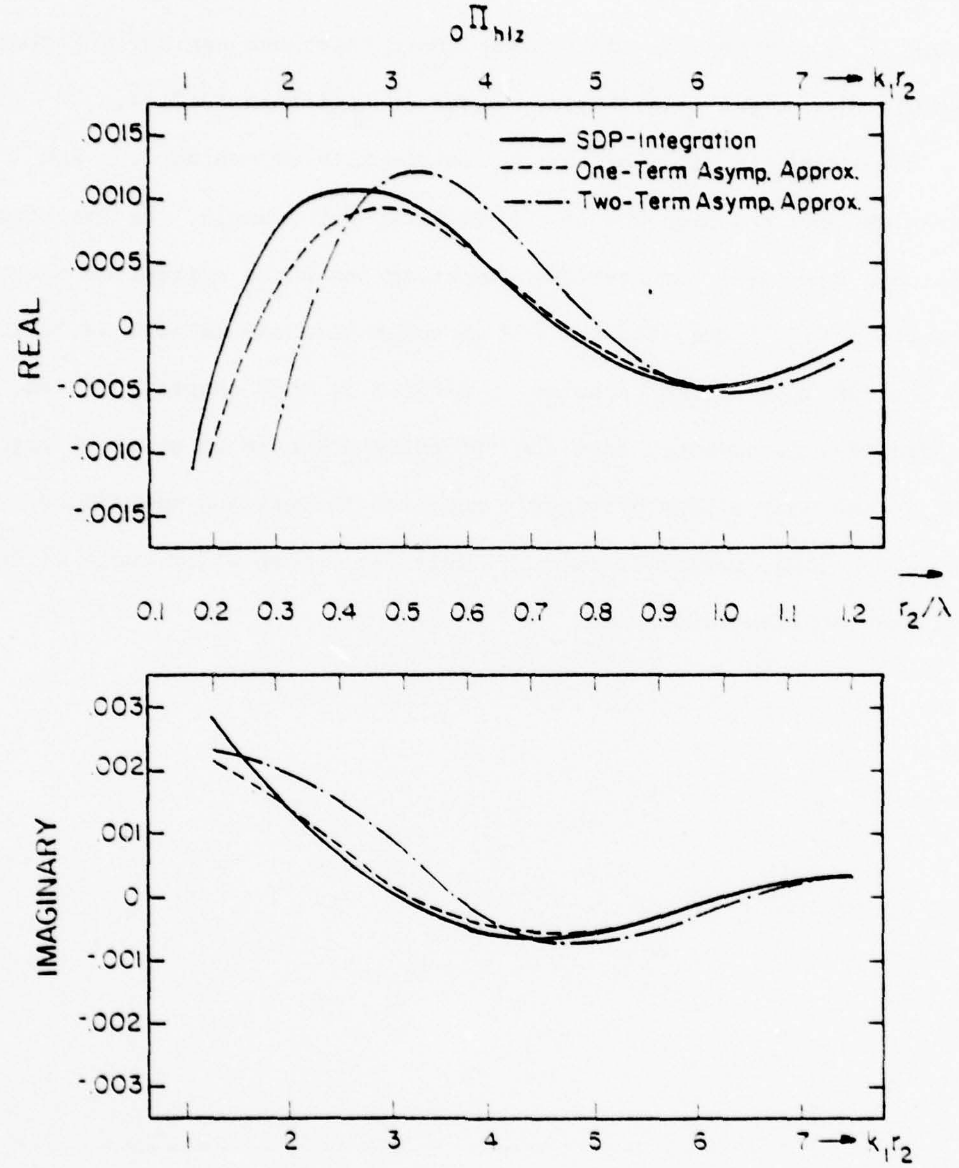

Figure 12. Comparing the SDP integration with the one- and the two-term asymptotic expansions of $_0\Pi_{h1z}$. The parameters are identical to those in Figure 10.

demonstrate the branch-cut effect, Figure 13 is included to show the minimum k_1r_2 contours in the κ-plane above which one can neglect the possible branch-cut contribution (based on condition (3.24)).

The computing time, of course, is the main reason why the RCM approximations are used whenever possible. For example, the execution time on a Cyber 175 computer for computing the three correction vector potentials is $\approx$ 1 msec for the RCM approximation and as high as 50-100 msec for the SDP integration technique presented in this chapter. It should be pointed out, however, that the SDP integration is an order of magnitude faster than many of the previously reported integration techniques [3] - [9], [12], making it more suitable for a much wider range of low-frequency applications.

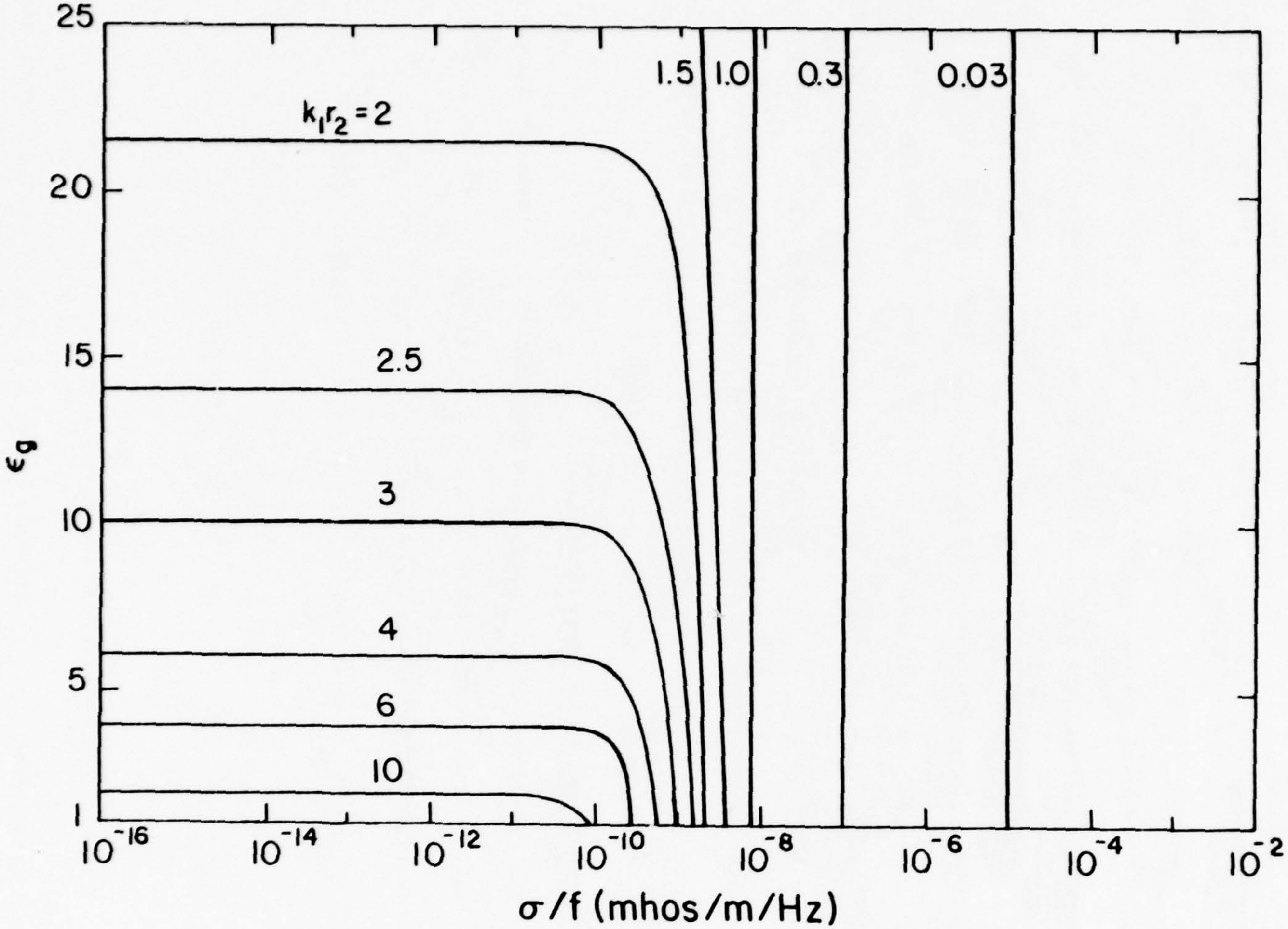

Figure 13. Minimum k_1r_2 contours as a function of κ. Once a branch point is captured, a branch-cut integration is negligible if the k_1r_2 is greater than the minimum values depicted in this graph.

4. COMPUTATIONS OF THE VECTOR POTENTIALS WITHOUT SOMMERFELD INTEGRATION

The conventional approach for analyzing antenna problems over lossy ground involves repeated evaluations of the Sommerfeld integrals appearing in the expressions for the vector potentials, viz., Equations (3.8) - (3.10). Even though the SDP procedure discussed in the previous chapter is an efficient integration technique, the computation time needed for evaluating these integrals severely limits the physical dimensions of the antenna problems being analyzed. In this chapter, a novel approach is introduced by initially approximating the well-behaved transform domain expressions of these integrals, derived in Chapter 2, and then performing the inverse transform operations via a set of exact identities. The resulting space domain expressions are valid for a wide range of parameters, with their computation times being comparable to those of the RCM approximation.

4.1 Transform Domain Expressions

The transform domain expressions for the three correction vector potential components shown in Equations (2.21c), (2.31c), and (2.32) can be rewritten in the following forms:

$$_0\tilde{\Pi}_{h1x} = I_{h0} \frac{1}{jk_1^2(1-\kappa)} (\gamma_1 - \gamma_2) \exp(-j\gamma_1 z_2) \tag{4.1}$$

$$_0\tilde{\Pi}_{h1z} = I_{h0} \frac{j\alpha}{k_1^2\kappa} \left[1 - (\kappa + 1) \frac{\gamma_2}{\kappa\gamma_1 + \gamma_2}\right] \exp(-j\gamma_1 z_2) \tag{4.2}$$

$$_0\tilde{\Pi}_{v1z} = I_{v0} \frac{\kappa}{j(\kappa\gamma_1 + \gamma_2)} \exp(-j\gamma_1 z_2) \tag{4.3}$$

where $z_2 = z + h$, and $\gamma_{1,2}$, defined in (2.15), are explicitly expressed as

$$\gamma_1 = (k_1^2 - \alpha^2 - \beta^2)^{1/2} \quad ; \quad \mathrm{Im}(\gamma_1) \leq 0 \tag{4.4a}$$

$$\gamma_2 = (\kappa k_1^2 - \alpha^2 - \beta^2)^{1/2} \quad ; \quad \mathrm{Im}(\gamma_2) \leq 0 \quad . \tag{4.4b}$$

In addition, the free-space Green's function g can also be expressed in the transform domain (see Equations (2.41b) and (2.31b)) yielding the following transform pair:

$$\tilde{g}(\alpha,\ \beta,\ z_2) = \frac{1}{2j\gamma_1} \exp\ (-j\gamma_1 z_2) \tag{4.5a}$$

$$g(x,\ y,\ z_2) = \exp\ (-jk_1 r_2)/4\pi r_2 \quad ; \quad r_2 = [x^2 + y^2 + z_2^2]^{1/2} \quad . \tag{4.5b}$$

By applying a successive $\partial/\partial z$ operator to (4.5), an infinite set of transform pairs is obtained, viz.,

$$\tilde{Q}_n = \gamma_1^{n-1} \exp\ (-j\gamma_1 z_2) \tag{4.6a}$$

$$Q_n = 2(j)^{n+1} \frac{\partial^n}{\partial z^n} g(x,\ y,\ z_2) \quad ; \quad n = 0,1,2,... \tag{4.6b}$$

where Q is expressed in a closed form for all n and can be numerically evaluated quite rapidly (see Appendix III).

An examination of the Fourier transformed vector potentials in (4.1) - (4.3) and the $\tilde{Q}_n$ in (4.6a) reveals two important and useful properties. First, all of the expressions have an identical z-variation term that corresponds to a space-domain solution emanating at the image point P_2. Second, it is apparent that all of the equations are well-behaved in the Fourier domain and decay exponentially to zero outside the circle $\alpha^2 + \beta^2 = k_1^2$. These properties give rise to the possibility of performing the inverse transform operation on Equations (4.1) - (4.3) via the use of the (4.6) identities. The major obstacle to such a procedure is the existence

of γ_2 in these expressions which is overcome in the following section by an appropriate approximation.

4.2 Approximating γ_2 and Space-Domain Results

All three Fourier transform domain expressions in (4.1) - (4.3) can be put into the following general form

$$ {}_0\tilde{\Pi} = f(\gamma_1, \gamma_2) \exp(-j\gamma_1 z_2) \quad . \tag{4.7}$$

As mentioned in the previous section, an important property of Equation (4.7) is the exponential term which rapidly decays to zero outside the circle $\alpha^2 + \beta^2 = k_1^2$ (also see Figure 14). This fact enables one to replace γ_2, defined in (4.4b), by the first term of its Taylor's series expansion $\bar{\gamma}_2$, that is,

$$\gamma_2 = k_1\sqrt{\kappa}\left[1 - \frac{\alpha^2 + \beta^2}{2k_1^2\kappa} - \frac{1}{8}\left(\frac{\alpha^2 + \beta^2}{k_1^2\kappa}\right)^2 - \ldots\right] \quad ; \quad \alpha^2 + \beta^2 \leq k_1^2|\kappa| \tag{4.8a}$$

$$\bar{\gamma}_2 = k_1\sqrt{\kappa} \quad . \tag{4.8b}$$

For most practical values of κ, i.e., $|\kappa| \geq 10$, the approximation in (4.8b) is excellent inside the circle $\alpha^2 + \beta^2 \leq k_1^2$. Fortunately, as demonstrated in Figure 14, the decaying exponential in (4.7) can easily overcome the errors introduced by (4.8b) in the region $\alpha^2 + \beta^2 \geq k_1^2$ thereby making this a valid approximation throughout the $\alpha\beta$-plane for a wide range of κ and z_2 parameters, namely,

$$ {}_0\tilde{\bar{\Pi}} \simeq f(\gamma_1, \bar{\gamma}_2) \exp(-jk_1 z_2) \tag{4.9}$$

where the bar on top represents the approximate quantities. It should be noted that Kuo and Mei [12, Eq. 8] have recently verified and used the aforementioned approximation for simplifying the space domain expressions,

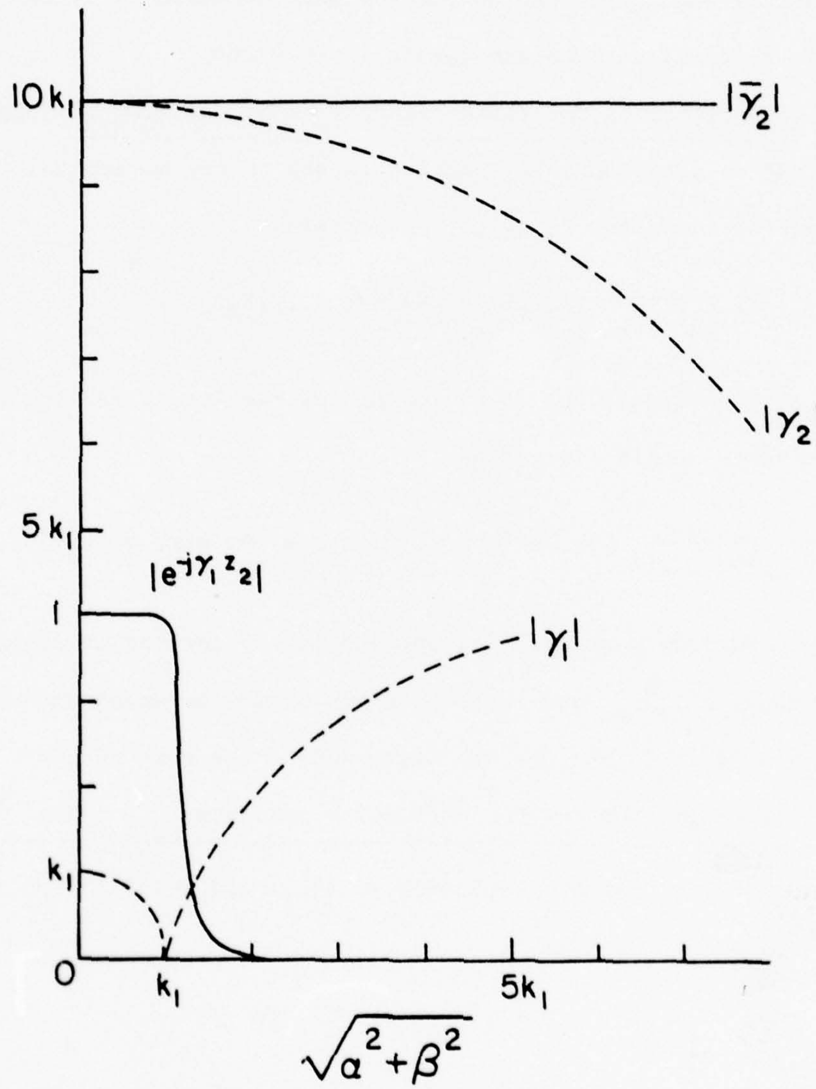

Figure 14. The plot of the functions $|\bar{\gamma}_2|$, $|\gamma_2|$, $|\gamma_1|$, and $|e^{-j\gamma_1 z_2}|$ versus $\sqrt{\alpha^2 + \beta^2}$. Note that for $|\kappa|$ large enough, the following approximation holds: $\gamma_2 e^{-j\gamma_1 z_2} \simeq \bar{\gamma}_2 e^{-j\gamma_1 z_2}$.

while Chang et al. [6] have employed an equivalent approximation for representing the vector potential in the vertical current element problem in terms of an incomplete Hankel function. The approximate transform domain vector potential quantities can now be treated individually in order to obtain their respective transform domain expressions.

4.2.1 Approximation for the horizontal component ($_0\bar{\Pi}_{h1x}$). Applying the approximation introduced in Equation (4.8b) to the horizontal correction vector potential component in (4.1), one obtains

$$_0\tilde{\bar{\Pi}}_{h1x} = I_{h0} \frac{1}{jk_1^2(1-\kappa)} (\gamma_1 - k_1\sqrt{\kappa}) \exp(-j\gamma_1 z_2) \quad , \tag{4.10}$$

and direct application of the (4.6) identities results in the following closed-form space domain expression:

$$_0\bar{\Pi}_{h1x} = \frac{-2I_{h0}}{k_1^2(1-\kappa)} \left[jk_1\sqrt{\kappa}\frac{\partial}{\partial z} g(x, y, z_2) + \frac{\partial^2}{\partial z^2} g(x, y, z_2)\right] \quad . \tag{4.11}$$

Note that the various partials of g are explicitly derived in Appendix III. The useful range of $_0\bar{\Pi}_{h1x}$ and the comparison of its accuracy and efficiency with other available techniques are discussed in the next section.

4.2.2 Approximation for the vertical components ($_0\bar{\Pi}_{h1z}$ and $_0\bar{\Pi}_{v1z}$). Again the variable γ_2 can be eliminated in (4.2) and (4.3) by applying the approximation in (4.8b), that is,

$$_0\tilde{\bar{\Pi}}_{h1z} = I_{h0} \frac{j\alpha}{k_1^2\kappa} \left[1 - j(\kappa + 1) \frac{c}{j(\gamma_1 + c)}\right] \exp(-j\gamma_1 z_2) \tag{4.12}$$

$$_0\tilde{\bar{\Pi}}_{v1z} = I_{v0} \frac{1}{j(\gamma_1 + c)} \exp(-j\gamma_1 z_2) \quad , \tag{4.13}$$

where the constant c is defined as

$$c = k_1/\sqrt{\kappa} \quad . \tag{4.14}$$

Application of the identities in Equation (4.6) results in the following space domain forms:

$$ {}_0\bar{\Pi}_{h1z} = \frac{I_{h0}}{k_1^2 \kappa} \left[-2 \frac{\partial^2}{\partial x \partial z} g(x, y, z_2) - jc(\kappa + 1) \frac{\partial}{\partial x} S(x, y, z_2) \right] \qquad (4.15) $$

$$ {}_0\bar{\Pi}_{v1z} = I_{v0} S(x, y, z_2) \quad . \qquad (4.16) $$

Unfortunately, the function S, whose transform domain expression is defined as

$$ \tilde{S}(\alpha, \beta, z_2) = {}_0\tilde{\bar{\Pi}}_{v1z}/I_{v0} = \frac{1}{j(\gamma_1 + c)} \exp(-j\gamma_1 z_2) \quad , \qquad (4.17) $$

cannot be expressed in a simple closed form. However, by using the (4.6) identities, it can be shown that S satisfies the following first-order inhomogeneous linear differential equation:

$$ \frac{\partial}{\partial z} [S(\rho, z_2) \exp(-jcz_2)] = 2 \exp(-jcz_2) \frac{\partial}{\partial z} g(\rho, z_2) \quad , \qquad (4.18) $$

where, for convenience, the functional dependences of S and g have been reduced from (x, y, z_2) to (ρ, z_2). By integrating (4.18) with respect to z_2, and after some algebraic manipulations, the following expression is derived for S:

$$ S(\rho, z_2) = [S(\rho, z_2') - 2g(\rho, z_2')] \exp[jc(z_2 - z_2')] + 2g(\rho, z_2) $$

$$ + 2jc \exp(jcz_2) \int_{z_2'}^{z_2} g(\rho, z) \exp(-jcz) \, dz \quad . \qquad (4.19) $$

The secondary height z_2' is an arbitrary starting point needed for obtaining a unique solution to the (4.18) differential equation. Since no simple starting point can be found at which $S(\rho, z_2')$ is known, it is assumed that z_2' is large enough so that the RCM approximation in Equation (3.27) is

applicable (see Figure 15), that is,

$$S(\rho,\ z_2') = \frac{2\kappa \cos \theta_2'}{\kappa \cos \theta_2' + \sqrt{\kappa - \sin^2 \theta_2'}}\ g(\rho,\ z_2') \tag{4.20}$$

where angle θ_2' is defined in Figure 15. A similar procedure can be used for computing $\frac{\partial}{\partial x}$ S, required for $_0\bar{\Pi}_{h1z}$ in Equation (4.15), by simply differentiating (4.19) with respect to x:

$$\frac{\partial}{\partial x} S(\rho,\ z_2) = [\frac{\partial}{\partial x} S(\rho,\ z_2') - 2 \frac{\partial}{\partial x} g(\rho,\ z_2')] \exp\ [jc(z_2 - z_2')] + 2 \frac{\partial}{\partial x} g(\rho,\ z_2)$$

$$+ 2jc \exp\ (jcz_2) \int_{z_2'}^{z_2} \frac{\partial}{\partial x} g(\rho,\ z) \exp\ (-jcz)\ dz \quad , \tag{4.21}$$

and by using the asymptotic expression in (3.29), the following initial value at point z_2' is obtained:

$$\frac{\partial}{\partial x} S(\rho,\ z_2') = \frac{2j}{c(\kappa + 1)} \left[\frac{\partial^2}{\partial x \partial z} g(\rho,\ z_2') + k_1^2 \kappa \cos \phi_2 \sin \theta_2' \cos \theta_2' \right.$$

$$\left. \cdot \frac{\cos \theta_2' - \sqrt{\kappa - \sin^2 \theta_2'}}{\kappa \cos \theta_2' + \sqrt{\kappa - \sin^2 \theta_2'}}\ g(\rho,\ z_2')\right] \quad . \tag{4.22}$$

In summary, the procedure for computing the vertical vector potential components at the point $(\rho,\ z_2)$, as demonstrated in Figure 15, is to start from a higher observation point $(\rho,\ z_2')$, at which the RCM expressions are valid, and simply use Equation (4.19) or (4.21) to integrate down to $(\rho,\ z_2)$. This procedure effectively computes a correction term for the RCM approximations of the vertical vector potential components in the region where RCM alone breaks down. The useful range and the accuracy of this procedure are discussed in the following section.

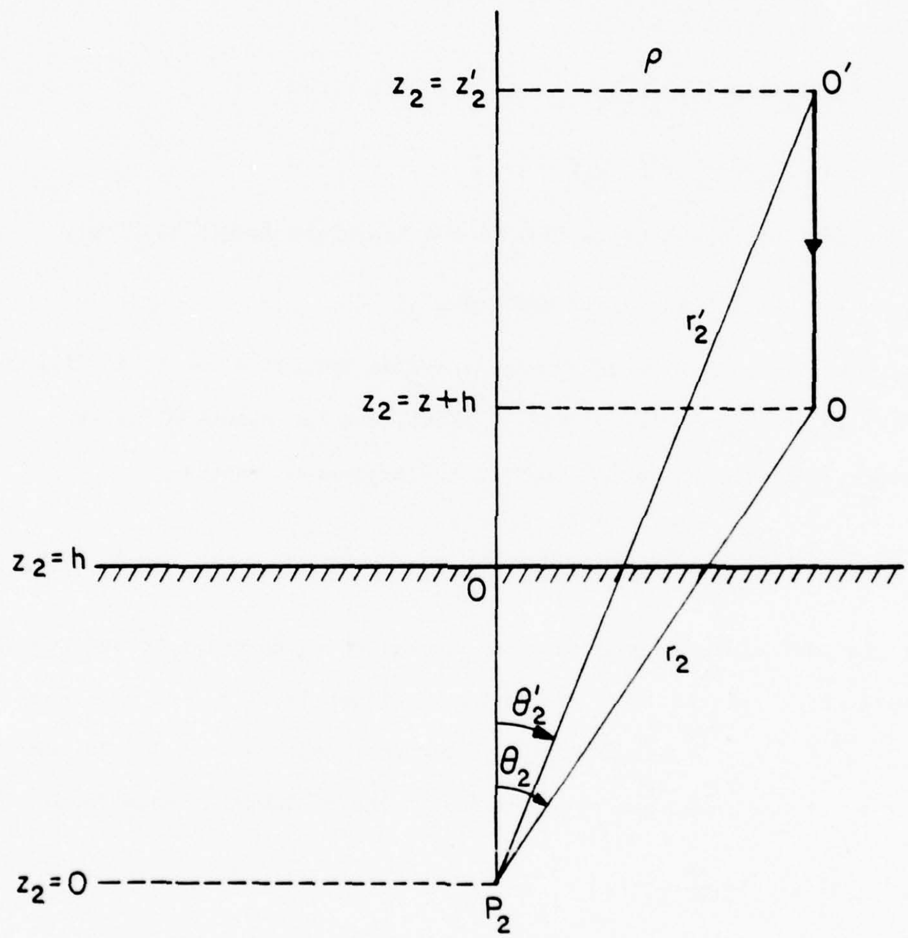

Figure 15. The geometry for computing the vertical vector potential components. r_2' is chosen to be large enough so that the RCM expressions are valid at 0'. Therefore, the vector potential values along the interval 0'0 are obtained by using the initial initial value at 0' and integrating down along the z-axis.

4.3 Error Estimation for the Approximate Expressions

In the previous section, only the approximation in (4.8) was made to derive the horizontal vector potential component in Equation (4.11). The approximated term T in this vector potential component, for convenience, can be expressed in the following forms:

$$\tilde{T} = \gamma_2 \exp(-j\gamma_1 z_2) \tag{4.23a}$$

$$\tilde{\bar{T}} = \bar{\gamma}_2 \exp(-j\gamma_1 z_2) \tag{4.23b}$$

$$\bar{T} = -2k_1\sqrt{\kappa}\,\frac{\partial}{\partial z}\, g(\rho,\, z_2) \quad . \tag{4.23c}$$

The error introduced by (4.23b) in the transform domain is simply

$$\Delta\tilde{T} = \tilde{T} - \tilde{\bar{T}} = (\gamma_2 - \bar{\gamma}_2)\exp(-j\gamma_1 z_2) \quad , \tag{4.24}$$

and again referring to the Taylor's series expansion for γ_2 in (4.8a), which is convergent for $\alpha^2 + \beta^2 < k_1^2|\kappa|$, one can assume $\Delta\tilde{T}$ to be proportional to the second term of the expansion, namely,

$$\Delta\tilde{T} \simeq \frac{-(\alpha^2 + \beta^2)}{2k_1\sqrt{\kappa}}\exp(-j\gamma_1 z_2) \quad . \tag{4.25}$$

At the same time, a constraint is needed for z_2 in order to enforce the exponential term in (4.25) to decay sufficiently, i.e., to 1%, when $\alpha^2 + \beta^2 = k_1^2|\kappa|$. This important condition, which allows one to use (4.25) for error analysis, can be expressed in the following simple form:

$$k_1 z_2 > \frac{5}{\sqrt{|\kappa| - 1}} \quad . \tag{4.26}$$

By substituting $\alpha^2 + \beta^2$ from (4.4a) into Equation (4.25), one can obtain ΔT directly via the (4.6) identities, namely,

$$\Delta T = \frac{k_1}{\sqrt{\kappa}}\frac{\partial}{\partial z}\, g(\rho,\, z_2) + \frac{1}{k_1\sqrt{\kappa}}\frac{\partial^3}{\partial z^3}\, g(\rho,\, z_2) \quad . \tag{4.27}$$

The space domain expressions in (4.23c) and (4.27) can be used to define R_T, the relative error in the magnitude of $\bar{T}$, as

$$R_T = \left|\frac{\Delta T}{\bar{T}}\right| \leq \frac{1}{2|\kappa|} + \frac{1}{2k_1^2|\kappa|}\left|\frac{\frac{\partial^3}{\partial z^3} g(\rho, z_2)}{\frac{\partial}{\partial z} g(\rho, z_2)}\right| \quad ; \tag{4.28}$$

and by using the explicit expansions provided in Appendix III, the above relation can be further reduced to

$$R_T < \frac{1}{2|\kappa|} + \frac{1}{2|\kappa|}\left\{|5\cos^2\theta_2 - 3|\left[\frac{1}{(k_1 r_2)^2}\left(2 + \frac{1}{\sqrt{1 + (k_1 r_2)^2}}\right) + \frac{1}{k_1 r_2}\right] + \cos^2\theta_2\right\} . \tag{4.29}$$

Equation (4.29) is a useful upper bound for the error existing in the computed magnitude of ${}_0\bar{\Pi}_{h1x}$. The first term in the aforementioned equation sets a limit on the minimum required $|\kappa|$ value; for example, the error condition $R_T < 10\%$ requires $|\kappa| > 10$, while $R_T < 5\%$ will require $|\kappa| > 20$. Figures 16 and 17 demonstrate the valid regions in the (r_2, θ_2) plane as a function of $|\kappa|$ for two useful error conditions, namely, $R_T = 5\%$ and 10%, respectively. Table 4.1 is included to numerically verify the conditions (4.26) and (4.29) by comparing the approximate horizontal vector potential values in (4.11) with the corresponding exact SDP integration results of Chapter 3. As clearly demonstrated in this table, the actual computed errors in the magnitude are consistently below the R_T values obtained from Equation (4.29), for the various (κ, r_2, θ_2) combinations tested.

Unfortunately, because of the complicated nature of the approximate transform expressions (4.12) - (4.13), one cannot derive a simple error condition for the vertical potential components, as was derived for the horizontal case (Equation (4.29)). However, because of the similar nature

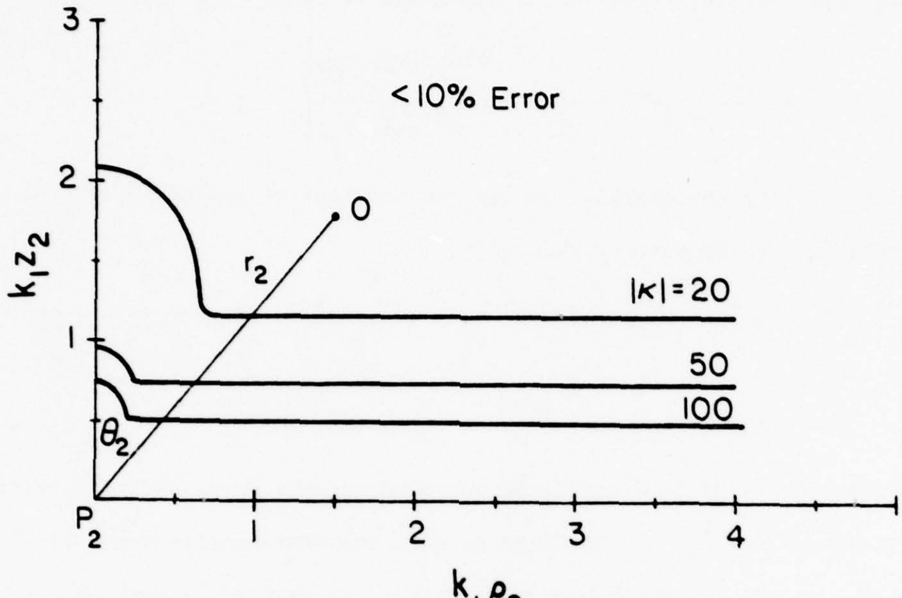

Figure 16. Examples of $|\kappa|$ contours for which < 10% error is ensured for observation points on or above it.

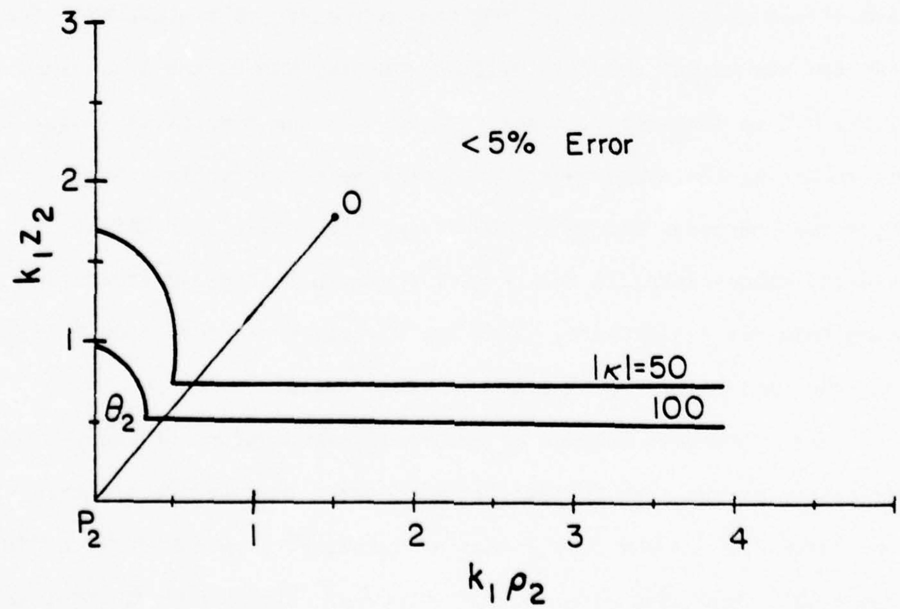

Figure 17. Examples of $|\kappa|$ contours for which < 5% error is ensured for observation points on or above it.

of the approximation for all three of the correction vector potential components, one can assume that conditions (4.26) and (4.29) also apply to the ${}_0\bar{\Pi}_{h1z}$ and ${}_0\bar{\Pi}_{v1z}$ expressions shown in Equations (4.15) - (4.16). This assumption is verified by the results in Tables 4.2 and 4.3 in which the vertical-correction-vector potential components are computed by using $k_1 r_2' = 10$ as a starting point. Even though these RCM initial values, in general, contain about 5% error, the net errors in all of the cases are well below the predicted ones (Equation (4.29)). Table 4.4 is also included to demonstrate the stability of the final vertical vector potential value as a function of starting point z_2'. Note that when $k_1 r_2' > 10$, the error in the final results stays within acceptable levels of the exact values primarily because the RCM approximation used to compute the starting point becomes reasonably accurate in this region.

Studying the results of this section, one can conclude that the proposed approximate formulas, i.e., (4.11), (4.15) and (4.16), can be employed in most practical antenna problems as long as $|\kappa| > 10$ and condition (4.26) is satisfied.

4.4 Advantages of the Approximate Expressions

The major advantage of the approximate technique introduced in the chapter is, of course, the computation of the vector potentials. For example, on the Cyber-175 computer, the computation time for computing the three vector potential expressions is $\simeq$ 1 msec for the RCM technique, $\simeq$ 5 msec for the approximate technique presented in this chapter, and finally $\simeq$ 50-100 msec for the SDP integration technique discussed in Chapter 3. Note that even though the approximate technique is slightly more time-consuming than the RCM method, it can be applied to a much

Table 4.1 Comparison of the RCM, exact, and the approximate evaluations of ${}_0\Pi_{v1z}$. For this example, f = 30 MHz, $\theta_2 = 45^o$, $\phi_2 = 0^o$, and $I_{v0} = 1$.

	k_1r_2	k_1z_2	Min. k_1z_2 Eq. (4.26)	RCM value $\times 10^2$	Exact integration $\times 10^2$	Approximate technique $\times 10^2$	% error Eq. (4.29)	% error actual
$\varepsilon_g=5$, $\sigma=.001$, $\lvert\kappa\rvert=5.04$	.1	.07	2.49	62.1-j7.49	79.6-j11.2	96.3-j17.2	1551.	16.0
	1.	.71	2.49	3.28-j5.33	3.22-j6.52	2.94-j7.13	33.3	8.7
	2.	1.41	2.49	-1.36-j2.82	-1.84-j2.95	-1.96-j2.88	20.4	4.0
	6.	4.24	2.49	1.01+j.272	1.06+j2.00	1.03-j2.09	16.0	2.9
	10.	7.07	2.49	-.518+j.351	-.507+j.383	-.518+j.351	15.5	5.5
$\varepsilon_g=10$, $\sigma=.01$, $\lvert\kappa\rvert=11.7$	.1	.07	1.53	70.5-j12.4	90.8-j15.8	96.6-j15.7	67.0	5.9
	1.	.71	1.53	3.41-j6.30	3.47-j7.76	3.42-j7.86	14.4	1.2
	2.	1.41	1.53	-1.73-j3.14	-2.23-j3.34	-2.28-j3.30	8.8	1.7
	6.	4.24	1.53	1.17+j.247	1.23+j.184	1.19+j.179	6.9	2.8
	10.	7.07	1.53	-.570+j.433	-.562+j.465	-.570+j.433	6.7	4.6
$\varepsilon_g=40$, $\sigma=1$, $\lvert\kappa\rvert=601$	.1	.07	.204	95.0-j13.2	99.5-j11.0	99.6-j11.0	13.0	.05
	1.	.71	.204	4.87-j8.26	5.09-j8.52	5.09-j8.52	.28	.06
	2.	1.41	.204	-2.16-j4.28	-2.22-j4.39	-2.22-j4.40	.17	.10
	6.	4.24	.204	1.55+j.388	1.57+j.386	1.57+j.386	.13	.35
	10.	7.07	.204	-.784+j.552	-.788+j.560	-.784+j.552	.13	.95

Table 4.2 Comparison of the RCM, exact, and the approximate evaluations of ${}_0\Pi_{h1x}$. For this example, f = 30 MHz, $\theta_2 = 45^o$, $\phi_2 = 0^o$, and $I_{h0} = 0$.

	k_1r_2	k_1z_2	Min. k_1z_2 Eq. (4.26)	RCM value $\times 10^2$	Exact integration $\times 10^2$	Approximate technique $\times 10^2$	% error Eq. (4.29)	% error actual
$\epsilon_g=5$, $\sigma=.001$, $\lvert\kappa\rvert=5.04$	.1	.07	2.49	24.9-j1.25	48.4-j7.82	1251.-j209.	1551.	96.1
	1.	.71	2.49	1.45-j2.03	1.11-j3.62	-.892+j1.51	33.3	29.4
	2.	1.41	2.49	-.462-j1.16	-.996-j1.18	-1.15-j1.16	20.4	9.7
	6.	4.24	2.49	.393+j1.36	.420+j.078	.452+j.084	16.0	7.1
	10.	7.07	2.49	-.216+j.125	-.205+j.146	-.222+j.156	15.5	7.3
$\epsilon_g=10$, $\sigma=.01$, $\lvert\kappa\rvert=11.7$	.1	.07	1.53	17.4+j.023	45.6-j9.38	452.6+j42.2	670.	90.3
	1.	.71	1.53	1.26-j1.22	.712-j2.55	.510-j2.72	14.4	9.4
	2.	1.41	1.53	-.171-j.859	-.576-j.847	-.592-j.858	8.8	1.9
	6.	4.24	1.53	.254+j.144	.278+j.105	.284+j.110	6.9	2.6
	10.	7.07	1.53	-.165+j.059	-.159+j.075	-.164+j.074	6.7	2.7
$\epsilon_g=40$, $\sigma=1$, $\lvert\kappa\rvert=601$	.1	.07	.204	-2.24-j1.52	-14.5+j5.41	-21.5-j3.74	13.0	9.8
	1.	.71	.204	.272-j.074	.206-j.342	.205-j.343	.28	.09
	2.	1.41	.204	.042-j1.35	-.024-j1.56	-.024-j1.56	.17	.03
	6.	4.24	.204	.025+j.040	.031+j.036	.031+j.036	.13	.03
	10.	7.07	.204	-.028-j.004	-.028-j.002	-.028-j.002	.13	.04

Table 4.3 Comparison of the RCM, exact, and the approximate evaluations of ${}_0\Pi_{h1z}$. For this example, f = 30 MHz, $\theta_2 = 45^o$, $\phi_2 = 0^o$, and $I_{v0} = 0$.

	k_1r_2	k_1z_2	Min. k_1z_2 Eq. (4.26)	RCM value $\times 10^2$	Exact integration $\times 10^2$	Approximate technique $\times 10^2$	% error Eq. (4.29)	% error actual
ϵ_g=5, σ=.001, |κ|=5.04	.1	.07	2.49	-12.5+j1.25	-14.3+j1.19	-2984.+j23.0	1551.	99.5
	1.	.71	2.49	-.677+j1.05	-.892+j1.51	-1.94+j4.14	33.3	61.9
	2.	1.41	2.49	.260+j.570	.463+j.699	.683+j.915	20.4	27.0
	6.	4.24	2.49	-2.01-j.058	-.225-j.027	-.238-j.032	16.0	5.6
	10.	7.07	2.49	.105-j.068	.100-j.082	.105-j.068	15.5	12.1
ϵ_g=10, σ=.01, |κ|=11.7	.1	.07	1.53	-11.6-j.126	-18.2+j2.63	-1170.-j448.5	670.	98.7
	1.	.71	1.53	-.753+j.903	-.676+j1.65	-1.16+j2.24	14.4	30.3
	2.	1.41	1.53	.182+j.552	.445+j.611	.456+j.680	8.8	8.6
	6.	4.24	1.53	-.179-j.074	-.202-j.043	-.199-j.049	8.8	3.2
	10.	7.07	1.53	.104-j.052	.997-j.066	.104-j.052	6.7	12.8
ϵ_g=40, σ=1., |κ|=601	.1	.07	.204	-2.24-j1.52	-14.5+j5.41	-21.5-j3.74	13.0	9.8
	1.	.71	.204	-.258+j.082	-.204+j.328	-.205+j.328	.28	.33
	2.	1.41	.204	-.035+j1.31	.026+j1.53	.026+j1.53	.17	.42
	6.	4.24	.204	-.025-j.037	.032-j.034	-.032-j.032	.13	4.1
	10.	7.07	.204	.027+j.003	.027+j.0005	.027+j.003	.13	10.4

Table 4.4 Demonstration of the stability of the approximate technique as a function of secondary height z_2'. In this example, $f = 18$ MHz, $r_2/\lambda = 0.6$, and $\theta_2 = 45^o$.

z_2/λ	z_2'/λ	Approximate ${}_0\Pi_{h1z} \times 10^3$
.42	.50	1.82-j.953
.42	.75	1.76-j1.39
.42	1.00	1.57-j1.31
.42	1.25	1.64-j1.22
.42	1.50	1.68-j1.29
.42	1.75	1.63-j1.30
.42	2.00	1.62-j1.25

At $z_2/\lambda = .42$ RCM ${}_0\Pi_{h1z} \times 10^3 = 1.64-j.773$

At $z_2/\lambda = .42$ Exact ${}_0\Pi_{h1z} \times 10^3$ 1.58-j1.29

wider range of parameters making it suitable for most practical antenna problems.

Another advantage of this technique is that the horizontal vector potential component ${}_0\bar{\Pi}_{h1x}$ is expressed in a simple closed form (Equation 4.11), while Kuo and Mei [12] have obtained yet another infinite integral form by applying virtually the same approximation as the one in Equation (4.8b) to the Sommerfeld integrals. Also the finite integrations needed for the vertical vector potential approximations, viz., Equations (4.19) and (4.21), will never have a singularity in their integration interval thus making the integrands well-behaved. In addition, these integrands are independent of z_2', thereby making it possible to compute the vertical vector potential values along the vertical interval $z_2'z_2$ by a single integration, i.e., by using the newly computed value of the vector potential as an initial value for computing the next point on the interval. This procedure, when needed, can appreciably improve the overall efficiency of the technique.

Finally, since the evaluation of the E- and the H-fields is of major importance, the approximate technique presented in this chapter also provides a computationally efficient formulation for computing the various field components. This can be simply demonstrated by observing the matrix Equations (2.9) and (2.10). The various mixed partial derivatives of Π_x and Π_z, needed for the field computations, can be easily expressed in terms of the various mixed partial derivatives of $g(\rho, z_2)$, which in turn are expressed in a computationally efficient closed form in Appendix III.

The following chapter demonstrates the ability of these approximate expressions to efficiently analyze several antenna structures radiating over a lossy half-space.

5. WIRE ANTENNAS RADIATING OVER A LOSSY HALF-SPACE

The approximate field solution to the current element problem radiating over a lossy half-space, developed in the previous chapter, in conjunction with the method of moments [17] can be employed to analyze a wide variety of thin-wire antenna problems radiating over a lossy half-space. Initially, in this chapter, a general integral equation is derived containing the unknown antenna current. The method of moments is then used to reduce the integral equation into a numerically manageable matrix form, and finally, a digital computer program is developed for computing the antenna currents, impedance, and far-field patterns, given a specified antenna geometry. A number of simple antenna structures are considered and their behaviours are numerically predicted and presented in the final sections.

5.1 Antenna Integral Equation

Figure 18 depicts the geometry of an arbitrary wire antenna over a lossy half-space, with (r_a, θ_a, ϕ_a) defining a point on the antenna-axis. For simplicity, it is assumed that the antenna is entirely in the xz-plane ($\phi_a = 0$), since the field computation due to currents in the y-direction can easily be handled by a digital computer program by simply rotating the xy-plane by 90° about the z-axis. Assuming that the antenna is excited by the field $\vec{E}^{exc}(\vec{r}_a)$, and having a loading function $\Lambda(\vec{r}_a)$ ohms/meter, one can write a general integral equation enforcing the total E-field along the antenna equal to that induced by the possible loading function, that is,

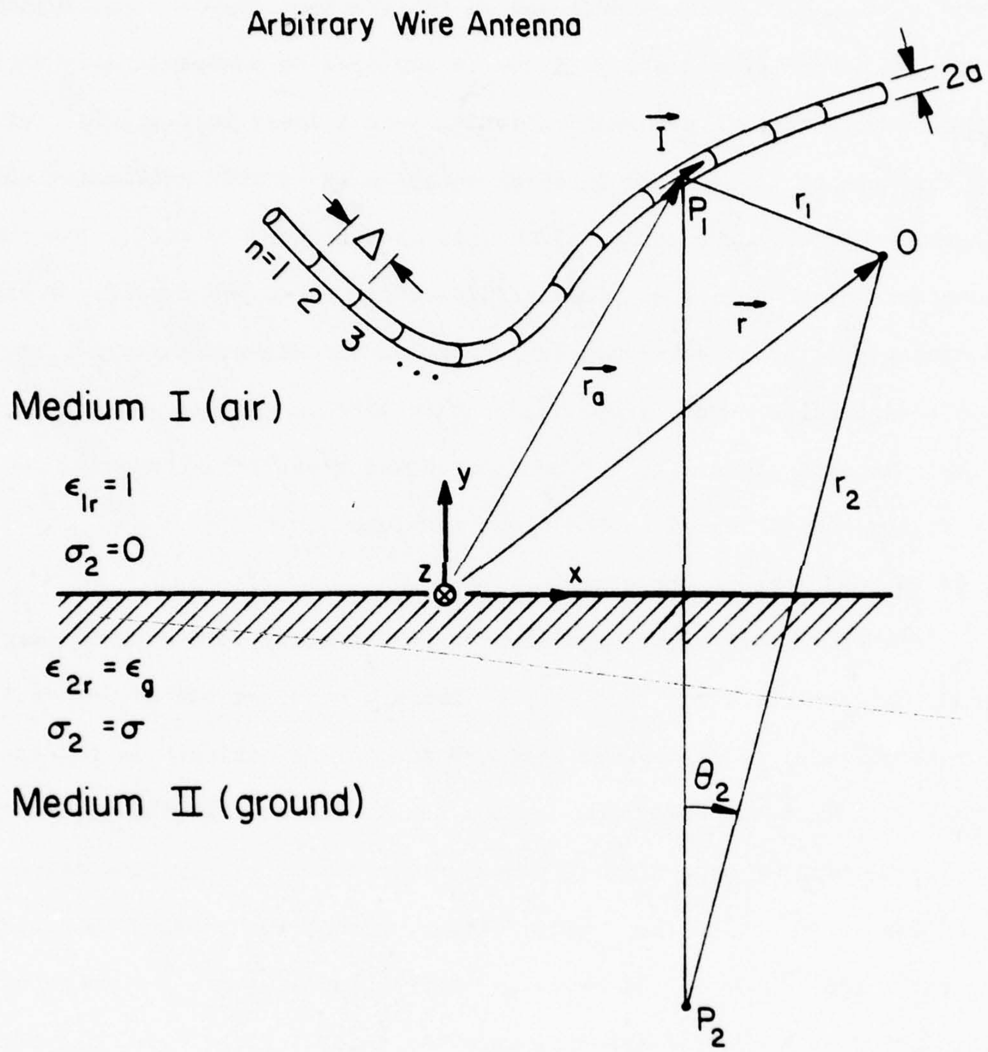

Figure 18. The geometry of an arbitrarily shaped wire antenna located over a lossy half-space.

$$\hat{I}(\vec{r}_a) \cdot \vec{E}^{exc}(\vec{r}_a) + \hat{I}(\vec{r}_a) \cdot \int_{antenna} \left[\vec{G}_v(\vec{r}_a,\vec{r}\,'_a)\hat{z} \cdot \vec{I}(\vec{r}\,'_a) + \vec{G}_h(\vec{r}_a,\vec{r}\,'_a)\hat{x} \cdot \vec{I}(\vec{r}\,'_a)\right] dr'_a$$

$$= \Lambda(\vec{r}_a)\vec{I}(\vec{r}_a) \quad , \tag{5.1}$$

where $\hat{I}(\vec{r}_a)$ is a unit vector along the antenna direction and the kernels $\vec{G}_v(\vec{r}_a,\vec{r}\,'_a)$ and $\vec{G}_h(\vec{r}_a,\vec{r}\,'_a)$ are the E-fields induced at point $\vec{r}_a$ due to a one-ampere electric current element located at $\vec{r}\,'_a$ and oriented in the z- and the x-directions, respectively. The matrix Equation (2.9), which formulates the electric-field components in terms of the vector potentials, is used to write:

$$\vec{E} = \vec{D}_x \Pi_x + \vec{D}_z \Pi_z \quad , \tag{5.2}$$

where the vector operators $\vec{D}_x$ and $\vec{D}_z$ are defined as:

$$\vec{D}_x = \hat{x}\left(k_1^2 + \frac{\partial^2}{\partial x^2}\right) + \hat{y}\left(\frac{\partial^2}{\partial x \partial y}\right) + \hat{z}\left(\frac{\partial^2}{\partial x \partial z}\right) \tag{5.3a}$$

$$\vec{D}_z = \hat{x}\left(\frac{\partial^2}{\partial x \partial z}\right) + \hat{y}\left(\frac{\partial^2}{\partial y \partial z}\right) + \hat{z}\left(k_1^2 + \frac{\partial^2}{\partial z^2}\right) \quad . \tag{5.3b}$$

By using the general formula in (5.2), one can directly write the two kernels, $\vec{G}_v$ and $\vec{G}_h$, in terms of the incident, perfect reflection, and the correction vector potential components (see Equations (2.20), (2.30), and (2.32)), namely,

$$\vec{G}_v(\vec{r}_a,\vec{r}\,'_a) = \vec{G}^i_v(\vec{r}_a,\vec{r}\,'_a) + \vec{G}^r_v(\vec{r}_a,\vec{r}\,'_a) + {}_0\vec{G}_v(\vec{r}_a,\vec{r}\,'_a), \tag{5.4}$$

where

$$\vec{G}^i_v(\vec{r}_a,\vec{r}\,'_a) = (j\omega\varepsilon_0)^{-1}\vec{D}_z g(\vec{r}_a - \vec{r}\,'_a) \tag{5.5a}$$

$$\vec{G}^r_v(\vec{r}_a,\vec{r}\,'_a) = (j\omega\varepsilon_0)^{-1}\vec{D}_z g(\vec{r}_a - \vec{r}\,'_a - 2h\hat{z}) \tag{5.5b}$$

$${}_0\vec{G}_v(\vec{r}_a,\vec{r}\,'_a) = \vec{D}_z \, {}_0\Pi_{v1z}(\vec{r}_a - \vec{r}\,'_a - 2h\hat{z})\Big|_{I_v = 1} \quad , \tag{5.5c}$$

and

$$\vec{G}_h(\vec{r}_a,\vec{r}_a') = \vec{G}_h^i(\vec{r}_a,\vec{r}_a') + \vec{G}_h^r(\vec{r}_a,\vec{r}_a') + {}_0\vec{G}_h(\vec{r}_a,\vec{r}_a') \quad , \tag{5.6}$$

where

$$\vec{G}_h^i(\vec{r}_a,\vec{r}_a') = (j\omega\varepsilon_0)^{-1}\vec{D}_x g(\vec{r}_a - \vec{r}_a') \tag{5.7a}$$

$$\vec{G}_h^r(\vec{r}_a,\vec{r}_a') = (j\omega\varepsilon_0)^{-1}\vec{D}_x g(\vec{r}_a - \vec{r}_a' - 2h\hat{z}) \tag{5.7b}$$

$$_0\vec{G}_h(\vec{r}_a,\vec{r}_a') = \left[\vec{D}_x\ {}_0\Pi_{h1x}(\vec{r}_a - \vec{r}_a' - 2h\hat{z}) + \vec{D}_z\ {}_0\Pi_{h1z}(\vec{r}_a - \vec{r}_a' - 2h\hat{z})\right]_{I_h = 1} \ . \tag{5.7c}$$

Note that in the above equations, $h = r_a' \cos(\theta_a')$ is the height of the current source above the half-plane interface and g is the free-space Green's function defined in (4.5b).

The correction vector potential formulation of Chapter 4, namely, Equations (4.11), (4.15), and (4.16), along with the expansions presented in Appendix III, enable one to compute the scattered components of the two kernels, viz., $\vec{G}_v^r, {}_0\vec{G}_v, \vec{G}_h^r$, and ${}_0\vec{G}_h$, without difficulty. However, because of the singular nature of g, the free-space solution of the kernels, $\vec{G}_v^i$ and $\vec{G}_h^i$, should not be computed directly. Instead, as has been successfully reported [11], [14], [18], and [19], the thin-wire approximation is used to shift the observation point r_a to the antenna surface, and in order to further smooth out the singularities, the finite difference scheme is employed to perform the D_x and D_z operations defined in (5.3).

5.2 Method of Moments

As developed by Harrington [17], the method of moments is a convenient approximation for transforming the antenna integral equation into a numerically manageable matrix form. In this work, pulse-basis and delta-matching functions

are chosen since they eliminate the need for integrating the kernels $\vec{G}_v$ and $\vec{G}_h$. The number of unknown patches on the antenna N should be large enough so that the patch length Δ is at most 1/6 of the wavelength. The approximated current along the antenna is therefore represented as:

$$\vec{I} = \sum_{n=1}^{N} I_n \hat{I}_n \quad , \tag{5.8}$$

for which I_n is an unknown constant value over the n^{th} patch and zero outside of it, also $\hat{I}_n$ is a known unit vector tangent to the antenna at the center of the n^{th} patch (see Figure 18). Substituting (5.8) into (5.1) and letting subscripts $n = 1,2,3,\cdots$ denote "evaluation at the center of the n^{th} patch," and letting $[\vec{I}]$ and $[\bar{E}^{exc}]$ be column vectors containing the current and the tangential excitation field values at successive patches, one finally arrives at

$$[\bar{E}^{exc}] = -[Z^{imp}][\bar{I}] + [\Lambda][\bar{I}] \quad , \tag{5.9}$$

where $[\Lambda]$ is a diagonal matrix with elements $\Lambda_1, \Lambda_2, \cdots, \Lambda_n$; and $[Z^{imp}]$ is an $n \times n$ square matrix with its i^{th} row and j^{th} column element defined as:

$$Z_{ij}^{imp} = \Delta \hat{I}(\vec{r}_{ai}) \cdot [\hat{z} \cdot \hat{I}(\vec{r}_{aj})\vec{G}_v(\vec{r}_{ai},\vec{r}_{aj}) + \hat{x} \cdot \hat{I}(\vec{r}_{aj})\vec{G}_h(\vec{r}_{ai},\vec{r}_{aj})] \quad . \tag{5.10}$$

Note that i and j also refer to patch numbers, and Δ is the patch length. The matrix Equation (5.9) can be solved for the unknown currents $[\bar{I}]$, and by replacing the excitation E-field in terms of the excitation voltage $[\bar{V}]$, one arrives at

$$[\bar{I}] = [Y^{ant}][\bar{V}] \tag{5.11a}$$

$$[Y^{ant}] = \Delta^{-1}\{-[Z^{imp}] + [\Lambda]\}^{-1} \quad . \tag{5.11b}$$

Once $[Y^{ant}]$ is constructed for a given structure, the antenna currents can

be directly computed for a given voltage source excitation. As was discussed in the previous section, the thin-wire approximation and the finite-difference scheme are employed for evaluating the free-space solution components of the kernels, viz., $\vec{G}_v^i$ and $\vec{G}_h^i$. A power series, derived by Harrington [20], is used for the thin-wire approximation computations, and based on the conclusions made in [11], [14], [18], and [19], the finite difference parameter δ is chosen to be equal to $\Delta/2$, e.g.,

$$\left.\frac{\partial^2}{\partial x^2} f\right|_{x_0} \simeq \frac{f(x_0 + \delta) + f(x_0 - \delta) - 2f(x_0)}{\delta^2} \quad ; \quad \delta = \Delta/2 \quad . \tag{5.12}$$

The free-space solution obtained by using the above approach has been thoroughly tested and, as an example, the generated impedance curves shown in Figures 19 and 20 agree well with the ones reported by Jordan et al. [21].

5.3 Far-Field Radiation Pattern

The RCM expressions, shown in Equations (3.27) - (3.29), are the logical choices for representing the correction vector potential components in the far-field region ($k_1 r >> 10$). Working in the spherical coordinate system (r,θ,ϕ), and neglecting all terms containing r^{-2}, r^{-3}, ..., one can easily show

$$\nabla\nabla.\vec{\Pi} \cong -k^2 \Pi_r \hat{r} \quad , \tag{5.13}$$

where $\vec{\Pi}$ is the total vector potential. The total electric field $\vec{E}$, from Equation (2.8), can therefore be shown to have no $\hat{r}$-component, namely,

$$\vec{E}(r,\theta,\phi) = (k^2 + \nabla\nabla.)\vec{\Pi} = k^2[(\cos\theta\cos\phi\,\Pi_x - \sin\theta\,\Pi_z)\hat{\theta} - \sin\phi\,\Pi_x\hat{\phi}] \quad . \tag{5.14}$$

As expected, the above far-field expression represents two plane waves

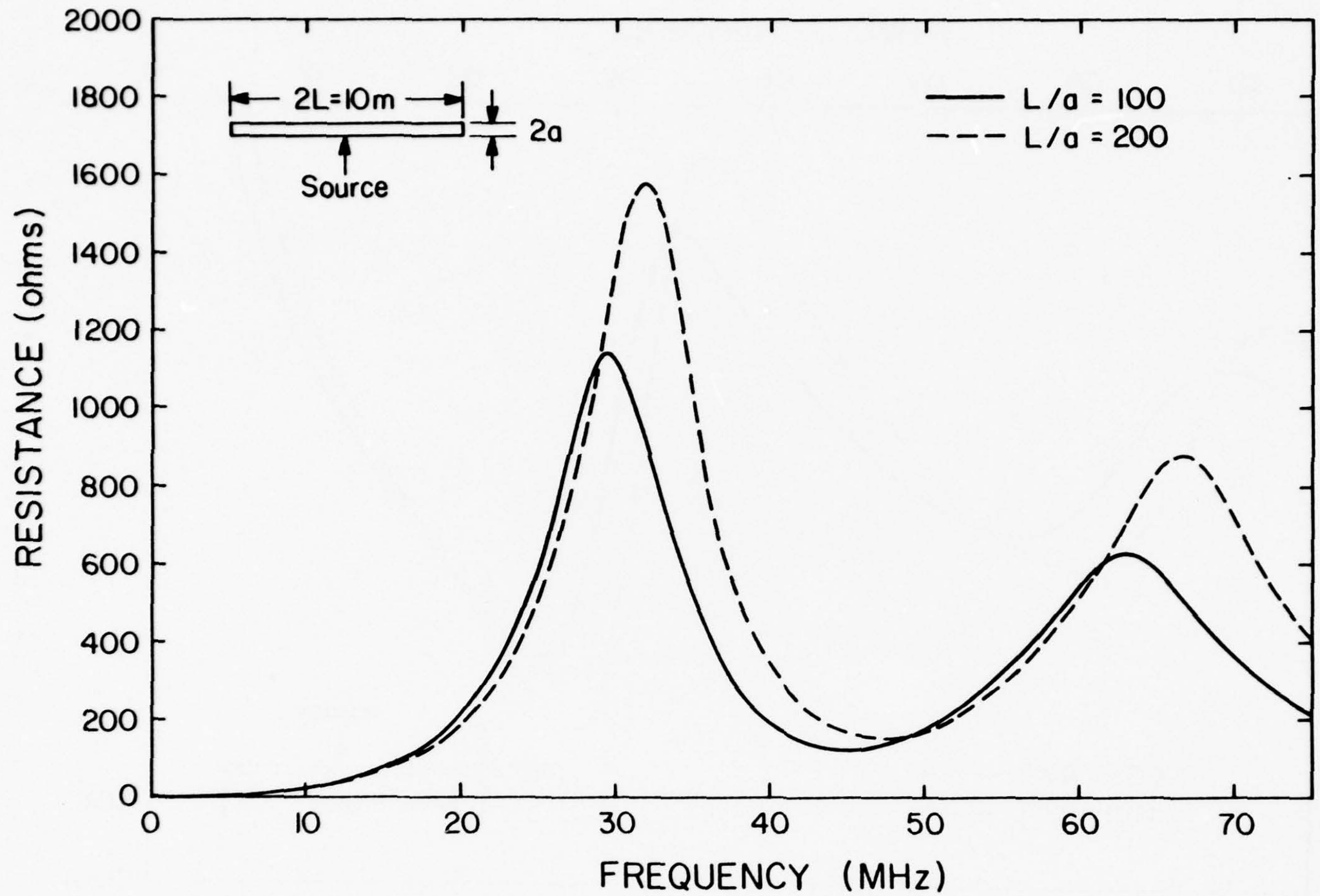

Figure 19. Input resistance of an unloaded dipole antenna (2L = 10m) radiating in free space.

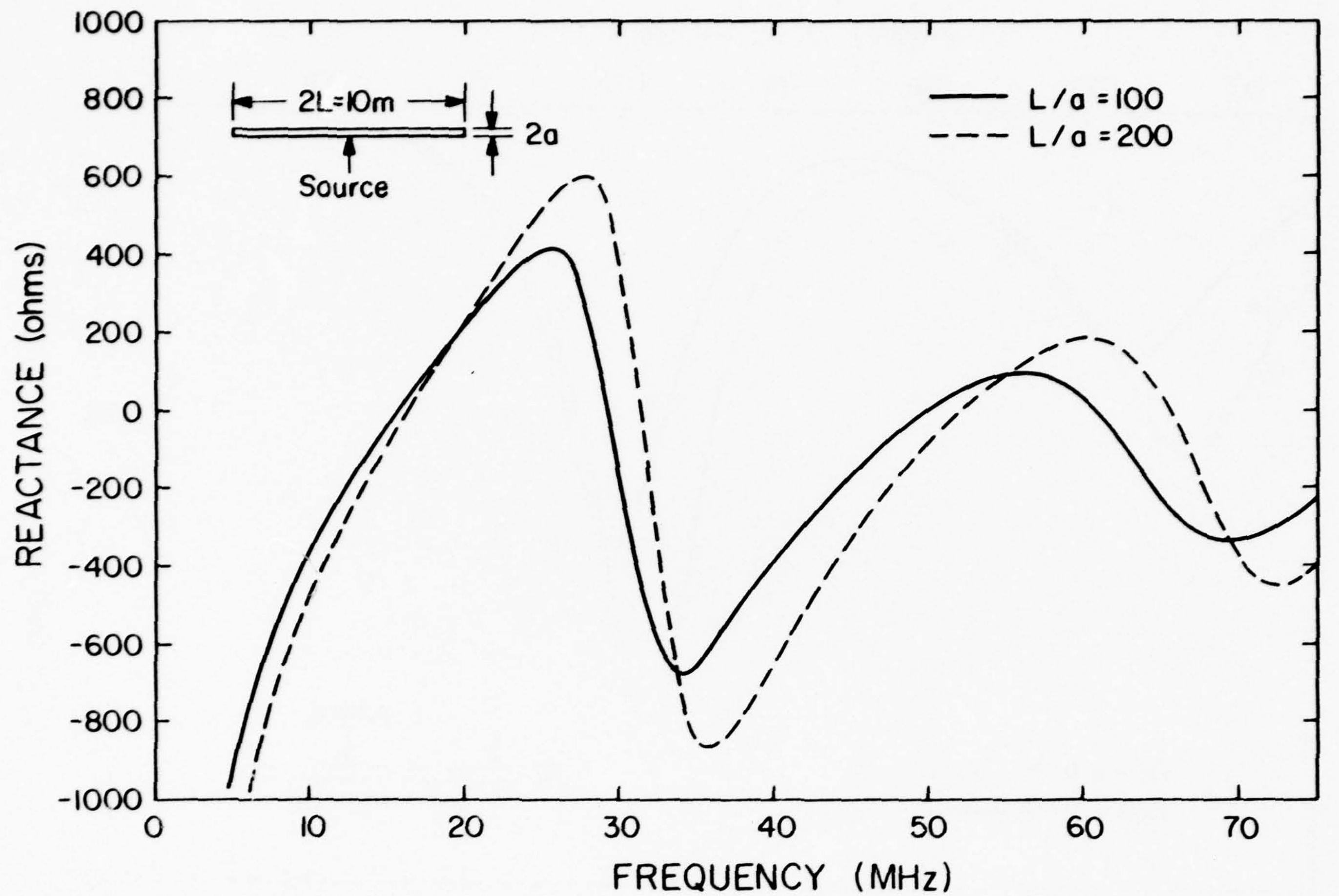

Figure 20. Input reactance of an unloaded dipole antenna (2L = 10m) radiating in free space.

(polarized in the $\hat{\theta}$- and the $\hat{\phi}$- directions) propagating away from the (x,y,z) origin defined in Figure 18. In summary, the far-electric-field radiation pattern due to a current element with no $\hat{y}$-component can be readily computed by initially evaluating the total vector potential components via the RCM approximation and then using Equation (5.14) to obtain the E-field values at the desired observation points.

The far-field pattern for a given antenna structure is simply obtained by applying the superposition theorem to the individual radiation patterns of the antenna current segments defined in the method of moments approximation. Radiation pattern examples are included for the various antenna structures analyzed in the following sections.

5.4 Horizontal Antenna over Lossy Half-Space

The general developments of Sections 5.1 - 5.3 are applied to the horizontal antenna shown in Figure 21. Fortunately, because of the symmetries present in this geometry, the $[Z^{imp}]$ matrix in Equation (5.9) takes the following form (Toeplitz matrix):

$$[Z^{imp}] = \begin{bmatrix} a_1 & a_2 & a_3 & \cdot & \cdot & \cdot & a_n \\ a_2 & a_1 & a_2 & \cdot & \cdot & \cdot & a_{n-1} \\ a_3 & a_2 & a_1 & \cdot & \cdot & \cdot & a_{n-2} \\ \cdot & \cdot & \cdot & \cdot & \cdot & \cdot & \cdot \\ \cdot & \cdot & \cdot & \cdot & \cdot & \cdot & \cdot \\ \cdot & \cdot & \cdot & \cdot & \cdot & \cdot & \cdot \\ a_n & a_{n-1} & a_{n-2} & \cdot & \cdot & \cdot & a_1 \end{bmatrix} . \tag{5.15}$$

Therefore, one needs to compute only one row of this matrix and use the aforementioned symmetry to complete it. The main program, HORIZ (see Appendix IV),

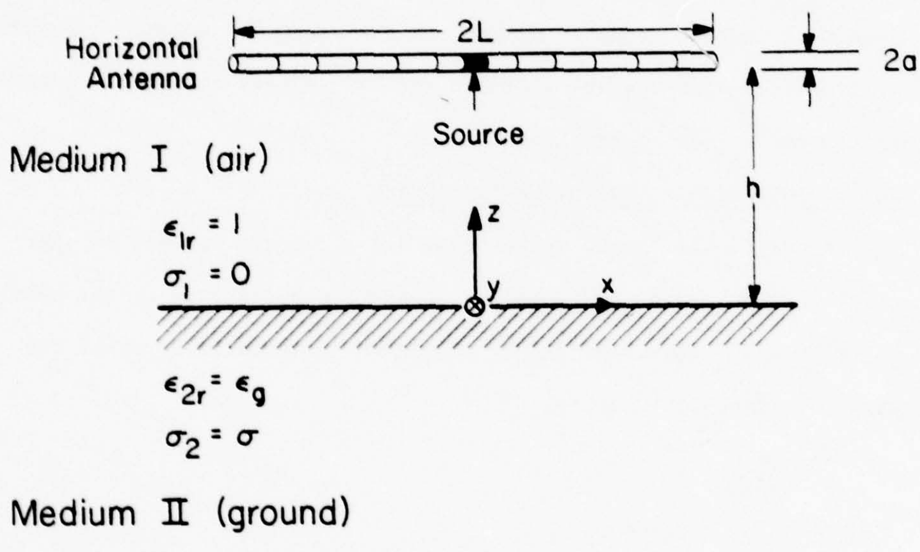

Figure 21. Center-fed horizontal dipole over a lossy half-space.

is developed to analyze the horizontal antenna of Figure 21. Using this program, Figures 22 and 23 are generated to show the impedance variations of a $2L = 10$ meters center-fed horizontal antenna located $h = 3$ meters above various lossy grounds. Radiation pattern of this antenna at 15 MHz is also shown in Figures 24 and 25.

5.5 Vertical Antenna over Lossy Half-Space

The vertical dipole shown in Figure 26 is the next geometry considered. Unfortunately, as was the case for the horizontal antenna, the total $[Z^{imp}]$ matrix is not in a Toeplitz form. However, main program VERT (in Appendix IV) is designed to take maximum advantage of the available symmetry. As an example, Figure 27 is included to show the radiation pattern of a $2L = 10$ meters, $h = 8$ meters, center-fed vertical dipole at resonance ($f = 15$ MHz) located over various lossy grounds.

5.6 Inverted Vee-Dipole

As a complicated example, the inverted Vee-dipole of Figure 28 is considered. Again, as in the two previous sections, symmetry is used in the main program VEEDIP (Appendix IV) in constructing the $[Z^{imp}]$ matrix. The program is tested for an inverted Vee-dipole structure having $L = 7.5$ meters, $h = 10$ meters, and $\Psi = 90^{o}$; Figures 29 and 30 demonstrate the radiation pattern of this structure at 10 MHz and for various lossy grounds.

In all three of these examples, care has been taken not to violate the conditions $|\kappa| > 10$ and Equation (4.26) to ensure the accuracy of the results. Also, since the $[Z^{imp}]$ matrix for these examples turns out to be symmetric, a special inversion routine (XINVZ in Appendix IV) is employed to save an appreciable amount of computer time.

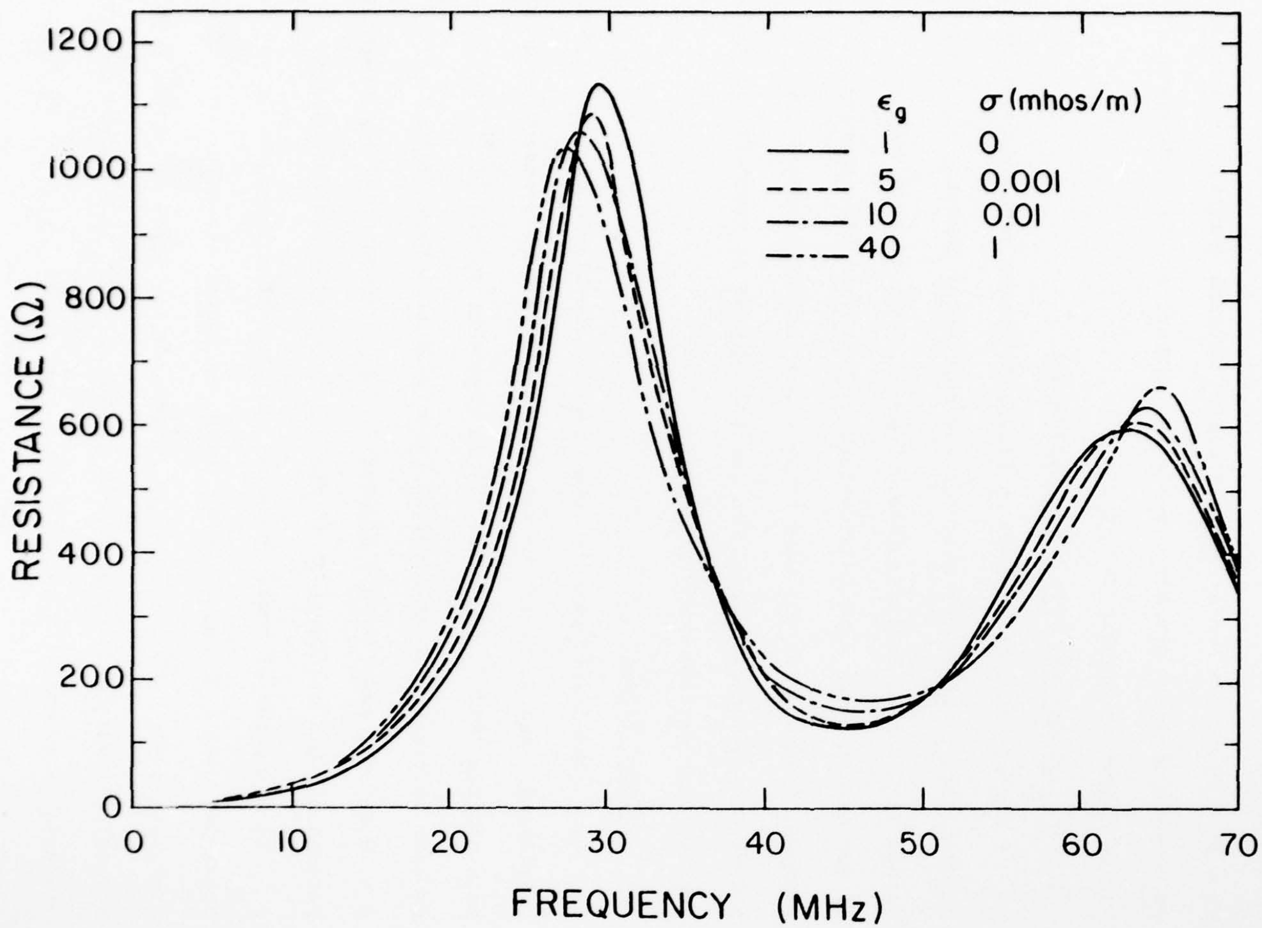

Figure 22. Input resistance of a center-fed horizontal dipole antenna as a function of frequency and the ground parameters. Note that $2L = 10m$, $2a = 0.1m$, and $h = 3m$.

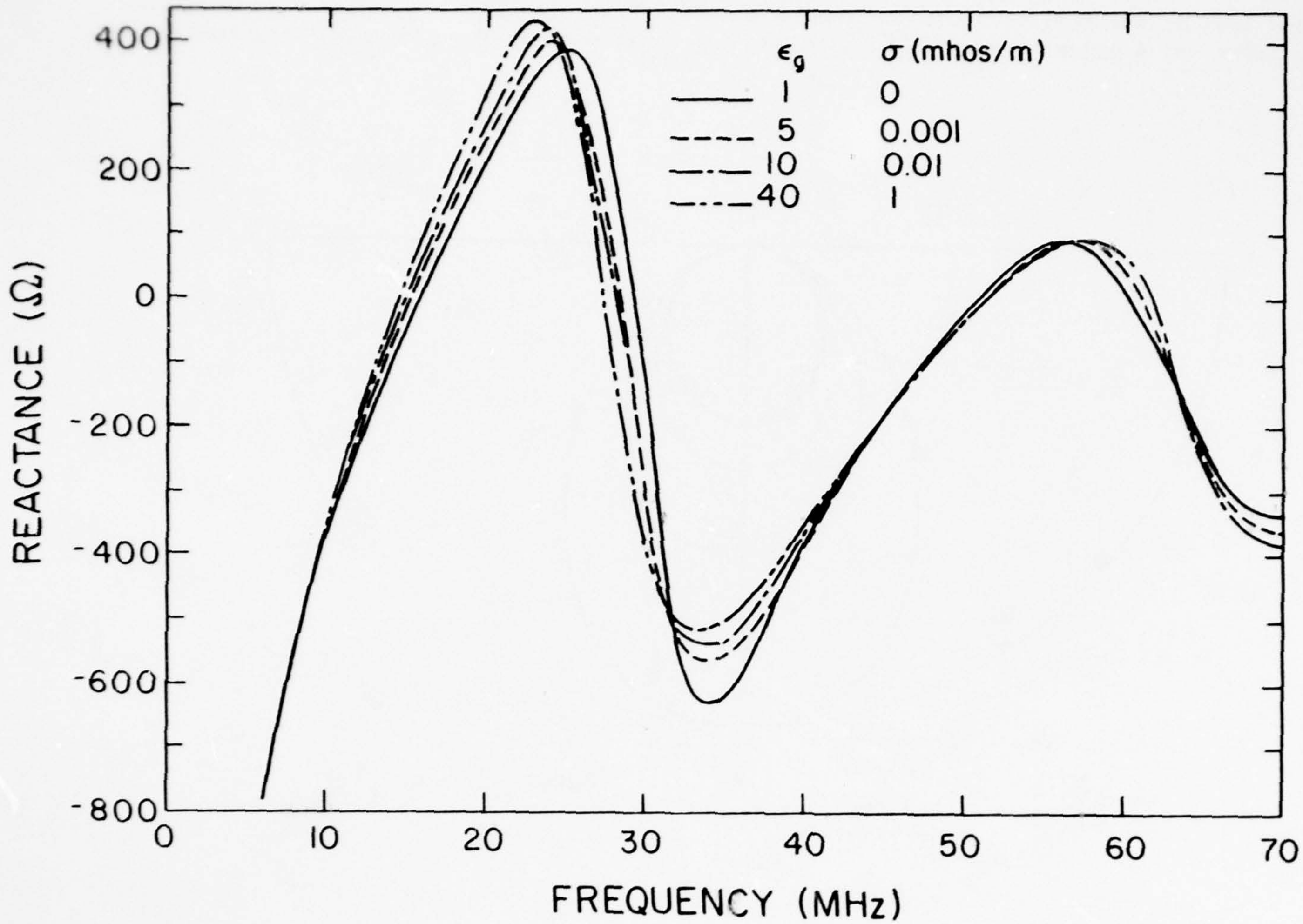

Figure 23. Input reactance of the antenna defined in Figure 22.

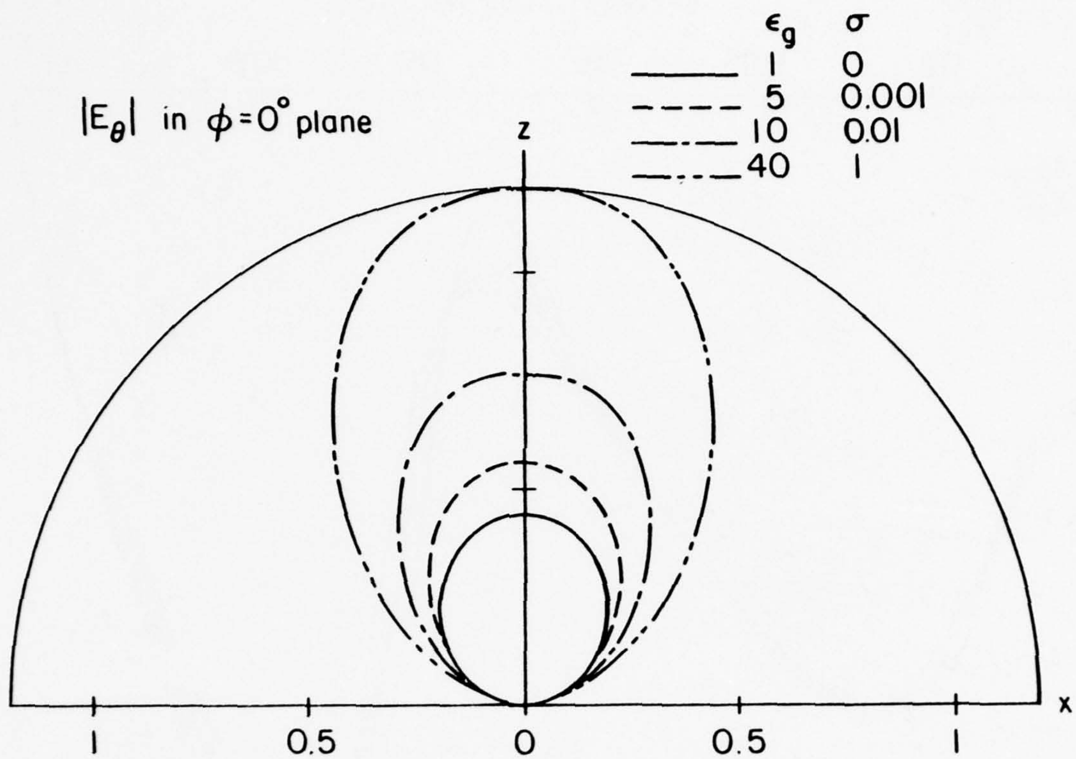

Figure 24. Far-field radiation pattern for the horizontal antenna defined in Figure 22 at 15 MHz. Note that the patterns are computed at $k_1 r = 500$, and in this plane, $|E_\phi|$ is negligible.

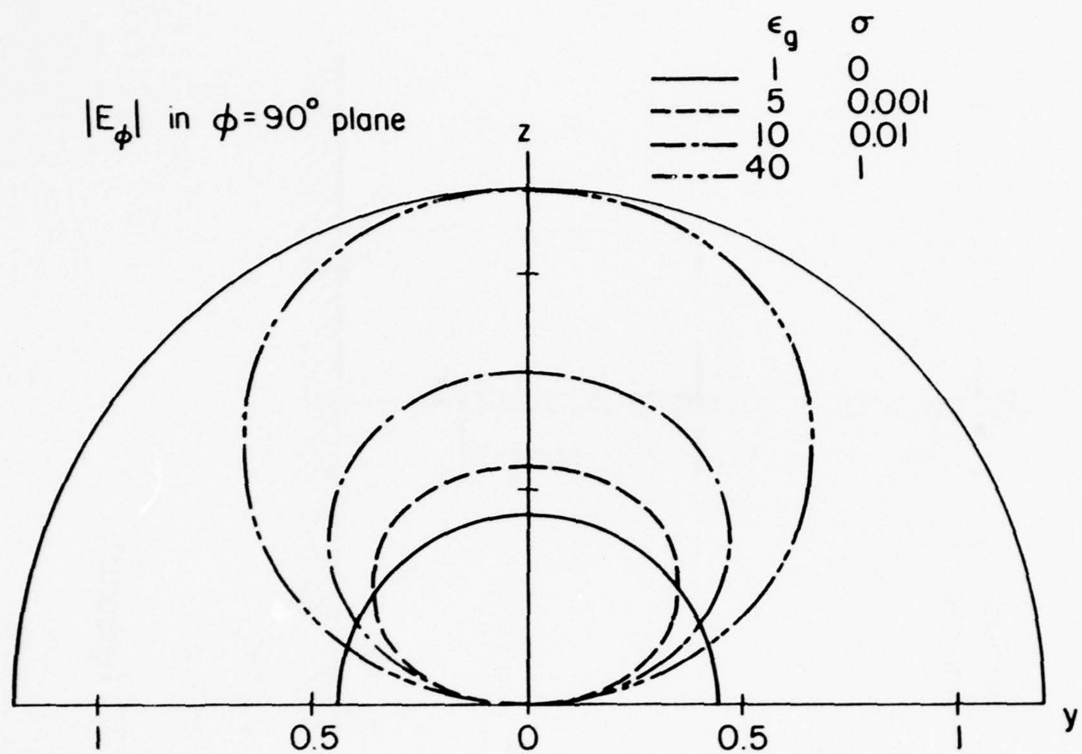

Figure 25. Far-field radiation pattern for the horizontal antenna defined in Figure 22 at 15 MHz. Note that the patterns are computed at $k_1 r = 500$, and in this plane, $|E_\theta|$ is negligible.

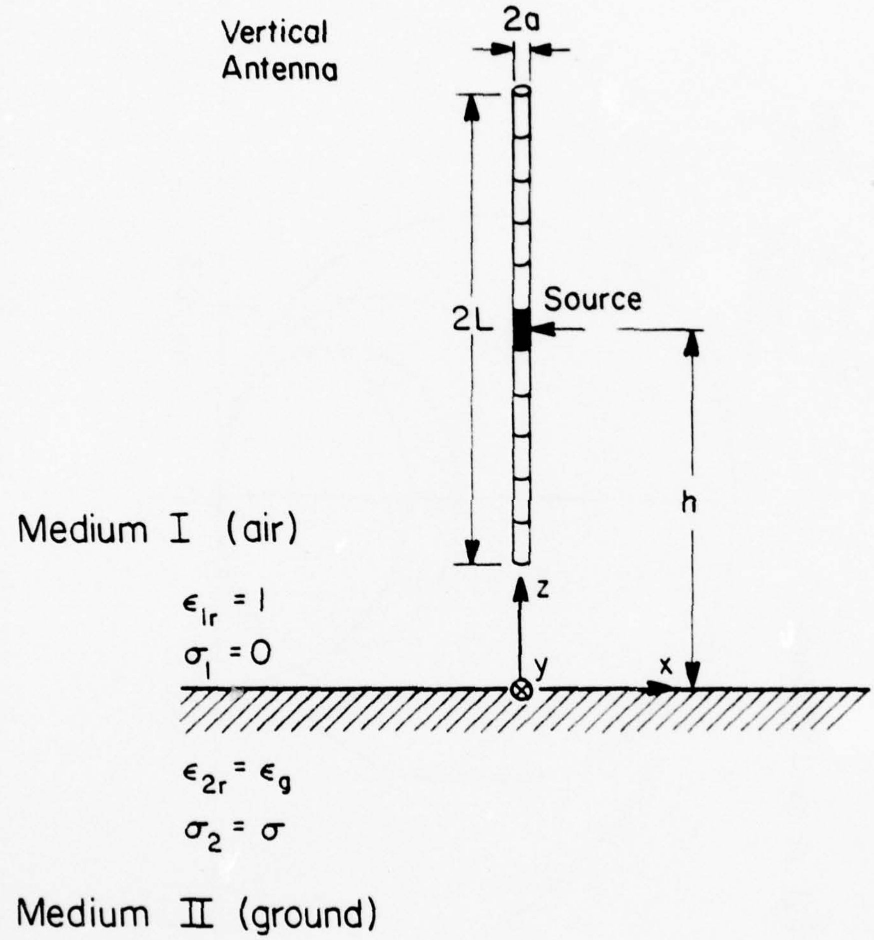

Figure 26. Center-fed vertical dipole over a lossy half-space.

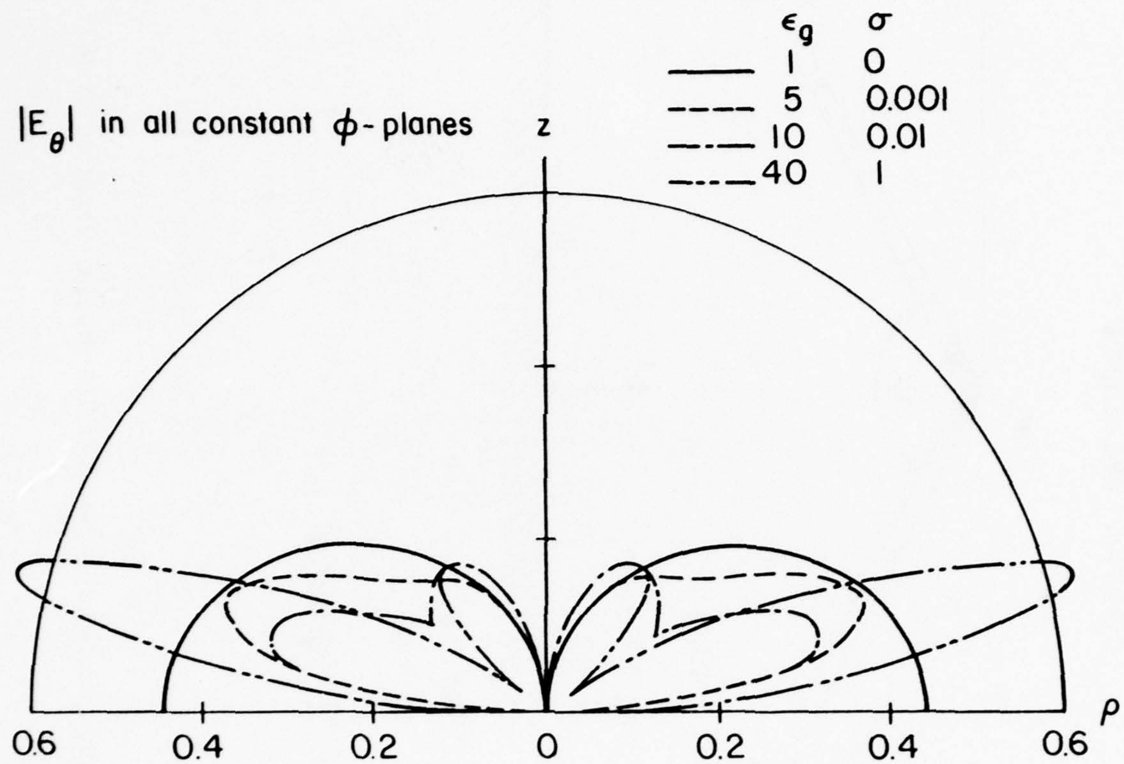

Figure 27. The far-field radiation pattern for a center-fed vertical dipole (2L = 10m, h = 8m, and 2a = 0.1m) at 15 MHz. Note that the patterns are computed at $k_1 r = 500$, and in this example, $|E_\phi|$ is negligible.

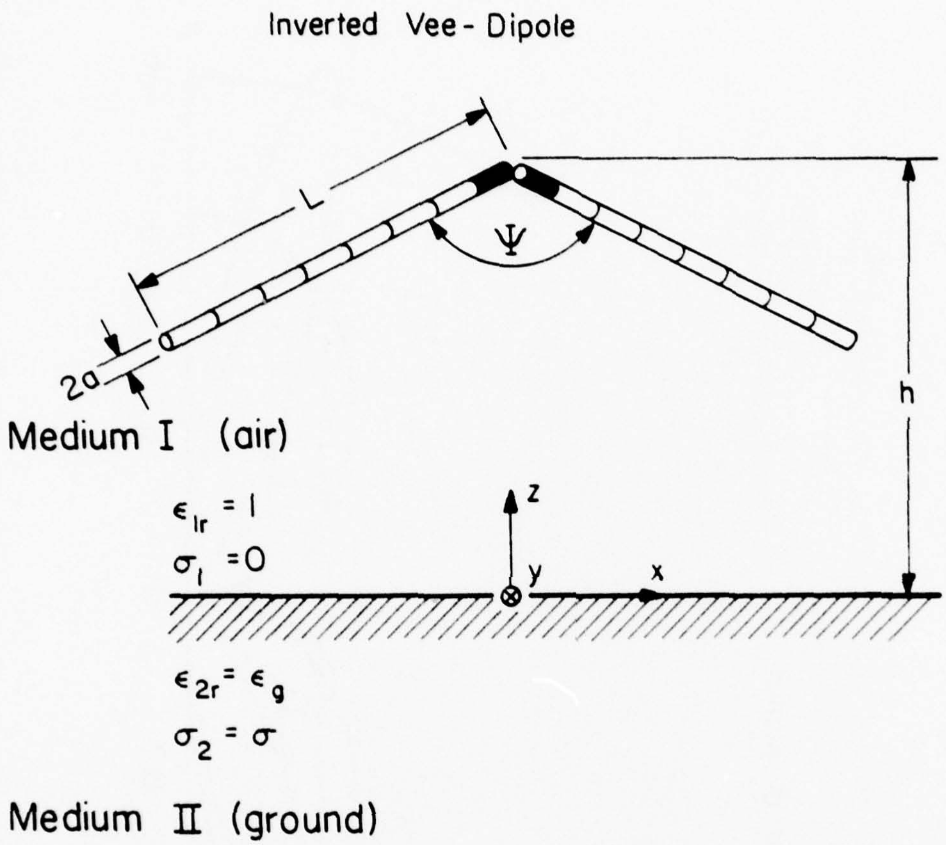

Figure 28. Center-fed inverted Vee-dipole over a lossy half-space.

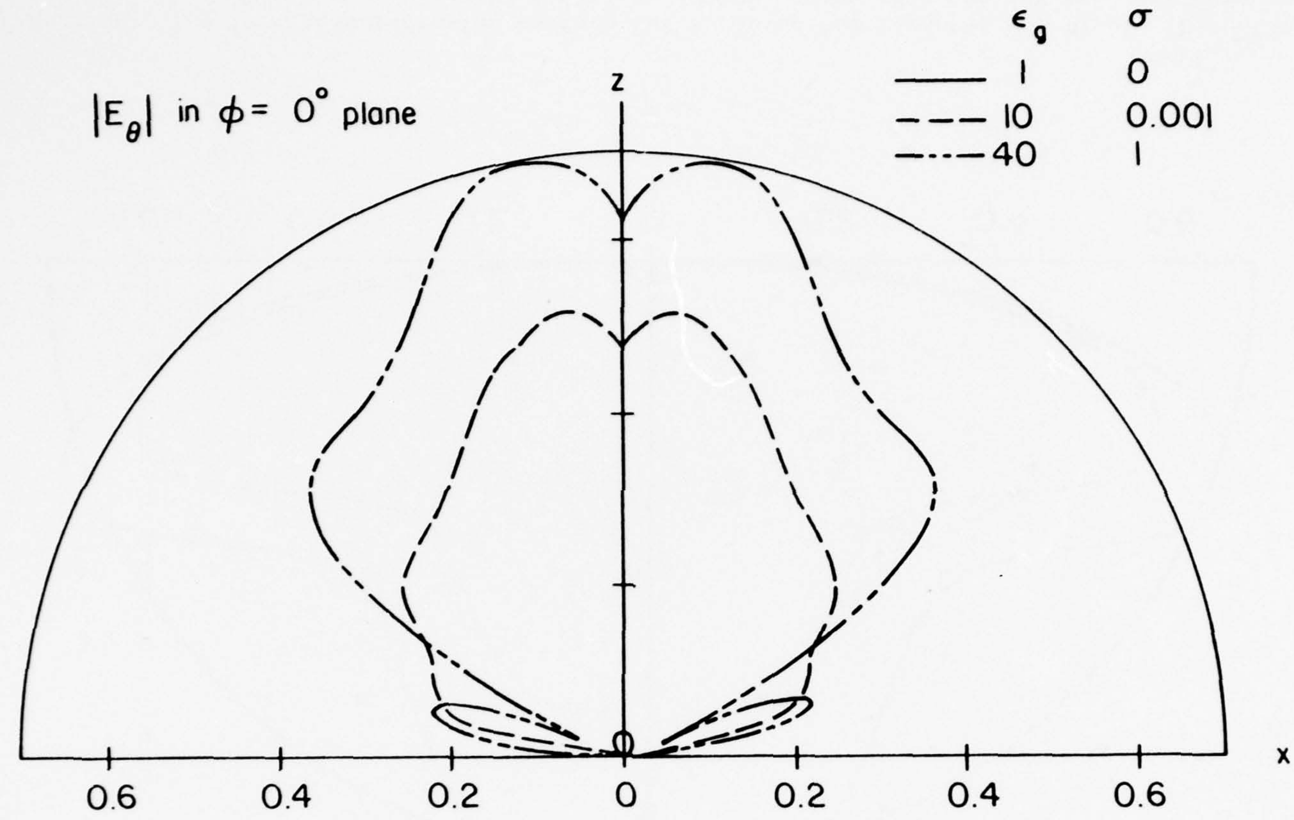

Figure 29. The far-field radiation pattern for a center-fed inverted Vee-dipole ($L = 7.5m$, $h = 10m$, $\Psi = 90^{o}$, and $2a = 0.1m$) at 10 MHz. Note that the patterns are computed at $k_1 r = 500$, and in this plane, $|E_\phi|$ is negligible.

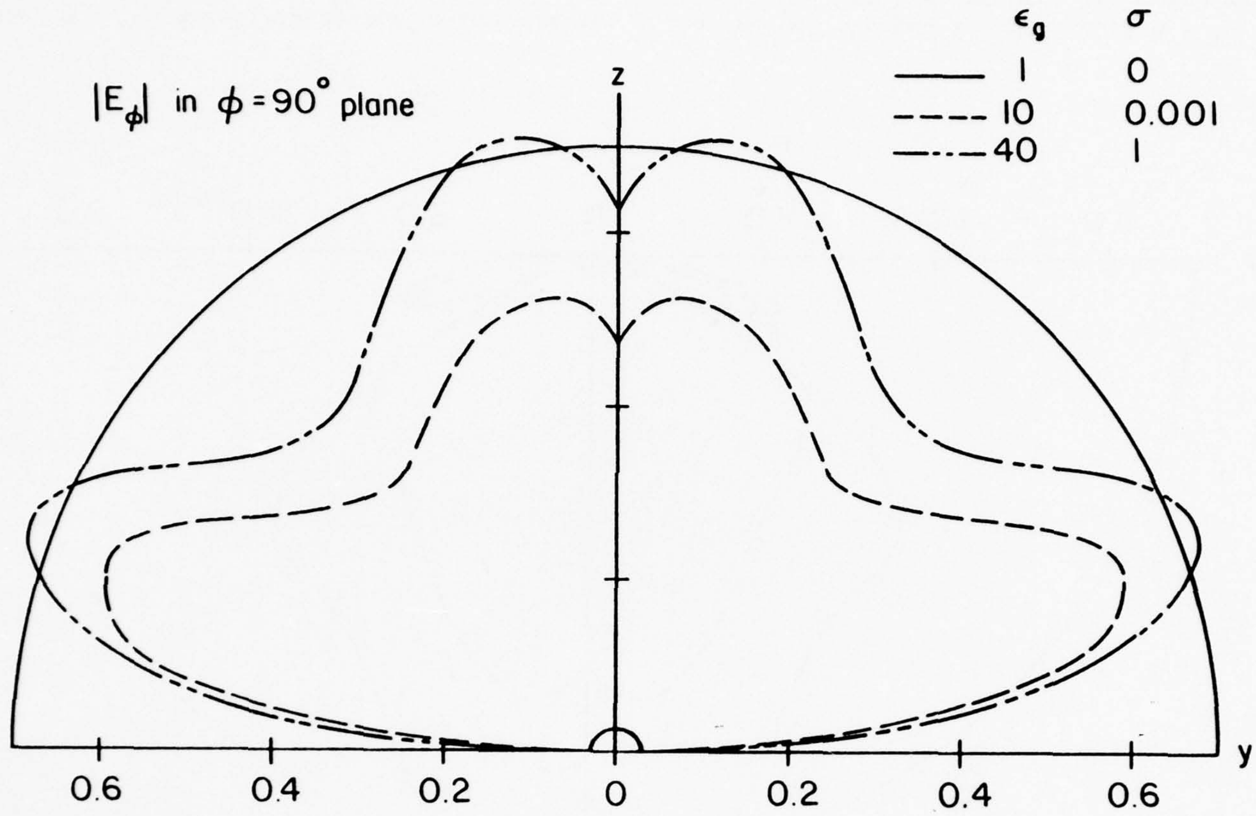

Figure 30. The far-field radiation pattern for a center-fed inverted Vee-dipole ($L = 7.5$m, $h = 10$m, $\psi = 90^o$, and $2a = 0.1$m) at 10 MHz. Note that the patterns are computed at $k_1 r = 500$, and in this plane, $|E_\theta|$ is negligible.

6. CONCLUSIONS

Based on the steepest descent path (SDP) integration technique, an efficient numerical integration procedure is developed in Chapter 3 for computing the Sommerfeld infinite integrals present in the vector potential expressions of a current element radiating over a lossy half-space. Even though this procedure is about an order of magnitude faster than the latest reported Sommerfeld integration techniques, the computation time for a typical antenna problem can still become prohibitive. The reflection coefficient method (RCM) approximations, which are simply the first term in the asymptotic expansion of the Sommerfeld integrals, offer a simple closed-form solution valid only at the high end of the frequency spectrum and which cannot be employed in many practical situations. Also, the addition of the second term in the aforementioned asymptotic expansion to the RCM approximations is ruled out, since the resulting vertical vector potential components diverge from their respective exact integration values.

Chapter 4 presents a novel approach in which the transform domain representation of the vector potentials is approximated such that the resulting space-domain expressions do not require any kind of infinite integration. This approach has the merit of being computationally over an order of magnitude faster than the SDP technique of Chapter 3, while being accurate over a wide range of parameters of practical interest and, in addition, offers a simple and numerically manageable procedure for obtaining the near E- and H-field components.

The general computer program, listed in Appendix IV, is developed by employing the approximate formulas of Chapter 4 and is used to solve several

antenna geometries. With minor modifications, this program can be adapted to analyze most three-dimensional thin-wire antenna structures over a lossy half-space.

APPENDIX I

EVALUATION OF ${}_0\Pi_{h1x}$, ${}_0\Pi_{h1z}$, AND ${}_0\Pi_{v1z}$ AT $\theta_2 = 0$

In this appendix, the behavior of Equations (2.47) - (2.49) is studied at $\theta_2 = 0$. In their present forms, these integrals are not defined at $\rho_2 = 0$, although it is clear that their equivalent forms in (2.42) - (2.44) are bounded. Equation (2.47) can be expressed here for convenience as

$$
{}_0\Pi_{v1z} = \frac{I_{v0}}{4\pi j} \int_{-\infty}^{\infty} \frac{\kappa\lambda}{\kappa\sqrt{k_1^2 - \lambda^2} + \sqrt{\kappa k_1^2 - \lambda^2}} H_0^{(2)}(\rho_2\lambda) e^{-jz_2\sqrt{k_1^2-\lambda^2}} \, d\lambda \tag{I.1}
$$

where $\rho_2 = r_2 \sin\theta_2$. The Hankel function in (I.1) is not bounded at $\theta_2 = 0$. To circumvent this difficulty, one replaces $H_0^{(2)}$ with its expansion from [22]

$$
H_0^{(2)}(\rho_2\lambda) = J_0(\rho_2\lambda) - j\left[\frac{2}{\pi} \operatorname{Ln} \frac{\gamma\rho_2\lambda}{2} J_0(\rho_2\lambda) + \frac{2}{\pi}\sum_{m=1}^{\infty} \frac{(-1)^{m+1}}{(m!)^2} \left(\frac{\rho_2\lambda}{2}\right)^{2m} \phi(m)\right] \tag{I.2}
$$

where γ is Euler's constant and $\phi(m)$ represents the harmonic series, i.e.,

$$
\phi(m) = 1 + 1/2 + 1/3 + \ldots + 1/m \quad . \tag{I.3}
$$

Note that both J_0 and the summation terms in (I.2) are even functions of λ, hence, their contributions to the integral (I.1) are zero. Substituting (I.2) into (I.1), one finally arrives at

$$
{}_0\Pi_{v1z} = \frac{I_{v0}}{4\pi j} \int_{-\infty}^{\infty} \frac{\kappa\lambda}{\kappa\sqrt{k_1^2 - \lambda^2} + \sqrt{\kappa k_1^2 - \lambda^2}} \frac{-2j}{\pi} J_0(r_2 \sin\theta_2\,\lambda) \cdot \operatorname{Ln}(r_2\lambda)\, e^{-jz_2\sqrt{k_1^2-\lambda^2}} \, d\lambda \quad , \tag{I.4}
$$

which is obviously bounded at $\theta_2 = 0$. Introducing the change of variable $\lambda = k_1 \sin \xi$ into (I.4) and setting $\theta_2 = 0$, one finds

$$ {}_0\Pi_{v1z} = \frac{I_{v0}k_1}{4\pi j} \int_\Gamma \frac{\kappa \sin \xi \cos \xi}{\kappa \cos \xi + \sqrt{\kappa - \sin^2 \xi}} \frac{-2j}{\pi} \operatorname{Ln}(k_1 r_2 \sin \xi) \quad e^{-jk_1 r_2 \cos\xi} \, d\xi \; ; $$

$$ \theta_2 = 0 \qquad \text{(I.5)} $$

where path Γ is shown in Figure 2. In a similar fashion, one may obtain equivalent expressions for the remaining vector potential components at $\theta_2 = 0$, namely,

$$ {}_0\Pi_{h1x} = \frac{I_{v0}k_1}{4\pi j} \int_\Gamma \frac{\sin \xi \cos \xi}{\cos \xi + \sqrt{\kappa - \sin^2 \xi}} \frac{-2j}{\pi} \operatorname{Ln}(k_1 r_2 \sin \xi) \quad e^{-jk_1 r_2 \cos\xi} \, d\xi \; ; $$

$$ \theta_2 = 0 \qquad \text{(I.6)} $$

and

$$ {}_0\Pi_{v1z} = 0 \quad ; \quad \theta_2 = 0 \quad . \qquad \text{(I.7)} $$

APPENDIX II

ASYMPTOTIC EVALUATION

In this appendix, a general formulation is developed for a higher-order asymptotic evaluation of an integral with the following format:

$$u = \frac{1}{4\pi j} \int_{\Gamma} P(\xi)\, e^{-jkr\cos(\xi-\theta)}\, d\xi \quad , \tag{II.1}$$

where it is assumed that kr is a large parameter, $-\pi/2 < \theta < \pi/2$, $P(\xi)$ is a slowly varying function and path Γ is shown in Fig. 2. For large values of kr, one is usually interested in determining the asymptotic expression of (II.1); this is done by employing the method of the steepest-descent path integration. At the saddle point $\xi = \theta$, one can deform the integration path Γ to the steepest descent path (SDP) defined by $\mathrm{Re}[\cos(\xi - \theta)] = 1$. Assuming that in this deformation no poles or branch points are encountered, one may express (II.1) as

$$u = \frac{1}{4\pi j} \int_{SDP} P(\xi)\, e^{-jkr\cos(\xi-\theta)}\, d\xi \quad . \tag{II.2}$$

Since on the SDP the relation $\mathrm{Re}[\cos(\xi - \theta)] = 1$ holds, one can introduce the change of variable

$$\cos(\xi - \theta_2) = 1 - jt^2 \quad , \tag{II.3}$$

or equivalently,

$$t = \sqrt{2}\, e^{-j\pi/4} \sin\frac{\xi - \theta}{2} \quad , \tag{II.4}$$

in which t is a real variable taking the domain $[-\infty,\infty]$. Substituting (II.4) into (II.2), one arrives at

$$u = \frac{e^{-jkr-j\pi/4}}{2\sqrt{2}\ \pi} \int_{-\infty}^{\infty} Q(t)\ e^{-krt^2}\ dt \qquad \text{(II.5)}$$

where

$$Q(t) = P(\xi)\ \sec\frac{\xi - \theta}{2} \quad , \qquad \text{(II.6a)}$$

in which ξ is replaced with

$$\xi = \pm\left[\frac{\pi}{2} + j\mathrm{Ln}(t^2 + j + |t|\sqrt{t^2 + 2j})\right] + \theta \quad , \quad t \lessgtr 0 \qquad \text{(II.6b)}$$

and Ln is interpreted as being its principal value. The complete asymptotic expansion procedure [23] is now used for the asymptotic evaluation of (II.5). In this procedure, one first expands Q(t) in a Taylor series

$$Q(t) = \sum_{n=0}^{\infty} \frac{Q^{(n)}(0)}{\Gamma(n + 1)}\ t^n \qquad \text{(II.7)}$$

where $Q^{(n)}(0) = \frac{\partial n}{\partial t^n} Q(t)\Big|_{t=0}$ and Γ is the Gamma function. Then (II.7) is substituted into (II.5) to finally result in

$$u = \frac{e^{-jkr-j\pi/4}}{2\sqrt{2\pi}} \sum_{n=0}^{\infty} \frac{2^{-2n}}{n!}\ (kr)^{-n-1/2}\ Q^{(2n)}(0) \quad . \qquad \text{(II.8)}$$

In constructing the preceding equation, the following identity was used, viz.,

$$\int_{-\infty}^{\infty} t^n e^{-krt^2}\ dt = \begin{cases} (kr)^{-(1+n)/2}\ \Gamma[(1 + n)/2] & \text{for } n \text{ even} \\ 0 & \text{for } n \text{ odd} \end{cases} \quad . \qquad \text{(II.9)}$$

The task is now to determine $Q^{(2n)}$'s in terms of P. This is achieved by differentiating (II.6a) and arriving at

AD-A068 548 ILLINOIS UNIV AT URBANA-CHAMPAIGN ELECTROMAGNETICS LAB F/G 20/14
ANALYSIS OF ARBITRARILY SHAPED WIRE ANTENNAS RADIATING OVER A L--ETC(U)
MAR 79 P PARHAMI, R MITTRA DAAG29-77-G-0111
UNCLASSIFIED UIEM79-6 ARO-14686.4-EL NL

2 OF 2
AD
A068548

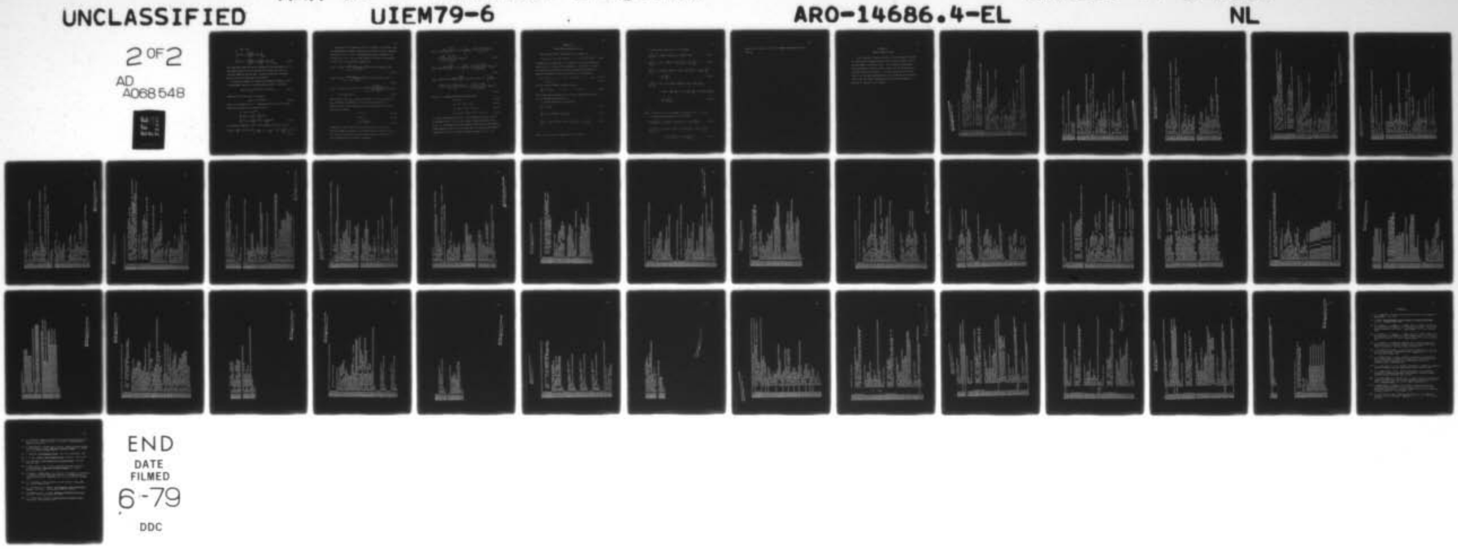

END
DATE
FILMED
6-79
DDC

$$\begin{cases} Q(0) = P(\theta) \\ Q^{(2)}(0) = 2j\left[\dfrac{d^2P(\xi)}{d\xi^2} + \dfrac{1}{4}P(\xi)\right]_{\xi=\theta} \\ Q^{(4)}(0) = -4\left[\dfrac{d^4P(\xi)}{d\xi^4} + \dfrac{5}{2}\dfrac{d^2P(\xi)}{d\xi^2} + \dfrac{9}{16}P(\xi)\right]_{\xi=\theta} \end{cases} \quad . \tag{II.10}$$

The higher-order terms can also be determined in the same fashion. It is worth emphasizing here that in deriving the preceding equations, the following assumption has been made: neither the poles nor the branch points of $P(\xi)$ are intercepted by the path SDP.

To present an example, the higher-order asymptotic expansion of the following Hankel function of the second kind and order ν is derived:

$$H_\nu^{(2)}(\Omega) = \frac{1}{\pi}\int_\Gamma e^{-j\nu\xi+j\nu\pi/2}\, e^{-j\Omega\cos\xi}\, d\xi \quad . \tag{II.11}$$

Comparing (II.11) with (II.1), one obtains

$$P(\xi) = 4j\, e^{-j\nu\xi+j\nu\pi/2} \quad , \tag{II.12}$$

where it is assumed that $\Omega >> \nu$. Substituting (II.12) into (II.10) and simplifying the result, one finally arrives at

$$\begin{cases} Q(0) = 4j\, e^{j\nu\pi/2} \\ Q^{(2)}(0) = -8\left[-\nu^2 + \dfrac{1}{4}\right] e^{j\nu\pi/2} \\ Q^{(4)}(0) = -16j\left[\nu^4 - \dfrac{5}{2}\nu^2 + \dfrac{9}{16}\right] e^{j\nu\pi/2} \end{cases} \quad . \tag{II.13}$$

The asymptotic expansion of $H_\nu^{(2)}$ is then determined using (II.8) to be

$$H_\nu^{(2)}(\Omega) = \sqrt{\frac{2}{\pi\Omega}}\, e^{-j(\Omega-\nu\pi/2-\pi/4)}\left[1 + \frac{j}{2\Omega}\left(\frac{1}{4} - \nu^2\right) - \frac{1}{8\Omega^2}\left(\nu^4 - \frac{5}{2}\nu^2 + \frac{9}{16}\right)\right] + O(\Omega^{-7/2}). \tag{II.14}$$

The purpose of this appendix has been to formulate the necessary steps for determining the asymptotic expansion of the vector potential components expressed in (2.47) - (2.49). Rearranging these three expressions into the form of Eq. (II.1), one can easily define a P function corresponding to each of the vector potential components as

$$P_{v1z}(\xi) = I_{v0}k_1\kappa \frac{\sin\xi\cos\xi}{\kappa\cos\xi + \sqrt{\kappa - \sin^2\xi}} H_0^{(2)}(k_1\rho_2 \sin\xi) \exp(jk_1\rho_2 \sin\xi) \tag{II.15}$$

$$P_{h1x}(\xi) = I_{h0}k_1 \frac{\sin\xi\cos\xi}{\cos\xi + \sqrt{\kappa - \sin^2\xi}} H_0^{(2)}(k_1\rho_2 \sin\xi) \exp(jk_1\rho_2 \sin\xi) \tag{II.16}$$

$$P_{h1z}(\xi) = -jI_{h0}k_1 \cos\phi_2 \sin^2\xi \cos\xi \frac{\cos\xi - \sqrt{\kappa - \sin^2\xi}}{\kappa\cos\xi + \sqrt{\kappa - \sin^2\xi}} H_1^{(2)}(k_1\rho_2 \sin\xi) \cdot \exp(jk_1\rho_2 \sin\xi) \tag{II.17}$$

where functions P_{v1z}, P_{h1x}, and P_{h1z} correspond to the ${}_0\Pi_{v1z}$, ${}_0\Pi_{h1x}$, and ${}_0\Pi_{h1z}$ expressions, respectively. Since the final results take a complicated form, the following notations are introduced for the ease of representation, namely,

$$c = \cos\theta_2 \tag{II.18a}$$

$$s = \sin\theta_2 \tag{II.18b}$$

$$q = \sqrt{\kappa - \sin^2\theta_2} \quad . \tag{II.18c}$$

Performing the rather tedious differentiation needed in (II.10) and using the asymptotic expansion for the Hankel functions derived in (II.14), one finally arrives at the following two-term asymptotic expression for the aforementioned vector potential components:

$$
{}_0\Pi_{v1z} = I_{v0}\,\frac{2\kappa c}{\kappa c + q}\,\frac{e^{-jk_1 r_2}}{4\pi r_2} + I_{v0}\,j\kappa c\left[\frac{-2}{\kappa c + q} + \frac{A_1(3c - 2/c) + A_2 + \kappa c}{(\kappa c + q)^2} + \frac{2s^2 A_1^2}{(\kappa c + q)^3}\right]\frac{e^{-jk_1 r_2}}{4\pi k_1 r_2^2} + O(k_1 r_2)^{-3} \qquad \text{(II.19)}
$$

$$
{}_0\Pi_{h1x} = I_{h0}\,\frac{2c}{c + q}\,\frac{e^{-jk_1 r_2}}{4\pi r_2} + I_{h0}\,jc\left[\frac{A_3}{c + q} + \frac{A_2 + c}{(c + q)^2}\right]\frac{e^{-jk_1 r_2}}{4\pi k_1 r_2^2} + O(k_1 r_2)^{-3} \qquad \text{(II.20)}
$$

$$
{}_0\Pi_{h1z} = I_{h0}\,2\cos\phi_2\,sc\,\frac{c - q}{\kappa c + q}\,\frac{e^{-jk_1 r_2}}{4\pi r_2} + I_{h0}\cos\phi_2\,jsc(c - q)\left[\frac{A_4}{\kappa c + q} + \frac{A_1(5c - 2/c + 2s^2/q) + A_2 + \kappa c}{(\kappa c + q)^2} + \frac{2s^2 A_1^2}{(\kappa c + q)^3}\right]\frac{e^{-jk_1 r_2}}{4\pi k_1 r_2^2} + O(k_1 r_2)^{-3} \qquad \text{(II.21)}
$$

where $A_1 - A_4$ expressions take the following form:

$$A_1 = \kappa q + c \qquad \text{(II.22a)}$$

$$A_2 = (s^4 - 2\kappa s^2 + \kappa)/q^3 \qquad \text{(II.22b)}$$

$$A_3 = 2s^2/q^2 + (3c - 2/c)/q - 2 \qquad \text{(II.22c)}$$

$$A_4 = s^2 c/q^3 + s^2/q^2 + 2(3c - 1/c)/q - 6 \quad ; \qquad \text{(II.22d)}$$

s,c, and q were defined in (II.18). It is interesting to point out that in deriving (II.19) - (II.21), one initially encounters singular terms at $\theta_2 = 0$. As expected, after some algebraic manipulations, these singular terms completely cancel out in all three cases, and the two-term asymptotic expressions for the vector potentials remain bounded for $0 \leq \theta_2 < 90$.

APPENDIX III

VARIOUS PARTIAL DERIVATIVES OF g

The free-space Green's function g, which is defined as

$$g = g(x_1, x_2, x_3) = \exp(-jkr)/4\pi r \quad ; \quad r = [x_1^2 + x_2^2 + x_3^2]^{1/2} \tag{III.1}$$

is singular only at the point $r = 0$, therefore, its partial derivatives exist for all $r > 0$ and can be represented in a closed form. In order to express these derivatives in an organized manner and suitable for numerical evaluation, the auxiliary function R_i is introduced as

$$R_i = (-1)^i\{1 \times 2 \times 4 \times \ldots \times (2i-2) + jkr[1 \times 3 \times 5 \times \ldots \times (2i-3)]\}r^{-2i};$$
$$i = 1,2,3,\ldots \tag{III.2}$$

where R_i has the following convenient property

$$\frac{\partial}{\partial x_j} R_i = x_j R_{i+1} \quad ; \quad i = 1,2,\ldots \quad ; \quad j = 1,2,3 \quad . \tag{III.3}$$

The various partial derivatives of g can now be expressed in terms of x_j, R_2, and lower-order partials of g.

a) Partial derivatives of one variable

$$\frac{\partial}{\partial x_j} g = x_j R_1 g \tag{III.4}$$

$$\frac{\partial^2}{\partial x_j^2} g = (R_1 + x_j^2 R_2)g + x_j R_1 \frac{\partial}{\partial x_j} g \tag{III.5}$$

$$\frac{\partial^3}{\partial x_j^3} g = (3x_j R_2 + x_j^3 R_3)g + 2(R_1 + x_j^2 R_2) \frac{\partial}{\partial x_j} g + x_j R_1 \frac{\partial^2}{\partial x_j^2} g \tag{III.6}$$

. . .

. . .

where $j = 1,2,3$ holds for Equations (III.4) - (III-6).

b) Mixed partial derivatives of two variables

$$\frac{\partial^2}{\partial x_j\ \partial x_k} g = x_j x_k R_2 g + x_k R_1 \frac{\partial}{\partial x_j} g = x_j x_k (R_1^2 + R_2) g \tag{III.7}$$

$$\frac{\partial^3}{\partial x_j^2\ \partial x_k} g = x_k (R_2 + x_j^2 R_3) g + 2 x_j x_k R_2 \frac{\partial}{\partial x_j} g + x_k R_1 \frac{\partial^2}{\partial x_j^2} g \tag{III.8}$$

$$\frac{\partial^4}{\partial x_j^3\ \partial x_k} g = x_k (3 x_j R_3 + x_j^3 R_4) g + 3 x_k (R_2 + x_j^2 R_3) \frac{\partial}{\partial x_j} g + 3 x_j x_k R_2 \frac{\partial^2}{\partial x_j^2} g$$
$$+ x_k R_1 \frac{\partial^3}{\partial x_j} g \tag{III.9}$$

$$\frac{\partial^4}{\partial x_j^2\ \partial x_k^2} g = [R_2 + (x_j^2 + x_k^2) R_3 + x_j^2 x_k^2 R_4] g + x_k (R_2 + x_j^2 R_3) \frac{\partial}{\partial x_k} g$$
$$+ 2 x_j (R_2 + x_k^2 R_3) \frac{\partial}{\partial x_j} g + (R_1 + x_k^2 R_2) \frac{\partial^2}{\partial x_j^2} g + 2 x_j x_k R_2 \frac{\partial^2}{\partial x_j\ \partial x_k} g$$
$$+ x_k R_1 \frac{\partial^3}{\partial x_j^2\ \partial x_k} g \tag{III.10}$$

. . .

. . .

where $j \neq k$ and $j,k = 1,2,3$ is assumed for Equations (III.7) - (III.10).

c) Mixed partial derivatives of three variables

$$\frac{\partial^3}{\partial x_j\ \partial x_k\ \partial x_\ell} g = x_j x_k x_\ell R_3 g + 2 x_k x_\ell R_2 \frac{\partial}{\partial x_j} g + x_\ell R_1 \frac{\partial^2}{\partial x_j\ \partial x_k} g \tag{III.11}$$

$$\frac{\partial^4}{\partial x_j^2\ \partial x_k\ \partial x_\ell} g = x_k x_\ell (R_3 + x_j^2 R_4) g + 3 x_j x_k x_\ell R_3 \frac{\partial}{\partial x_j} g + 2 x_k x_\ell R_2 \frac{\partial^2}{\partial x_j^2} g$$
$$+ x_j x_\ell R_2 \frac{\partial^2}{\partial x_j\ \partial x_k} g + x_\ell R_1 \frac{\partial^3}{\partial x_j^2\ \partial x_k} g \tag{III.12}$$

. . .

. . .

where $j \neq k \neq \ell$ and $j,k,\ell = 1,2,3$ is assumed for Equations (III.11) - (III.12).

APPENDIX IV

COMPLETE COMPUTER LISTING

In this appendix, a complete listing of a Fortran program is listed for analyzing wire antenna structures over a lossy half-space, based on the developments of Chapters 4 and 5. Also included are subroutines for evaluating the correction vector potential via the SDP integration technique introduced in Chapter 3. To avoid confusion, care has been taken to use the same symbols and names in the program as were introduced in the text, and comment statements have been included frequently to describe the function of each routine.

```
      PROGRAM HORIZ(INPUT,OUTPUT)
C
C
C     CENTER-FED HORIZONTAL WIRE ANTENNA
C     ANTL=   ANTENNA-LENGTH (METERS)
C     RADIUS=   ANTENNA-RADIUS (METERS)
C     H=   ANTENNA-HEIGHT ABOVE THE LOSSY HALF-SPACE
C     EPSR, SIGMA=   GROUND PARAMETERS,  SIGMA IN MHOS/METERS
C      N=   NUMBER OF CURRENT PATCHES (ODD FOR A CENTER-FED ANTENNA)
C     PHIOP=  THE PHI-PLANE IN WHICH PATTERN IS COMPUTED(AS A FUNCTION OF THETA)
C
C      **********INPUT***********
C
C      READ FREQUENCY (MHZ)
C      READ EPSR,SIGMA (DEFINING THE GROUND)
C      IF EPSR<0.   ,   THEN READ A NEW FREQUENCY
C      READ PHIOP (DEGREES) , PATTERN-PLANE
C      IF PHIOP<0.   , PATTERN NOT COMPUTED AND NEW GROUND IS READ
C
C
      IMPLICIT COMPLEX(C,J)
      REAL COS,CABS
      COMPLEX KAPPA,ZIOI(21,21),JANT(21),ZI(21),ZR(21),ZL(21)
      COMMON/PI/   PI,EPS0,CJ
      COMMON/OBS/   R2,TH2,PHI2
      COMMON/PARAM/   AK1,KAPPA,C1A
      COMMON/PATTERN/   R0,TH0,PHI0
      COMMON/PATCH/   XCORR,YCORR,ZCORR
      PI=4.*ATAN(1.)    $   EPS0=1.E-9/(36.*PI)    $   CJ=(0.,1.)
 2121    CONTINUE
C
      READ900,FREQ
 900   FORMAT(G14.6)
C
      IF(FREQ.LT.0.)    STOP
      FREQ=FREQ*1.E6
 1111    CONTINUE
      READ900,EPSR
      IF(EPSR.LT.0.)    GO TO 2121
      READ900,SIGMA
      AK1=2.*PI*FREQ/3.E8
      KAPPA=EPSR-CJ*SIGMA/(2.*PI*FREQ*EPS0)
      C1A=1./(CJ*2.*PI*FREQ*EPS0)
C
      ANTL=10.    $    H=3.    $    RADIUS=.05    $    N=21
C
      PRINT820,FREQ,KAPPA
 820    FORMAT(//,"FREQ=",G14.4,5X,"KAPPA=",G12.4,",",G14.6)
      PRINT830,ANTL,RADIUS,H,N
 830    FORMAT(//"ANT-L=",G10.5,"ANT-RAD=",G12.6,"ANT-HEIGHT=",
     +G10.5,"    N=",I4)
```

```
C
C*****    COMPUTE THE IMPEDANCE MATRIX
C
 DEL=ANTL/N
C
C**USE FINITE-DIFFERENCE TECHNIQUE FOR EINC
C
 DO 100 I=1,N
 X=(I-1)*DEL
 XR=X+DEL/2.

 CALL SI(DEL,RADIUS,X,ZI(I))
 CALL SI(DEL,RADIUS,XR,ZR(I))
 100   CONTINUE
 ZL(1)=ZR(1)
 DO 210   I=2,N
 210   ZL(I)=ZR(I-1)
 DO 120 J=1,N
 ZTOT(1,J)=(ZR(J)+ZL(J)-2.*ZI(J))/(DEL/2.)**2+AK1**2*ZI(J)
 ZTOT(1,J)=-ZTOT(1,J)*DEL*CI0
 120   CONTINUE
 IF(EPSR.EQ.1..AND.SIGMA.EQ.0.)    GO TO 200
C
C***    ADD THE GROUND CONTRIBUTIONS TO THE MATRIX ELEMENTS
C
 Z2=2.*H    $    PHI2=0.
 C1=(0.,0.)    $    C2=-DEL**2*CI0
 DO 110    I=1,N
 RHO2=(I-1)*DEL
 R2=SQRT(RHO2**2+Z2**2)
 TH2=ACOS(Z2/R2)
 CALL SESAPP(DEX,DEY,DEZ,C1,C2)
 ZTOT(1,I)=ZTOT(1,I)+DEX
 110   CONTINUE
C
C***USE SYMMETRY TO COMPLETE THE MATRIX
C
 200   CONTINUE
 850   FORMAT(/,4("(",G10.4," ,",G10.4,")"))
 DO 300 I=1,N
 DO 300 J=I,N
 IF(I.EQ.1)    GO TO 310
 ZTOT(I,J)=ZTOT(I-1,J-1)
 310   ZTOT(J,I)=ZTOT(I,J)
 300   CONTINUE
C
C***INVERT THE MATRIX AND COMPUTE CURRENTS AND THE IMPEDANCE
C
 CALL LINV2(N,21,ZTOT,DDET,IER)
 NO2=N/2+1
```

```
      DO 400 I=1,N
      JANT(I)=ZTOT(I,NO2)
400   CONTINUE
      PRINT849
849   FORMAT(///,"ANTENNA CURRENTS(AMPS), DUE TO 1-VOLT EXCITATION")
      PRINT850,(JANT(I),I=1,N)
      UZIMP=1./JANT(NO2)
      PRINT860,UZIMP
860   FORMAT(///,"ANTENNA IMPEDANCE(OHMS)= (",G14.6,"  ,",G14.6," )",//)
C
C***COMPUTE THE E-FIELD PATTERNS IN THE PHI=PHIØP PLANE
C
      AK1R0=500.
      R0=AK1R0/AK1
3131  READ900,PHIØP
      IF(PHIØP.LT.0.)   GO TO 1111
      PRINT970
      PHIØ=PHIØP*PI/180.
      DO 700 I=1,45
      THØP=2.*I
      THØ=THØP*PI/180.
      UETH=UEPHI=(0.,0.)
C
C
      DO 750   K=1,N
      ZCORR=0   $   YCORR=0.
      XCORR=(K-(N+1)/2)*DEL
      UIZ=(0.,0.)
      UIX=JANT(K)
      CALL SEPAT(UIX,UIZ,U1,U2)
      UETH=UETH+U1*DEL
      UEPHI=UEPHI+U2*DEL
750   CONTINUE
      ETH=CABS(UETH)   $   EPHI=CABS(UEPHI)
      PRINT975,AK1R0,THØP,PHIØP,ETH,EPHI
700   CONTINUE
970   FORMAT(///)
975   FORMAT(" K1R0=",G8.2," THØ=",G8.2," PHIØ=",G8.2,
     +" MAG-ETH=",G14.6," MAG-EPHI=",G14.6)
      GO TO 3131
      END
```

```
      PROGRAM VERTIC(INPUT,OUTPUT)
C
C
C     CENTER-FED VERTICAL WIRE ANTENNA
C     ANTL=   ANTENNA-LENGTH (METERS)
C     RADIUS=   ANTENNA-RADIUS (METERS)
C     H=   ANTENNA-HEIGHT ABOVE THE LOSSY HALF-SPACE (MEASURED FROM ANTENNA-CENTER)
C     EPSR, SIGMA=   GROUND PARAMETERS,  SIGMA IN MHOS/METERS
C      N=   NUMBER OF CURRENT PATCHES (ODD FOR A CENTER-FED ANTENNA)
C     PHI0P=  THE PHI-PLANE IN WHICH PATTERN IS COMPUTED(AS A FUNCTION OF THETA)
C
C      **********INPUT***********
C
C      READ FREQUENCY (MHZ)
C      READ EPSR,SIGMA (DEFINING THE GROUND)
C      IF EPSR<0.    ,    THEN READ A NEW FREQUENCY
C      READ PHI0P (DEGREES) , PATTERN-PLANE
C      IF PHI0P<0.    , PATTERN NOT COMPUTED AND NEW GROUND IS READ
C
C
      IMPLICIT COMPLEX(C,U)
      REAL COS,CABS
      COMPLEX KAPPA,ZTOT(21,21),JANT(21),ZI(21),ZR(21),ZL(21)
      COMPLEX ZEXTRA(41)
C---ZEXTRA MUST BE DIMENSIONED AT LIST 2*N+1 LONG
      COMMON/PI/   PI,EPS0,CJ
      COMMON/OBS/   R2,TH2,PHI2
      COMMON/PARAM/   AK1,KAPPA,CIN
      COMMON/PATTERN/   R0,TH0,PHI0
      COMMON/PATCH/   XCORR,YCORR,ZCORR
      PI=4.*ATAN(1.)   $   EPS0=1.E-9/(36.*PI)   $   CJ=(0.,1.)
 2121   CONTINUE
C
      READ900,FREQ
 900    FORMAT(F14.6)
C
      IF(FREQ.LT.0.)     STOP
      FREQ=FREQ*1.E6
 1111   CONTINUE
      READ900,EPSR
      IF(EPSR.LT.0.)     GO TO 2121
      READ900,SIGMA
      PRINT900,FREQ,EPSR,SIGMA
      AK1=2.*PI*FREQ/3.E8
      KAPPA=EPSR-CJ*SIGMA/(2.*PI*FREQ*EPS0)
      CIN=1./(CJ*2.*PI*FREQ*EPS0)
C
      ANTL=10.   $   H=0.   $   RADIUS=.05   $   N=21
C
      PRINT620,FREQ,KAPPA
 620    FORMAT(//,"FREQ=",G14.4,5X,"KAPPA=",G12.4,",",G14.6)
```

```
PRINT830,ANTL,RADIUS,H,N
830   FORMAT(//"ANT-L=",G10.5,"ANT-RAD=",G12.6,"ANT-HEIGHT=",
+G10.5,"    N=",I4)
C
C*****    COMPUTE THE IMPEDANCE MATRIX
C
DEL=ANTL/N
C
C**USE FINITE-DIFFERENCE TECHNIQUE FOR EINC
C

DO 100 I=1,N
X=(I-1)*DEL
XR=X+DEL/2.
CALL SI(DEL,RADIUS,X,ZI(I))
CALL SI(DEL,RADIUS,XR,ZR(I))
100   CONTINUE
ZL(1)=ZR(1)
DO 210   I=2,N
210   ZL(I)=ZR(I-1)
DO 120 J=1,N
ZTOT(1,J)=(ZR(J)+ZL(J)-2.*ZI(J))/(DEL/2.)**2+AK1**2*ZI(J)
ZTOT(1,J)=-ZTOT(1,J)*DEL*CI0
120   CONTINUE
DO 150 I=2,N
DO 150 J=1,N
150   ZTOT(I,J)=ZTOT(I-1,J-1)
IF(EPSR.EQ.1..AND.SIGMA.EQ.0.)    GO TO 200
C
C***    ADD THE GROUND CONTRIBUTIONS TO THE MATRIX ELEMENTS
C
RHO2=0.    $    PHI2=0.    $    TH2=0.
C2=(0.,0.)    $    C1=-DEL**2*CI0
NPP=2.*N-1
DO 110 I=1,NPP
R2=Z2=2.*H-ANTL+I*DEL
CALL SESAPP(DEX,DEY,DEZ,C1,C2)
ZEXTRA(I)=DEZ
110   CONTINUE
DO 115    I=1,N
DO 115    J=I,N
ZTOT(I,J)=ZTOT(I,J)+ZEXTRA(I+J-1)
115   CONTINUE
C
C***USE SYMMETRY TO COMPLETE THE MATRIX
C
200   CONTINUE
850   FORMAT(/,4("(",G10.4," ,",G10.4,")"))
DO 500 I=2,N
K=I-1
```

```
      DO 300 J=1,N
      ZTOT(I,J)=ZTOT(J,I)
300   CONTINUE
C
C***INVERT THE MATRIX AND COMPUTE CURRENTS AND THE IMPEDANCE
C
      CALL XINV2(N,21,ZTOT,UDET,IER)
      NO2=N/2+1
      DO 400 I=1,N
      JANT(I)=ZTOT(I,NO2)
400   CONTINUE
      PRINT849
849   FORMAT(///,"ANTENNA CURRENTS(AMPS), DUE TO 1-VOLT EXCITATION")
      PRINT850,(JANT(I),I=1,N)
      UZIMP=1./JANT(NO2)
      PRINT860,UZIMP
860   FORMAT(///,"ANTENNA IMPEDANCE(OHMS)= (",G14.6,"  ,",G14.6," )",//)
C
C***COMPUTE THE E-FIELD PATTERNS IN THE PHI=PHI0P PLANE
C
      AK1R0=500.
      R0=AK1R0/AK1

3131  READ900,PHI0P
      IF(PHI0P.LT.0.)   GO TO 1111
      PRINT970
      PHI0=PHI0P*PI/180.
      DO 700 I=1,45
      TH0P=2.*I
      TH0=TH0P*PI/180.
      UETH=UEPHI=(0.,0.)
C
C
      DO 750   K=1,N
      XCURR=0.   $   YCURR=0.
      ZCURR=H-ANTL/2.+(K-.5)*DEL
      UIX=(0.,0.)
      UIZ=JANT(K)
      CALL SEPAT(UIX,UIZ,U1,U2)
      UETH=UETH+U1*DEL
      UEPHI=UEPHI+U2*DEL
750   CONTINUE
      ETH=CABS(UETH)   $   EPHI=CABS(UEPHI)
      PRINT975,AK1R0,TH0P,PHI0P,ETH,EPHI
700   CONTINUE
970   FORMAT(///)
975   FORMAT(" K1R0=",G8.2," TH0=",G8.2," PHI0=",G8.2,
     +" MAG-ETH=",G14.6," MAG-EPHI=",G14.6)
      GO TO 3131
      END
```

```
      PROGRAM VEEDIP(INPUT,OUTPUT)
C
C
C     INVERTED VEE-DIPOLE ANTENNA OVER GROUND
C     ANTLEG=   THE LENGTH OF EACH ANTENNA LEG (METETRS)
C     RADIUS=   ANTENNA-RADIUS (METERS)
C     H=   ANTENNA-HEIGHT ABOVE THE LOSSY HALF-SPACE (MEASURED FROM ANTENNA-CENTER)
C     EPSR, SIGMA=   GROUND PARAMETERS,  SIGMA IN MHOS/METERS
C      N=   NUMBER OF CURRENT PATCHES (EVEN FOR A CENTER-FED ANTENNA)
C     PHI0P=  THE PHI-PLANE IN WHICH PATTERN IS COMPUTED(AS A FUNCTION OF THETA)
C
C      *********INPUT**********
C
C     READ FREQUENCY (MHZ)
C      READ EPSR,SIGMA (DEFINING THE GROUND)
C      IF EPSR<0,     ,     THEN READ A NEW FREQUENCY
C      READ PHI0P (DEGREES) , PATTERN-PLANE
C      IF PHI0P<0,    , PATTERN NOT COMPUTED AND NEW GROUND IS READ
C
C
      IMPLICIT COMPLEX(C,U)
      REAL COS,CABS
      COMPLEX KAPPA,ZTOT(22,22),JANT(22),ZI(22),ZR(22),ZL(22)
      COMMON/PI/   PI,EPS0,CJ
      COMMON/OBS/   R2,TH2,PHI2
      COMMON/PARAM/   AK1,KAPPA,C10
      COMMON/PATTERN/   R0,TH0,PHI0
      COMMON/PATCH/   XCURR,YCURR,ZCURR
      PI=4.*ATAN(1.)    $   EPS0=1.E-9/(36.*PI)    $   CJ=(0.,1.)
 2121   CONTINUE
C
      READ900,FREQ
 900    FORMAT(F14.6)
C
      IF(FREQ.LT.0.)    STOP
      FREQ=FREQ*1.E6
 1111    CONTINUE
      READ900,EPSR
      IF(EPSR.LT.0.)    GO TO 2121
      READ900,SIGMA
      READ900,ANTS1
      PRINT900,FREQ,EPSR,SIGMA
      AK1=2.*PI*FREQ/3.E8
      KAPPA=EPSR-CJ*SIGMA/(2.*PI*FREQ*EPS0)
      C10=1./(CJ*2.*PI*FREQ*EPS0)
C
      ANTLEG=7.5    $    H=10.    $    RADIUS=.05    $    N=22
C
      PRINT820,FREQ,KAPPA
```

```
620   FORMAT(//,"FREQ=",G14.4,5X,"KAPPA=",G12.4,",",G14.6)
PRINT630,ANTLEG,ANTSI,RADIUS,H
630   FORMAT(//"ANTENNA-LEG=",G10.5,"INVERTED-VEE ANGLE=",G10.5,
+"ANT-RADIUS=",G10.5,"ANT-HEIGHT=",G10.5)
PRINT635,N
635   FORMAT(/"  N= ",I5)
ANTSI=ANTSI*PI/180.
C
C*****   COMPUTE THE IMPEDANCE MATRIX
C
NO2=N/2
DEL=ANTLEG/NO2

C
C**USE FINITE-DIFFERENCE TECHNIQUE FOR EINC(SYMMETRY IS USED)
C
DO 100 I=1,NO2
X=(I-1)*DEL
XR=X+DEL/2.
CALL SI(DEL,RADIUS,X,ZI(I))
CALL SI(DEL,RADIUS,XR,ZR(I))
100   CONTINUE
ZL(1)=ZR(1)
DO 110   I=2,NO2
110   ZL(I)=ZR(I-1)
DO 120 J=1,NO2
ZTOT(1,J)=(ZR(J)+ZL(J)-2.*ZI(J))/(DEL/2.)**2+AK1**2*ZI(J)
ZTOT(1,J)=ZTOT(1+NO2,J+NO2)=-ZTOT(1,J)*DEL*CI0
120   CONTINUE
DO 150 I=2,NO2
DO 150 J=I,NO2
150   ZTOT(I,J)=ZTOT(I+NO2,J+NO2)=ZTOT(I-1,J-1)
C
C
DO 160 I=1,NO2
K=NO2+1-I
DO 160 J=1,K
X=(NO2-I+.5)*DEL+(J-.5)*DEL*COS(PI-ANTSI)+2.*RADIUS*SIN(PI-ANTSI)
RHO=ABS((J-.5)*DEL*SIN(PI-ANTSI)-2.*RADIUS*COS(PI-ANTSI)+RADIUS)
CALL SI(DEL,RHO,X,UZI)
CALL SI(DEL,RHO,X+DEL/2.,UZIXR)
CALL SI(DEL,RHO,X-DEL/2.,UZIXL)
CALL SI(DEL,RHO+DEL/2.,X+DEL/2.,UZIRRXR)
CALL SI(DEL,RHO-DEL/2.,X-DEL/2.,UZIRLXL)
CALL SI(DEL,RHO+DEL/2.,X-DEL/2.,UZIRRXL)
CALL SI(DEL,RHO-DEL/2.,X+DEL/2.,UZIRLXR)
DEPAR=(UZIXR+UZIXL-2.*UZI)/(DEL/2.)**2+AK1**2*UZI
DEVER=(UZIRRXR+UZIRLXL-UZIRRXL-UZIRLXR)/DEL**2
DET=DEPAR*COS(PI-ANTSI)+DEVER*SIN(PI-ANTSI)
ZTOT(I,J+NO2)=ZTOT(NO2+1-J,N+1-I)=-DET*DEL*CI0
160   CONTINUE
IF(EPSR.EQ.1..AND.SIGMA.EQ.0.)   GO TO 200
```

THIS PAGE IS BEST QUALITY PRACTICABLE
FROM COPY FURNISHED TO DDC

```
C
C***   ADD THE GROUND CONTRIBUTIONS TO THE MATRIX ELEMENTS(SUMMETRY IS USED)
C
DO 210   I=1,NO2
DO 210   J=1,NO2
RHO2=ABS(FLOAT(I-J))*DEL*SIN(ANTSI/2.)
Z2=2.*(H-(NO2-I+.5)*DEL*COS(ANTSI/2.))+ABS(FLOAT(I-J))*DEL*COS(ANTSI/2.)
PHI2=0.
R2=SQRT(RHO2**2+Z2**2)
TH2=ATAN(RHO2/Z2)
C1=-DEL**2*C10*COS(ANTSI/2.)
C2=-DEL**2*C10*SIN(ANTSI/2.)
CALL SESAPP(UEX,UEY,UEZ,C1,C2)
UET=UEX*SIN(ANTSI/2.)+UEZ*COS(ANTSI/2.)
ZTOT(I,J)=ZTOT(I,J)+UET
ZTOT(N+1-J,N+1-I)=ZTOT(N+1-J,N+1-I)+UET
210   CONTINUE
DO 220   I=1,NO2
DO 220   J=1,NO2
IF(I.NE.1.AND.J.NE.1)   GO TO 220
RHO2=(NO2-I+J)*DEL*SIN(ANTSI/2.)
Z2=2.*H-(NO2-I+J)*DEL*COS(ANTSI/2.)

PHI2=0.
R2=SQRT(RHO2**2+Z2**2)
TH2=ATAN(RHO2/Z2)
CALL SESAPP(UEX,UEY,UEZ,C1,C2)
UET=UEX*SIN(ANTSI/2.)-UEZ*COS(ANTSI/2.)
ZTOT(I,J+NO2)=ZTOT(I,J+NO2)+UET
220   CONTINUE
DO 230   I=2,NO2
K=NO2+2
DO 230   J=K,N
ZTOT(I,J)=ZTOT(I-1,J-1)
230   CONTINUE
C
C***USE SYMMETRY TO COMPLETE THE MATRIX
C
200   CONTINUE
650   FORMAT(/,4("(",G10.4," ,",G10.4,")"))
DO 300 I=2,N
K=I-1
DO 300 J=1,K
ZTOT(I,J)=ZTOT(J,I)
300   CONTINUE
C
C***INVERT THE MATRIX AND COMPUTE CURRENTS AND THE IMPEDANCE
C
CALL XINVZ(N,22,ZTOT,DDET,IER)
DO 400 I=1,N
JANT(I)=ZTOT(I,N/2)+ZTOT(I,N/2+1)
```

```
400   CONTINUE
PRINT849
849   FORMAT(///,"ANTENNA CURRENTS(AMPS), DUE TO 1-VOLT EXCITATION
+ APPLIED TO EACH OF THE TWO CENTER PATCHES")
PRINT850,(JANT(I),I=1,N)
UZIMP=2./JANT(N/2)
PRINT860,UZIMP
860   FORMAT(///,"ANTENNA IMPEDANCE(OHMS)= (",G14.6,"   ,",G14.6," )",//)
C
C**COMPUTE THE E-FIELD PATTERNS IN THE PHI=PHIØP PLANE
C
AK1RØ=500.
RØ=AK1RØ/AK1
3131   READ900,PHIØP
IF(PHIØP.LT.0.)   GO TO 1111
PRINT970
PHIØ=PHIØP*PI/180.
DO 700 I=1,46
THØP=2.*(I-1)
THØ=THØP*PI/180.
DETH=DEPHI=(0.,0.)
C
C
DO 750   K=1,NU2
YCURR=0.
ZCURR=H-(NU2-I+.5)*DEL*COS(ANTSI/2.)
XCURR=-(NU2-I+.5)*DEL*SIN(ANTSI/2.)
UIX=JANT(K)*SIN(ANTSI/2.)
UIZ=JANT(K)*COS(ANTSI/2.)
CALL SEPAT(UIX,UIZ,U1,U2)
DETH=DETH+U1*DEL
DEPHI=DEPHI+U2*DEL
XCURR=-XCURR

UIX=JANT(N-K+1)*SIN(ANTSI/2.)
UIZ=-JANT(N-K+1)*COS(ANTSI/2.)
CALL SEPAT(UIX,UIZ,U1,U2)
DETH=DETH+U1*DEL
DEPHI=DEPHI+U2*DEL
750   CONTINUE
ETH=CABS(DETH)    $    EPHI=CABS(DEPHI)
PRINT975,AK1RØ,THØP,PHIØP,ETH,EPHI
700   CONTINUE
970   FORMAT(///)
975   FORMAT(" K1RØ=",G8.2," THØ=",G8.2," PHIØ=",G8.2,
+" MAG-ETH=",G14.6," MAG-EPHI=",G14.6)
GO TO 3131
END
```

```
      SUBROUTINE SEPAT(UIX,UIZ,UETH,UEPHI)
C
C
C     COMPUTE THE FAR-FIELD APPROXIMATION FOR E-THETA AND E-PHI.
C     THE OBSERVATION POINT IS LOCATED AT (R0,TH0,PHI0),
C     AND THE CURRENT ELEMENT IS LOCATED AT (XCURR,YCURR,ZCURR)
C     WITH UIX AMPS IN THE X-DIRECTION AND
C          UIZ AMPS IN THE Z-DIRECTION.
C
C
      IMPLICIT COMPLEX (C,U)
      REAL COS
      COMPLEX KAPPA
      COMMON/PI/    PI,EPS0,CJ
      COMMON/OBS/    R2,TH2,PHI2
      COMMON/PATTERN/    R0,TH0,PHI0
      COMMON/PATCH/    XCURR,YCURR,ZCURR
      COMMON/PARAM/    AK1,KAPPA,CI0
C
C
      Z2=R0*COS(TH0)+ZCURR
      X2=R0*SIN(TH0)*COS(PHI0)-XCURR
      Y2=R0*SIN(TH0)*SIN(PHI0)-YCURR
      R2=SQRT(X2**2+Y2**2+Z2**2)
      TH2=ACOS(Z2/R2)
      PHI2=0.
      IF(X2.NE.0..OR.Y2.NE.0.)    PHI2=ATAN2(Y2,X2)
C
C
      CALL SRCH1(U1,U2,U3)
      R1=SQRT(X2**2+Y2**2+(Z2-2.*ZCURR)**2)
      UG1=CEXP(-CJ*AK1*R1)/(4.*PI*R1)
      UG2=CEXP(-CJ*AK1*R2)/(4.*PI*R2)
      UPIX=UIX*CI0*(UG1-UG2+U2)
      UPIZ=UIZ*CI0*(UG1-UG2+U1)+UIX*CI0*U3
      UETH=AK1**2*(COS(TH0)*COS(PHI0)*UPIX-SIN(TH0)*UPIZ)
      UEPHI=-AK1**2*SIN(PHI0)*UPIX
      RETURN
      END
```

```
SUBROUTINE SRCM1(CPØVIZ,CPØHIX,CPØHIZ)
C
C
C     COMPUTING THE 1ST TERM OF THE ASYMPTOTIC EXPANSION
C
C
IMPLICIT COMPLEX(C,U)
REAL COS,C
COMPLEX KAPPA,U
COMMON/PI/ PI,EPS0,CJ
COMMON/OBS/ R,TH,PHI
COMMON/PARAM/ AK1,KAPPA,CIU
CG=CEXP(-CJ*AK1*R)/(4.*PI*R)
C=COS(TH)
S=SIN(TH)
U=CSQRT(KAPPA-S**2)
CPØVIZ=2.*KAPPA*C/(KAPPA*C+U)*CG
CPØHIX=2.*C/(C+U)*CG
CPØHIZ=2.*COS(PHI)*S*C*(C-U)/(KAPPA*C+U)*CG
RETURN
END
C
C
C
SUBROUTINE SRCM2(CPØVIZ,CPØHIX,CPØHIZ)
C
C
C    COMPUTING THE 2ND TERM IN THE ASYMPTOTIC EXPANSION
C
C
IMPLICIT COMPLEX(C,U)
REAL COS,C
COMPLEX KAPPA,U,A1,A2,A3,A4,B1,B2
COMMON/PI/ PI,EPS0,CJ
COMMON/OBS/ R,TH,PHI
COMMON/PARAM/ AK1,KAPPA,CIU
CG2=CEXP(-CJ*AK1*R)/(4.*PI*AK1*R**2)
C=COS(TH)
S=SIN(TH)
U=CSQRT(KAPPA-S**2)
A1=KAPPA*U+C
A2=(S**4-2.*KAPPA*S**2+KAPPA)/U**3
A3=2.*S**2/U**2+(3.*C-2./C)/U-2.
A4=S**2*C/U**3+S**2/U**2+2.*(3.*C-1./C)/U-6.
B1=KAPPA*C+U
B2=C+U
CPØVIZ=CJ*KAPPA*C*(-2./B1+(A1*(3.*C-2./C)+A2+KAPPA*C)/
+B1**2+2.*S**2*A1**2/B1**3)*CG2
CPØHIX=CJ*C*(A3/B2+(A2+C)/B2**2)*CG2
CPØHIZ=COS(PHI)*CJ*S*C*(C-U)*CG2
CPØHIZ=CPØHIZ*(A4/B1+(A1*(5.*C-2./C+2.*S**2/U)+A2+KAPPA*C)/
+B1**2+2.*S**2*A1**2/B1**3)
RETURN
END
```

THIS PAGE IS BEST QUALITY PRACTICABLE
FROM COPY FURNISHED TO DDC

```
SUBROUTINE SI(DELX,P,X,Z)
C
C    INTEGRATION OF THE FREE SPACE GREENS FUNCTION
C    FROM X-DEL/2 TO X+DEL/2 , X IS MEASURED ALONG THE
C    SOURCE AND P IS THE LATERAL DISLACEMENT FROM THE
C    SOURCE POINT.
C
COMPLEX CMPLX,CEXP,Z,KAPPA
COMMON/PARAM/    AK,KAPPA,C10
REAL I1,I2,I3,I4
PI=3.141592654
AL=DELX/2.
R=SQRT(P**2+X**2)
IF(R.GE.10.*AL) GO TO 100
S1=SQRT(P**2+(X+AL)**2)
S2=SQRT(P**2+(X-AL)**2)
I1=ALOG((X+AL+S1)/(X-AL+S2))
I2=2.*AL
I3=.5*(AL+X)*S1+.5*(AL-X)*S2+.5*P**2*I1
I4=2.*AL*P**2+1./3.*(2.*AL**3+6.*AL*X**2)
Z=I1-(0.,1.)*AK*(I2-R*I1)-.5*AK**2*(I3-2.*R*I2+R**2*I1)
Z=Z+(0.,1.)*AK**3/6.*(I4-3.*R*I3+3.*R**2*I2-R**3*I1)
Z=Z*CEXP(-(0.,1.)*AK*R)/(4.*PI)
RETURN
100 CONTINUE
AOR=AL/R
XOR=X/R
A0=1.+1./6.*AOR**2*(-1.+3.*XOR**2)
A0=A0+1./40.*AOR**4*(3.-30.*XOR**2+35.*XOR**4)
A1=1./6.*AOR*(-1.+3.*XOR**2)
A1=A1+1./40.*AOR**3*(3.-30.*XOR**2+35.*XOR**4)
A2=-1./6.*XOR**2-1./40.*AOR**2*(1.-12.*XOR**2+15.*XOR**4)
A3=1./60.*AOR*(3.*XOR**2-5.*XOR**4)
A4=1./120.*XOR**4
Z=A0+(0.,1.)*AK*AL*A1+(AK*AL)**2*A2
  Z=Z+(0.,1.)*(AK*AL)**3*A3+(AK*AL)**4*A4
Z=Z*2.*AOR*CEXP(-(0.,1.)*AK*R)/(4.*PI)
RETURN
END
```

```
      SUBROUTINE SPIAPP(CPØV1Z,CPØM1X,CPØM1Z)
C
C
C     COMPUTE THE VECTOR POTENTIALS VIA THE APPROXIMATE TECHNIQUE
C
C
      IMPLICIT COMPLEX(C,U)
      COMPLEX KAPPA
      REAL COS
      COMMON/PI/    PI,EPS0,CJ
      COMMON/OBS/    R2,TH2,PHI2
      COMMON/PARAM/    AK1,KAPPA,C10
      Z2=R2*COS(TH2)    $    RHO2=R2*SIN(TH2)
      STORER=R2    $    STORET=TH2
      CALL SDGPI(UG,UGZ,UGZ2,UGXZ,UGX,0,0)
      CPØM1X=-2./AK1**2/(1.-KAPPA)*(CJ*AK1*CSQRT(KAPPA)*UGZ+UGZ2)
      CONST=AK1/CSQRT(KAPPA)
      R2P=15./AK1
      IF(R2.GT.R2P)    GO TO 100
      Z2P=SQRT(R2P**2-RHO2**2)    $    R2=R2P    $    TH2=ATAN(RHO2/Z2P)
      CALL SDGPI(UGP,UGZP,UGZ2P,UGXZP,UGXP,0,0)
999   FORMAT(/6G14.6)
      R2=STORER    $    TH2=STORET
      CALL SUS(Z2P,Z2,UGP,UG,UGXZP,CONST,USZ,0)
      CALL SUS(Z2P,Z2,UGXP,UGX,UGXZP,CONST,USZX,1)
      CPØV1Z=USZ
      CPØM1Z=1./AK1**2/KAPPA*(-2.*UGXZ-CJ*CONST*(1.+KAPPA)*USZX)
      RETURN
100   CALL SRCM1(CPØV1Z,U2,CPØM1Z)
      RETURN
      END
C
C
C
      COMPLEX FUNCTION UGARGV(Z2P)
      IMPLICIT COMPLEX (C,U)
      COMPLEX KAPPA
      REAL COS
      COMMON/PI/    PI,EPS0,CJ
      COMMON/OBS/    R2,TH2,PHI2
      COMMON/PARAM/    AK1,KAPPA,C10
      STORER=R2    $    STORET=TH2    $    RHO2=R2*SIN(TH2)
      CONST=AK1/CSQRT(KAPPA)
      R2=SQRT(Z2P**2+RHO2**2)    $    TH2=ATAN(RHO2/Z2P)
      CALL SDGPI(UG,U1,U2,U3,U4,1,0)
      UGARGV=UG*CEXP(-CJ*CONST*Z2P)
      R2=STORER    $    TH2=STORET
      RETURN
      END
C
C
C
      COMPLEX FUNCTION UGARGH(Z2P)
      IMPLICIT COMPLEX (C,U)
```

```
      COMPLEX KAPPA
      REAL COS
      COMMON/PI/     PI,EPS0,CJ
      COMMON/OBS/     R2,TH2,PHI2
      COMMON/PARAM/     AK1,KAPPA,C10
      STORER=R2    $     STORET=TH2    $     RHO2=R2*SIN(TH2)
      CONST=AK1/CSQRT(KAPPA)
      R2=SQRT(Z2P**2+RHO2**2)    $     TH2=ATAN(RHO2/Z2P)
      CALL SDGPI(U1,U2,U3,U4,UGX,0,1)
      UGARGH=UGX*CEXP(-CJ*CONST*Z2P)
      R2=STORER    $     TH2=STORET
      RETURN
      END
C
C
C
      SUBROUTINE SDGPI(UG,UGZ,UGZ2,UGXZ,UGX,IV,IH)
      IMPLICIT COMPLEX (C,U)
      COMPLEX KAPPA
      REAL COS
      COMMON/PI/     PI,EPS0,CJ
      COMMON/OBS/     R2,TH2,PHI2
      COMMON/PARAM/     AK1,KAPPA,C10
      UG=CEXP(-CJ*AK1*R2)/(4.*PI*R2)
      IF(IV.EQ.1)     RETURN
      X2=R2*SIN(TH2)*COS(PHI2)
      UR1=UR(1)
      UGX=X2*UR1*UG
      IF(IH.EQ.1)     RETURN
      Z2=R2*COS(TH2)
      UGZ=Z2*UR1*UG
      UR2=UR(2)
      UGZ2=(UR1+Z2**2*UR2)*UG+Z2*UR1*UGZ
      UGXZ=X2*Z2*UR2*UG+X2*UR1*UGZ
      RETURN
      END
C
C
C
      COMPLEX FUNCTION UR(I)
      IMPLICIT COMPLEX (C,U)
      COMPLEX KAPPA
      COMMON/PI/     PI,EPS0,CJ
      COMMON/OBS/     R2,TH2,PHI2
      COMMON/PARAM/     AK1,KAPPA,C10
      K1=K2=1
      DO 100 K=1,I
      J1=2*K-2
      IF(J1.GT.1)     K1=K1*J1
      J2=2*K-3
      IF(J2.GT.1)     K2=K2*J2
  100 CONTINUE
```

```
      UR=(-1)**I*(K1+CJ*AK1*R2*R2)/R2**(2*I)
      RETURN
      END
C
C
C
      SUBROUTINE SUS(Z2P,Z2,UGP,UG,UGXZP,CONST,US,IX)
C
C
C     IX=0,    COMPUTES THE S-FUNCTION
C     IX=1,    COMPUTES THE DS/DX-FUNCTION
C     IX=2,    COMPUTES THE DS/DY-FUNCTION
C     IX=3,    COMPUTES THE D2S/DX2-FUNCTION
C     IX=4,    COMPUTES THE D2S/DXDY-FUNCTION
C     CAUTION:   INPUTS UGP , UG AND UGXZP MUST BE SUPPLIED ACCORDING TO IX
C
C
      IMPLICIT COMPLEX (C,U)
      REAL COS
      COMPLEX KAPPA
      COMMON/PI/   PI,EPS0,CJ
      COMMON/OBS/   R2,TH2,PHI2
      COMMON/PARAM/   AK1,KAPPA,C10
      EXTERNAL   UGARGV,UGARGH
      STORER=R2   $   STORET=TH2   $   STOREP=PHI2
      IF(ABS(Z2-Z2P).LT.1.E-12)   GO TO 100
      RHO2=R2*SIN(TH2)
      R2=SQRT(Z2P**2+RHO2**2)   $   TH2=ATAN(RHO2/Z2P)
  100   CALL SRCM1(U1,U2,U3)
      R2=STORER   $   TH2=STORET
      IF(IX.GE.2)   GO TO 500
      USP=U1
      IF(IX.EQ.1)   USP=CJ/CONST/(1.+KAPPA)*(2.*UGXZP+AK1**2*KAPPA*U3)
      USINT=(0.,0.)
      IF(ABS(Z2-Z2P).LT.1.E-12)   GO TO 200
      IF(IX.EQ.0)   CALL DUG12(Z2P,Z2,UGARGV,USINT)
      IF(IX.EQ.1)   CALL DUG12(Z2P,Z2,UGARGH,USINT)
  200   US=(USP-2.*UGP)*CEXP(CJ*CONST*(Z2-Z2P))+2.*UG+2.*CJ*
     +CONST*CEXP(CJ*CONST*Z2)*USINT
      RETURN
  500   CONTINUE
      DEL=.05*2.*PI/AK1
      X2=R2*SIN(TH2)*COS(PHI2)   $   Y2=R2*SIN(TH2)*SIN(PHI2)
      USINT=(0.,0.)
C
      IF(IX.NE.2)   GO TO 510
      RHO2D=SQRT(X2**2+(Y2+DEL)**2)
      R2=SQRT(RHO2D**2+Z2P**2)   $   TH2=ATAN(RHO2D/Z2P)
      PHI2=ATAN2(Y2+DEL,X2)
      CALL SRCM1(U1DY,U2,U3)
      IF(ABS(Z2-Z2P).GT.1.E-12)   CALL DUG12(Z2P,Z2,UGARGV,USIDY)
      RHO2D=SQRT(X2**2+(Y2-DEL)**2)
      R2=SQRT(RHO2D**2+Z2P**2)   $   TH2=ATAN(RHO2D/Z2P)
```

THIS PAGE IS BEST QUALITY PRACTICABLE
FROM COPY FURNISHED TO DDC

```
      PHI2=ATAN2(Y2-DEL,X2)
      CALL SRCM1(U1DYM,U2,U3)
      IF(ABS(Z2-Z2P).GT.1.E-12)   CALL DUG12(Z2P,Z2,UGARGV,USIDYM)
      USP=(U1DY-U1DYM)/2./DEL
      IF(ABS(Z2-Z2P).GT.1.E-12)   USINT=(USIDY-USIDYM)/2./DEL
      R2=STORER    $    TH2=STORET    $    PHI2=STOREP
      GO TO 200
C
  510 IF(IX.NE.3)   GO TO 520
      RHO2D=SQRT((X2+DEL)**2+Y2**2)
      R2=SQRT(RHO2D**2+Z2P**2)    $    TH2=ATAN(RHO2D/Z2P)
      PHI2=ATAN2(Y2+.000001*DEL,X2+DEL)
      CALL SRCM1(U1,U2,U3DX)
      IF(ABS(Z2-Z2P).GT.1.E-12)   CALL DUG12(Z2P,Z2,UGARGH,USIDX)
      RHO2D=SQRT((X2-DEL)**2+Y2**2)
      R2=SQRT(RHO2D**2+Z2P**2)    $    TH2=ATAN(RHO2D/Z2P)
      PHI2=ATAN2(Y2+.000001*DEL,X2-DEL)
      CALL SRCM1(U1,U2,U3DXM)
      IF(ABS(Z2-Z2P).GE.1.E-12)   CALL DUG12(Z2P,Z2,UGARGH,USIDXM)
      U3=(U3DX-U3DXM)/2./DEL
      IF(ABS(Z2-Z2P).GT.1.E-12)   USINT=(USIDX-USIDXM)/2./DEL
      USP=CJ/CONST/(1.+KAPPA)*(2.*UGXZP+AK1**2*KAPPA*U3)
      R2=STORER    $    TH2=STORET    $    PHI2=STOREP
      GO TO 200
C
  520 IF(IX.NE.4)   RETURN
      RHO2D=SQRT(X2**2+(Y2+DEL)**2)
      R2=SQRT(RHO2D**2+Z2P**2)    $    TH2=ATAN(RHO2D/Z2P)
      PHI2=ATAN2(Y2+DEL,X2)
      CALL SRCM1(U1,U2,U3DY)
      IF(ABS(Z2-Z2P).GE.1.E-12)   CALL DUG12(Z2P,Z2,UGARGH,USIDY)
      RHO2D=SQRT(X2**2+(Y2-DEL)**2)
      R2=SQRT(RHO2D**2+Z2P**2)    $    TH2=ATAN(RHO2D/Z2P)
      PHI2=ATAN2(Y2-DEL,X2)
      CALL SRCM1(U1,U2,U3DYM)
      IF(ABS(Z2-Z2P).GT.1.E-12)   CALL DUG12(Z2P,Z2,UGARGH,USIDYM)
      U3=(U3DY-U3DYM)/2./DEL
      IF(ABS(Z2-Z2P).GE.1.E-12)   USINT=(USIDY-USIDYM)/2./DEL
      USP=CJ/CONST/(1.+KAPPA)*(2.*UGXZP+AK1**2*KAPPA*U3)
      R2=STORER    $    TH2=STORET    $    PHI2=STOREP
      GO TO 200
C
      END
```

```
SUBROUTINE SESAPP(UEX,UEY,UEZ,CIV,CIH)
C
C
C     COMPUTE THE THREE COMPLEX SCATTERED E-FIELD COMPONENTS IN THE
C     (X2,Y2,Z2) COORDINATE SYSTEM USING THE APPROXIMATE PROCEDURE
C     DEVELOPED IN CHAPTER 4.
C
C
IMPLICIT COMPLEX(C,U)
COMPLEX KAPPA,UDG(17),UDGP(17)
REAL COS
COMMON/PI/   PI,EPS0,CJ
COMMON/ODS/   R2,TH2,PH12
COMMON/PARAM/   AK1,KAPPA,C10
Z2=R2*COS(TH2)   $   RHO2=R2*SIN(TH2)
STORER=R2   $   STORET=TH2
CONST=AK1/CSQRT(KAPPA)
CALL SDGES(UDG)
R2P=15./AK1
IF(R2.GT.R2P)   GO TO 100
Z2P=SQRT(R2P**2-RHO2**2)
R2=R2P   $   TH2=ATAN(RHO2/Z2P)
CALL SDGES(UDGP)
GO TO 110
100   Z2P=Z2
DO 105 I=1,17
105   UDGP(I)=UDG(I)
110   CONTINUE
R2=STORER   $   TH2=STORET
C
UG=UDG(1)   $   UGP=UDGP(1)
UGX=UDG(2)   $   UGXP=UDGP(2)
UGY=UDG(3)   $   UGYP=UDGP(3)
UGZ=UDG(4)   $   UGZP=UDGP(4)
UGX2=UDG(5)   $   UGX2P=UDGP(5)
UGZ2=UDG(6)   $   UGZ2P=UDGP(6)
UGXY=UDG(7)   $   UGXYP=UDGP(7)
UGXZ=UDG(8)   $   UGXZP=UDGP(8)
UGYZ=UDG(9)   $   UGYZP=UDGP(9)
UGX2Z=UDG(10)   $   UGX2ZP=UDGP(10)
UGXZ2=UDG(11)   $   UGXZ2P=UDGP(11)
UGX2Z2=UDG(12)   $   UGX2Z2P=UDGP(12)
UGXZ3=UDG(13)   $   UGXZ3P=UDGP(13)
UGXYZ=UDG(14)   $   UGXYZP=UDGP(14)
UGX2YZ=UDG(15)   $   UGX2YZP=UDGP(15)
UGXY2Z=UDG(16)   $   UGXY2ZP=UDGP(16)
UGXYZ2=UDG(17)   $   UGXYZ2P=UDGP(17)
C
 UEX=UEY=UEZ=(0.,0.)
IF(CABS(CIH).LT.1.E-14)   GO TO 500
C
C
C2=-2./AK1**2/(1.-KAPPA)
C1=C2*CJ*AK1*CSQRT(KAPPA)
```

```
      C0=-1.
      UPIX=C0*UG+C1*UGZ+C2*UGZ2
      UPIXX2=C0*UGX2+C1*UGX2Z+C2*UGX2Z2
      UEX=UEX+C1H*(AK1**2*UPIX+UPIXX2)
      UPIXXY=C0*UGXY+C1*UGXYZ+C2*XYZ2
      UEY=UEY+C1H*UPIXXY
      UPIXXZ=C0*UGXZ+C1*UGXZ2+C2*UGXZ3

      UEZ=UEZ+C1H*UPIXXZ
C
C
500   CONTINUE
      CALL SUS(Z2P,Z2,UGP,UG,UGXZP,CONST,US,0)
      CALL SUS(Z2P,Z2,UGXP,UGX,UGXZP,CONST,USX,1)
      CALL SUS(Z2P,Z2,UGYP,UGY,UGXZP,CONST,USY,2)
      CALL SUS(Z2P,Z2,UGX2P,UGX2,UGX2ZP,CONST,USX2,3)
      CALL SUS(Z2P,Z2,UGXYP,UGXY,UGXYZP,CONST,USXY,4)
      USZ=CJ*CONST*US+2.*UGZ
      USZ2=CJ*CONST*USZ+2.*UGZ2
      USXZ=CJ*CONST*USX+2.*UGXZ
      USXZ2=CJ*CONST*USXZ+2.*UGXZ2
      USYZ=CJ*CONST*USY+2.*UGYZ
      USX2Z=CJ*CONST*USX2+2.*UGX2Z
      USXYZ=CJ*CONST*USXY+2.*UGXYZ
      C10=C1V
      C11=-C1H*CJ*CONST*(KAPPA+1.)/(AK1**2*KAPPA)
      C12=-C1H*2./(AK1**2*KAPPA)
      C13=-C1V
      UPIZ=C10*US+C11*USX+C12*UGXZ+C13*UG
      UPIZZ2=C10*USZ2+C11*USXZ2+C12*UGXZ3+C13*UGZ2
      UPIZYZ=C10*USYZ+C11*USXYZ+C12*UGXYZ2+C13*UGYZ
      UPIZXZ=C10*USXZ+C11*USX2Z+C12*UGX2Z2+C13*UGXZ
      UEX=UEX+UPIZXZ
      UEY=UEY+UPIZYZ
      UEZ=UEZ+AK1**2*UPIZ+UPIZZ2
      RETURN
      END
C
C
C
      SUBROUTINE SOGES(UDG)
      IMPLICIT COMPLEX(C,U)
      DIMENSION UDG(17)
      REAL COS
      COMPLEX KAPPA
      COMMON/PI/ PI,EPS0,CJ
      COMMON/OBS/ R2,TH2,PHI2
      COMMON/PARAM/ AK1,KAPPA,C1V
      UDG(1)=UG=CEXP(-CJ*AK1*R2)/(4.*PI*R2)
      RHO2=R2*SIN(TH2)    $    Z2=R2*COS(TH2)
      X2=RHO2*COS(PHI2)    $    Y2=RHO2*SIN(PHI2)
      UR1=UR(1)
      UDG(2)=UGX=X2*UR1*UG
      UDG(3)=UGY=Y2*UR1*UG
```

```
      UDG(4)=UGZ=Z2*UR1*UG
      UR2=UR(2)
      UDG(5)=UGX2=(UR1+X2**2*UR2)*UG+X2*UR1*UGX
             UGY2=(UR1+Y2**2*UR2)*UG+Y2*UR1*UGY
      UDG(6)=UGZ2=(UR1+Z2**2*UR2)*UG+Z2*UR1*UGZ
      UDG(7)=UGXY=X2*Y2*UR2*UG+X2*UR1*UGY
      UDG(8)=UGXZ=X2*Z2*UR2*UG+X2*UR1*UGZ
      UDG(9)=UGYZ=Y2*Z2*UR2*UG+Y2*UR1*UGZ
      UR3=UR(3)
             UGZ3=(3.*Z2*UR2+Z2**3*UR3)*UG+2.*(UR1+Z2**2*UR2)*UGZ+
     +Z2*UR1*UGZ2
      UDG(10)=UGX2Z=Z2*(UR2+X2**2*UR3)*UG+2.*X2*Z2*UR2*UGX+Z2*UR1*UGX2
      UDG(11)=UGXZ2=X2*(UR2+Z2**2*UR3)*UG+2.*X2*Z2*UR2*UGZ+X2*UR1*UGZ2
             UGXY2=X2*(UR2+Y2**2*UR3)*UG+2.*X2*Y2*UR2*UGY+X2*UR1*UGY2
      UR4=UR(4)
      UDG(12)=UGX2Z2=(UR2+(X2**2+Z2**2)*UR3+X2**2*Z2**2*UR4)*UG+
     +Z2*(UR2+X2**2*UR3)*UGZ+2.*X2*(UR2+Z2**2*UR3)*UGX+(UR1+Z2**2*UR2)*UGX2+
     +2.*X2*Z2*UR2*UGXZ+Z2*UR1*UGX2Z
      UDG(13)=UGXZ3=X2*(3.*Z2*UR3+Z2**3*UR4)*UG+3.*X2*(UR2+Z2**2*UR3)*UGZ+
     +3.*X2*Z2*UR2*UGZ2+X2*UR1*UGZ3
      UDG(14)=UGXYZ=X2*Y2*Z2*UR3*UG+2.*Y2*Z2*UR2*UGX+Z2*UR1*UGXY
      UDG(15)=UGX2YZ=Y2*Z2*(UR3+X2**2*UR4)*UG+3.*X2*Y2*Z2*UR3*UGX+
     +2.*Y2*Z2*UR2*UGX2+X2*Y2*UR2*UGXZ+Y2*UR1*UGX2Z
      UDG(16)=UGXY2Z=X2*Z2*(UR3+Y2**2*UR4)*UG+3.*X2*Y2*Z2*UR3*UGY+
     +2.*X2*Z2*UR2*UGY2+Y2*Z2*UR2*UGXY+Z2*UR1*UGXY2
      UDG(17)=UGXYZ2=X2*Y2*(UR3+Z2**2*UR4)*UG+3.*X2*Y2*Z2*UR3*UGZ+
     +2.*X2*Y2*UR2*UGZ2+Y2*Z2*UR2*UGXZ+Y2*UR1*UGXZ2
      RETURN
      END
```

```
      SUBROUTINE SOMINT(CPØV1Z,CPØH1X,CPØH1Z,IV,IH)
C
C
C     COMPUTE SOMMERFELD INTEGRALS
C     IV=Ø,     DO NOT COMPUTE THE VERTICAL INTEGRAL
C     IH=Ø,     DO NOT COMPUTE THE HORIZONTAL INTEGRALS
C
C
      IMPLICIT COMPLEX(C,U)
      COMPLEX KAPPA,BRV1Z,BRH1X,BRH1Z
      COMMON/PI/  PI,EPSØ,CJ
      COMMON/OBS/ R2,TH2,PHI2
      COMMON/PARAM/  AK1,KAPPA,CIO
      EXTERNAL V1ZARG,H1XARG,H1ZARG
      CPØV1Z=CPØH1X=CPØH1Z=(Ø.,Ø.)
      TMAX=3./SQRT(AK1*R2)
      A=REAL(CSQRT(KAPPA))
      B=AIMAG(CSQRT(KAPPA-1.))
      TH2MIN=ASIN(1./SQRT(A**2+B**2))-ATAN(B/A)
      TH2P=TH2MIN*180./PI
      PRINT805,TMAX,TH2P
805   FORMAT(" ","TMAX=",G10.2,"TH2MIN=",G10.2)
      IF(TH2.LT.TH2MIN)     GO TO 100
      BETA=Ø.   $   DEL=5.   $   IS=1
10    BETA=BETA+DEL
      UA=CSQRT(KAPPA-BETA**2)
      UB=CSQRT(KAPPA-1.-BETA**2)
      TH2P=ASIN(1./SQRT(REAL(UA)**2+AIMAG(UB)**2))-ATAN(AIMAG(UB)/REAL(UA))
      IF(ABS(TH2-TH2P).LT.1.E-4)    GO TO 20
      IF((TH2-TH2P)*IS.GT.Ø.)    GO TO 10
      DEL=-DEL/2.   $   IS=-IS
      GO TO 10
20    BETA1=BETA
      T1=SQRT(-SIN(TH2)*AIMAG(UA)+COS(TH2)*REAL(UB))
      PRINT810,T1,BETA1
810   FORMAT(" ","T1=",G10.2,"BETA1=",G10.2)
      IF(T1.GT.TMAX)    GO TO 100
      CALL BRINT(BETA1,BRV1Z,BRH1X,BRH1Z,IV,IH)
      IF(IV.EQ.Ø)    GO TO 30
      CALL DQG12(-TMAX,Ø.,V1ZARG,U1)
      CALL DQG12(Ø.,T1-.ØØ1*T1,V1ZARG,U2)
      CALL DQG12(T1+.ØØ1*T1,TMAX,V1ZARG,U3)
      CPØV1Z=U1+U2+U3+BRV1Z
30    IF(IH.EQ.Ø)    RETURN
      CALL DQG12(-TMAX,Ø.,H1XARG,UX1)
      CALL DQG12(-TMAX,Ø.,H1ZARG,UZ1)
      CALL DQG12(Ø.,T1-.ØØ1*T1,H1XARG,UX2)
      CALL DQG12(Ø.,T1-.ØØ1*T1,H1ZARG,UZ2)
      CALL DQG12(T1+.ØØ1*T1,TMAX,H1XARG,UX3)
      CALL DQG12(T1+.ØØ1*T1,TMAX,H1ZARG,UZ3)
      CPØH1X=UX1+UX2+UX3+BRH1X
      CPØH1Z=UZ1+UZ2+UZ3+BRH1Z
      RETURN
```

```
      100   IF(IV.EQ.0)    GO TO 110
      CALL DQG12(-TMAX,0.,V1ZARG,U1)
      CALL DQG12(0.,TMAX,V1ZARG,U2)
      CP0V1Z=U1+U2
      110   IF(IM.EQ.0)    RETURN
      CALL DQG12(-TMAX,0.,H1XARG,UX1)
      CALL DQG12(-TMAX,0.,H1ZARG,UZ1)
      CALL DQG12(0.,TMAX,H1XARG,UX2)

      UVZ=KAPPA/(KAPPA**2*COSXI**2-BETA**2)*UR*UM0
      10    IF(IMX.EQ.0)    GO TO 20
      CALL HNKL0(C1,UM0)
      UMX=UR/(KAPPA-1.)*UM0
      20    IF(IMZ.EQ.0)    RETURN
      CALL HNKL1(C1,UM1)
      UMZ=CJ*COS(PHI2)*(KAPPA+1.)/(KAPPA**2*COSXI**2-BETA**2)*SINXI
     +*COSXI*UR*UM1
      RETURN
      END
```

```
      SUBROUTINE PIWARG(IVZ,IMX,IMZ,T,UVZ,UMX,UMZ)
C
C
C     SOMMERFELD INTEGRANDS
C
C
      IMPLICIT COMPLEX(C,U)
      REAL COS
      COMPLEX KAPPA,XI,SINXI
      COMMON/PI/   PI,EPS0,CJ
      COMMON/OBS/   R2,TH2,PHI2
      COMMON/PARAM/   AK1,KAPPA,C10
      UVZ=UMX=UMZ=(0.,0.)
      CALL SQPTXI(T,TH2,XI)
      RHO2=R2*SIN(TH2)
      SINXI=CSIN(XI)
      COSXI=CCOS(XI)
      USQ=CSQRT(KAPPA-SINXI**2)
      IF(T.GT.0..AND.AIMAG(USQ).GT.0.)   USQ=-USQ
      C1=AK1*RHO2*SINXI
      UR=AK1/(2.*PI)*CEXP(-CJ*AK1*R2)/CSQRT(T**2+2.*CJ)
      UR=UR*SINXI*COSXI*CEXP(CJ*C1)*EXP(-AK1*R2*T**2)
      IF(IVZ.EQ.0)   GO TO 10
      IF(TH2.LT.1.E-6)   CH0=-2.*CJ/PI*CLOG(AK1*R2*SINXI)
      IF(TH2.GE.1.E-6)    CALL HNKL0(C1,CH0)
      UVZ=KAPPA*UR*CH0/(KAPPA*COSXI+USQ)
 10   IF(IMX.EQ.0)   GO TO 20
      IF(TH2.LT.1.E-6)  CH0=-2.*CJ/PI*CLOG(AK1*R2*SINXI)
      IF(TH2.GE.1.E-6)    CALL HNKL0(C1,CH0)
      UMX=UR*CH0/(COSXI+USQ)
 20   IF(IMZ.EQ.0)   RETURN
      IF(TH2.LT.1.E-6)   RETURN
      CALL HNKL1(C1,CH1)
      UMZ=-CJ*COS(PHI2)*UR*CH1*SINXI*(COSXI-USQ)/(KAPPA*COSXI+USQ)
      RETURN
      END
C
C
C
      COMPLEX FUNCTION V1ZARG(T)
      IMPLICIT COMPLEX(V)
      CALL PIWARG(1,0,0,T,V1ZARG,V2,V3)
      RETURN
      END
C
C
C
      COMPLEX FUNCTION H1XARG(T)
      IMPLICIT COMPLEX (H)
      CALL PIWARG(0,1,0,T,H1,H1XARG,H3)
      RETURN
      END
```

```
C
C
C
      COMPLEX FUNCTION M12ARG(T)
      IMPLICIT COMPLEX(M)
      CALL PI0ARG(0,0,1,T,M1,M2,M12ARG)
      RETURN
      END
C
C
C
      SUBROUTINE SQRTXI(T,TH2,XI)
      COMPLEX CMPLX,XI
      SQ1=SQRT(T**4+4.)
      ALPHA=(-T**2+SQ1)/2.
      BETA=(T**2+SQ1)/2.
      Q1=ACOS(ALPHA)
      Q2=ALOG(BETA+SQRT(BETA**2-1.))
      XI=CMPLX(Q1,Q2)*SIGN(1.,T)+TH2
      RETURN
      END
```

```
SUBROUTINE BRINT(BETA1,BRVIZ,BRHIX,BRHIZ,IV,IH)
C
C
C    COMPUTE BRANCH CUT CONTRIBUTIONS
C    IV=0    ;    DO NOT COMPUTE THE VERTICAL CASE
C    IH=0    ;    DO NOT COMPUTE THE HORIZONTAL CASE
C
C
COMPLEX BRVIZ,BRHIX,BRHIZ
EXTERNAL BARGVZ,BARGHX,BARGHZ
IF(IV.EQ.0)   GO TO 10
CALL DQG12(0.,BETA1,BARGVZ,BRVIZ)
10   IF(IH.EQ.0)   RETURN
CALL DQG12(0.,BETA1,BARGHX,BRHIX)
CALL DQG12(0.,BETA1,BARGHZ,BRHIZ)
RETURN
END
C
C
C
COMPLEX FUNCTION BARGVZ(BETA)
IMPLICIT COMPLEX (B)
REAL BETA
CALL BRARG(1,0,0,BETA,BARGVZ,B2,B3)
RETURN
END
C
C
C
COMPLEX FUNCTION BARGHX(BETA)
IMPLICIT COMPLEX (B)
REAL BETA
CALL BRARG(0,1,0,BETA,B1,BARGHX,B3)
RETURN
END
C
C
C
COMPLEX FUNCTION BARGHZ(BETA)
IMPLICIT COMPLEX (B)
REAL BETA
CALL BRARG(0,0,1,BETA,B1,B2,BARGHZ)
RETURN
END
C
C
C
SUBROUTINE BRARG(IVZ,IHX,IHZ,BETA,UVZ,UHX,UHZ)
IMPLICIT COMPLEX (C,U)
REAL COS
COMPLEX KAPPA,SINXI
COMMON/PI/    PI,EPS0,CJ
COMMON/OBS/    R2,TH2,PHI2
```

```
COMMON/PARAM/    AK1,KAPPA,C10
COSXI=-CJ*CSQRT((KAPPA-1.-BETA**2)
SINXI=CSQRT(KAPPA-BETA**2)
RHO2=R2*SIN(TH2)    $    Z2=R2*COS(TH2)
UR=AK1/(2.*PI*CJ)*BETA**2*CEXP(-CJ*AK1*Z2*COSXI)
C1=AK1*RHO2*SINXI
IF(IV2.EQ.0)    GO TO 10
CALL HNKL0(C1,UH0)

CALL DQG12(0.,TMAX,HIZARG,UZ2)
CPOM1X=UX1+UX2
CPOM1Z=UZ1+UZ2
RETURN
END
```

```
C------------------------------------------------------------------------
      SUBROUTINE XINVZ(N,NX,A,D,IERR)
C------------------------------------------------------------------------
C     PARAMETERS HAVE THE FOLLOWING MEANINGS
C     A - N BY N REAL, SYMMETRIC MATRIX TO BE INVERTED, ON OUTPUT A
C         CONTAINS A INVERSE.
C     D - DETERMINANT OF A.
C------------------------------------------------------------------------
      IMPLICIT COMPLEX(A-H,O-Z)
      DIMENSION A(NX,N),GAMMA(150)
C-----INITIALIZE DETERMINANT
      D=A(1,1)
C-----COMPUTE B(1)**(-1)
      A(1,1)=1./A(1,1)
      DO 70 I=2,N
      IM1=I-1
      DO 20 K=1,IM1
      GAMMA(K)=0.
C-----COMPUTE BV*U
      DO 10 KK=1,IM1
   10     GAMMA(K)=A(K,KK)*A(I,KK)+GAMMA(K)
   20     GAMMA(K)=-GAMMA(K)
      ALPHA=0.E0
C-----COMPUTE ALPHA
      DO 50 KK=1,IM1
   50     ALPHA=A(I,KK)*GAMMA(KK)+ALPHA
      ALPHA=A(I,I)+ALPHA
C-----IF ALPHA=0 THEN GO TO ERROR RETURN
      IF(CABS(ALPHA).LE.1.0E-15)GO TO 80
      Y=1./(ALPHA)
      DO 60 K=1,IM1
C-----STORE -BV*U/ALPHA
      A(I,K)=GAMMA(K)*Y
      A(K,I)=A(I,K)
      DO 40 KK=1,K
C-----STORE BV+BV*U*U'*BV
   40     A(K,KK)=A(K,KK)+GAMMA(K)*GAMMA(KK)*Y
      IF(K.EQ.1)GO TO 60
      KM1=K-1
      DO 50 KK=1,KM1
C-----STORE -(BV*U/ALPHA)'
   50     A(KK,K)=A(K,KK)
   60     CONTINUE
C-----STORE 1./ALPHA
      A(I,I)=Y
C-----UPDATE DETERMINANT
   70     D=ALPHA*D
      IERR=1.0
      RETURN
   80     IERR=1
      RETURN
      END
```

```
      SUBROUTINE HNKL1(Z,H1)
C
C
C     HANKEL FUNCTION, 1ST ORDER,SECOND TYPE
C     USAGE: INPUT COMPLEX*16 Z
C     USAGE, OUTPUT COMPLEX*16 H1
C     TO CALCULATE J0 AND Y0 HNKL USES AN ANALYTIC CONTINUATION
C     OF THE POLYNOMIAL FITS IN ABRAMOWITZ AND STEGUN PG 369
C
C
      COMPLEX AI,Z,H1,Y1,J1
      REAL PI
      PI=3.141592654
      AI=(0.E0,1.E0)
      IF(CABS(Z).LE.12.)GOTO10
      GOTO 20
   10 CONTINUE
      CALL YI(Z,Y1,J1)
      H1=J1-AI*Y1
      GOTO 99
   20 H1=CSQRT(2./(PI*Z))*CEXP(-1.*AI*(Z-3.*PI/4.))*(1.+15./(128.*Z**
+2)-AI*3./(8.*Z))
   99 RETURN
      END
      SUBROUTINE JI(Z,J1)
C
C
C     BESSEL FUNCTION, 1ST ORDER
C     USAGE  INPUT  COMPLEX*16 Z
C     USAGE   OUTPUT  COMPLEX*16 J1
C     ANALYTICAL CONTINUATION INTO THE FIRST QUADRANT OF THE
C     POLYNIMIAL FIT IN ABRAMOWITZ AND STEGUN PG 369
C
C
      COMPLEX J1,J1AS,J1AL,Z,Z1,AI
      REAL PI,AP,REAL,AIMAG
      PI=3.141592654
      AI=(0.E0,1.E0)
      Z1=CMPLX(ABS(REAL(Z)),ABS(AIMAG(Z)))
      AP=ATAN2(AIMAG(Z),REAL(Z))
      IF(CABS(Z).LE.3.0)J1=J1AS(Z1)
      IF(CABS(Z).GT.3.0)J1=J1AL(Z1)
      IF(AP.GT.PI/2..AND.AP.LT.PI)J1=CEXP(AI*PI)*CONJG(J1)
      IF(AP.LE.-1.*PI/2..AND.AP.GT.-1.*PI)J1=CEXP(AI*PI)*J1
      IF(AP.LT.0..AND.AP.GE.-1.*PI/2.)J1=CONJG(J1)
      RETURN
      END
      COMPLEX FUNCTION J1AS(Z)
      COMPLEX Z,W
      W=Z/3.
      J1AS=Z*(.5-.56249985*W**2+.21093573*W**4-.03954289*W**6+.
+00443319*W**8-.00031761*W**10+.00001109*W**12)
      RETURN
      END
```

THIS PAGE IS BEST QUALITY PRACTICABLE
FROM COPY FURNISHED TO DDC

```
      COMPLEX FUNCTION J1AL(Z)
      COMPLEX Z,W,F1,TH1
      W=3./Z
      F1=.79788456+.00000156*W+.01659667*W**2+.00017105*W**3-.
     +00249511*W**4+.00113653*W**5-.00020033*W**6
      TH1=Z-2.35619449+.12499612*W+.00005650*W**2-.00637879*W**3+.
     +00074348*W**4+.00079824*W**5-.00029166*W**6
      J1AL=F1*CCOS(TH1)/CSQRT(Z)
      RETURN
      END
      SUBROUTINE Y1(Z,Y1,J1)
C
C
C     NEUMANN FUNCTION,1ST ORDER, SUBROUTINE J1 IS CALLED
C     USAGE   INPUT  COMPLEX*16 Z
C     USAGE  OUTPUT COMPLEX*16 Y1
C     ANALYTIC CONTINUATION INTI THE FIRST QUADRANT OF THE
C     POLYNOMIAL FIT FOUND IN ABRAMOWITZ AND STEGUN PG 369
C
C
      COMPLEX Y1,Y1AS,Y1AL,Z,Z1,AI,J1
      REAL PI,AP,REAL,AIMAG
      PI=3.141592654
      AI=(0.E0,1.E0)
      Z1=CMPLX(ABS(REAL(Z)),ABS(AIMAG(Z)))
      CALL J1(Z1,J1)
      AP=ATAN2(AIMAG(Z),REAL(Z))
      IF(CABS(Z).LE.3.0)Y1=Y1AS(Z1,J1)
      IF(CABS(Z).GT.3.0)Y1=Y1AL(Z1)
      IF(AP.GT.PI/2..AND.AP.LT.PI)Y1=CEXP(AI*PI)*(CONJG(Y1)+2.*AI*
     +CONJG(J1))
      IF(AP.LE.-1.*PI/2..AND.AP.GT.-1.*PI)Y1=CEXP(AI*PI)*(Y1-2.*AI*J1)
      IF(AP.LT.0..AND.AP.GE.-1.*PI/2.)Y1=CONJG(Y1)
       IF(AP.GT.PI/2..AND.AP.LT.PI)  J1=-CONJG(J1)
       IF(AP.LT.-PI/2..AND.AP.GE.-PI)  J1=-J1
       IF(AP.LT.0..AND.AP.GE.-PI/2.)  J1=CONJG(J1)
      RETURN
      END
      COMPLEX FUNCTION Y1AS(Z,J1)
      COMPLEX Z,J1,W
      REAL PI
      PI=3.141592654
      W=Z/3.
      Y1AS=(1./Z)*((2./PI)*Z*CLOG(Z/2.)*J1-.6366198+.2212091*W**2+2.
     +1682709*W**4-1.3164827*W**6+.3123951*W**8-.0400976*W**10+.
     +0027873*W**12)
      RETURN
      END
      COMPLEX FUNCTION Y1AL(Z)
      COMPLEX Z,W,TH1,F1
      W=3./Z
      F1=.79788456+.00000156*W+.01659667*W**2+.00017105*W**3-.
     +00249511*W**4+.00113653*W**5-.00020033*W**6
```

```
      TH1=Z-2.35619449+.12499612*W+.00005650*W**2-.00637879*W**3+.
+00074348*W**4+.00079824*W**5-.00029166*W**6
      Y1AL=F1*CSIN(TH1)/CSQRT(Z)
      RETURN
      END
      SUBROUTINE HNKL0(Z,H)
C
C
C     HANKEL FUNCTION 0TH ORDER,2ND TYPE
C     USAGE  COMPLEX*16 Z
C     USAGE  COMPLEX*16 H
C     TO CALCULATE J0 AND Y0 HNKL USES AN ANALYTIC CONTINUATION
C     OF THE POLYNOMIAL FITS IN ABRAMOWITZ AND STEGUN PG 369
C
C
      COMPLEX AI,J0,Y0,Z,H
      REAL PI
      PI=3.141592654
      AI=(0.E0,1.E0)
      IF(CABS(Z).LE.12.)GOTO10
      GOTO 20
   10 CONTINUE
      CALL Y0(Z,Y0,J0)
      H=J0-AI*Y0
      GOTO 99
   20 H=CSQRT(2./(PI*Z))*CEXP(-1.*AI*(Z-PI/4.))*(1.-9./(2.*(8.*Z)**2)+
+AI/(8.*Z))
   99 RETURN
      END
      SUBROUTINE J0(Z,J0)
C
C
C     BESSEL FUNCTION, 0TH ORDER
C     USAGE  INPUT  COMPLEX*16 Z
C     USAGE   OUTPUT  COMPLEX*16 J0
C     ANALYTICAL CONTINUATION INTO THE FIRST QUADRANT OF THE
C     POLYNOMIAL FIT FOUND IN ABRAMOWITZ AND STEGUN PG 369
C
C
      COMPLEX J0,J0AS,J0AL,Z,Z1
      REAL PI,AP,REAL,AIMAG
      PI=3.141592654
      Z1=CMPLX(ABS(REAL(Z)),ABS(AIMAG(Z)))
      AP=ATAN2(AIMAG(Z),REAL(Z))
      IF(CABS(Z).LE.3.0)J0=J0AS(Z1)
      IF(CABS(Z).GT.3.0)J0=J0AL(Z1)
      IF(AP.GT.PI/2..AND.AP.LT.PI)J0=CONJG(J0)
      IF(AP.LT.0..AND.AP.GE.-1.*PI/2.)J0=CONJG(J0)
      RETURN
      END
      COMPLEX FUNCTION J0AS(Z)
      COMPLEX Z,W
      W=Z/3.
```

THIS PAGE IS BEST QUALITY PRACTICABLE
FROM COPY FURNISHED TO DDC

```
      JOAS=1.-2.2499997*W**2+1.2656208*W**4-.3163866*W**6+.0444479*W**
     +8-.0039444*W**10+.0002100*W**12
      RETURN
      END
      COMPLEX FUNCTION JOAL(Z)
      COMPLEX THO,FO,Z
      FO=.79788456-.00000077*(3/Z)-.00552740*(3/Z)**2-.00009512*(3/Z)*
     +*3+.00137237*(3/Z)**4-.00072805*(3/Z)**5+.00014476*(3/Z)**6
      THO=Z-.78539816-.04166397*(3/Z)-.00003954*(3/Z)**2+.00262573*(3/
     +Z)**3-.00054125*(3/Z)**4-.00029333*(3/Z)**5+.00013588*(3/Z)**6
      JOAL=FO*CCOS(THO)/CSQRT(Z)
      RETURN
      END
      SUBROUTINE Y0(Z,YO,JO)
C
C     NEUMANN FUNCTION,0TH ORDER,SUBROUTINE J0 IS CALLED
C     USAGE  INPUT COMPLEX*16 Z
C     USAGE  OUTPUT COMPLEX*16 YO
C     ANALYTIC CONTINUATION INTO THE FIRST QUADRANT OF THE
C     POLYNOMIAL FIT IN ABRAMOWITZ AND STEGUN PG 369
C
C
      COMPLEX YO,YOAS,YOAL,JO,Z,Z1,AI
      REAL PI,AP,REAL,AIMAG
      PI=3.141592654
      AI=(0.E0,1.E0)
      Z1=CMPLX(ABS(REAL(Z)),ABS(AIMAG(Z)))
      CALL J0(Z1,JO)
      AP=ATAN2(AIMAG(Z),REAL(Z))
      IF(CABS(Z).LE.3.0)YO=YOAS(Z1,JO)
      IF(CABS(Z).GT.3.0)YO=YOAL(Z1)
      IF(AP.GT.PI/2..AND.AP.LT.PI)YO=CONJG(YO)+2.*AI*CONJG(JO)
      IF(AP.LE.-1.*PI/2..AND.AP.GT.-1.*PI)YO=YO-2.*AI*JO
      IF(AP.LT.0..AND.AP.GE.-1.*PI/2.)YO=CONJG(YO)
       IF(AP.GT.PI/2..AND.AP.LT.PI)      JO=CONJG(JO)
       IF(AP.LT.0..AND.AP.GE.-PI/2.)    JO=CONJG(JO)
      RETURN
      END
      COMPLEX FUNCTION YOAS(Z,JO)
      COMPLEX Z,JO
      REAL PI
      PI=3.141592654
      YOAS=(2./PI)*CLOG(Z/2.)*JO+.36746691+.60559366*(Z/3.)**2-.
     +74350384*(Z/3)**4+.25300117*(Z/3)**6-.04261214*(Z/3)**8+.
     +00427916*(Z/3)**10-.00024846*(Z/3)**12
      RETURN
      END
      COMPLEX FUNCTION YOAL(Z)
      COMPLEX Z,THO,FO
      FO=.79788456-.00000077*(3/Z)-.00552740*(3/Z)**2-.00009512*(3/Z)*
     +*3+.00137237*(3/Z)**4-.00072805*(3/Z)**5+.00014476*(3/Z)**6
```

```
      THU=Z-.78539816-.04166397*(3/Z)-.00003954*(3/Z)**2+.00262573*(3/
     +Z)**3-.00054125*(3/Z)**4-.00029333*(3/Z)**5+.00013588*(3/Z)**6
      FUAL=FU*CSIN(THU)/CSQRT(Z)
      RETURN
      END
```

```
      SUBROUTINE DQG12(XL,XU,FCT,Y)
C
C     INTEGRATE COMPLEX FUNCTION FCT FROM XL TO XU
C     USING 12-POINT GAUSS QUADRITURE FORMULA,
C     EXACT FOR POLYNOMIALS UP TO DEGREE 23.
C
      COMPLEX Y,FCT
      EXTERNAL FCT
C
      A=.5*(XU+XL)
      B=XU-XL
      C=.49078031712335963E0*B
      Y=.23587668193255914E-1*(FCT(A+C)+FCT(A-C))
      C=.45205862818523743E0*B
      Y=Y+.53469662997659215E-1*(FCT(A+C)+FCT(A-C))
      C=.38495133709715234E0*B
      Y=Y+.80039164271673111E-1*(FCT(A+C)+FCT(A-C))
      C=.29365897714330872E0*B
      Y=Y+.10158371336153296E0*(FCT(A+C)+FCT(A-C))
      C=.18391574949909010E0*B
      Y=Y+.11674626826917740E0*(FCT(A+C)+FCT(A-C))
      C=.62616704255734458E-1*B
      Y=B*(Y+.12457352290670139E0*(FCT(A+C)+FCT(A-C)))
      RETURN
      END
```

REFERENCES

[1] A. N. Sommerfeld, "Uber die ausbrietung der wellen in der telegraphie," Ann. Physik, p. 665, 1909.

[2] A. Banos, Dipole Radiation in the Presence of Conducting Half-Space. New York: Pergamon Press, 1966.

[3] E. K. Miller, A. J. Poggio, G. J. Burke, and E. S. Selden, "Analysis of wire antennas in the presence of a conducting half-space: Part I. The vertical antenna in free space," Can. J. Phys., vol. 50, pp. 879-888, 1972.

[4] E. K. Miller, A. J. Poggio, G. J. Burke, and E. S. Selden, "Analysis of wire antennas in the presence of conducting half-space: Part II. The horizontal antenna in free space," Can. J. Phys., vol. 50, pp. 2614-2627, 1972.

[5] J. D. McCannon, "A comparative numerical study of several methods for analyzing a vertical thin-wire antenna over a lossy half-space," Ph.D. Thesis, University of Illinois, Urbana, Illinois, 1974.

[6] D. C. Chang and R. Fisher, "A unified theory on radiation of a vertical electric dipole above a dissipative earth," Radio Sci., vol. 9, no. 12, pp. 1129-1138, December 1974.

[7] T. K. Sarker and B. J. Strait, "Analysis of arbitrarily oriented thin wire antenna arrays over imperfect ground planes," Syracuse University Scientific Report 9, December 1975; prepared under Contract No. F19628-73-C-0047, AFCRL-TR-75-0641.

[8] D. L. Lager and R. J. Lytle, "Numerical evaluation of Sommerfeld integrals," Lawrence Livermore Laboratory Report UCRL-51688, October 23, 1974.

[9] D. L. Lager and R. J. Lytle, "Fortran subroutines for the numerical evaluation of Sommerfeld integrals under anderem," Lawrence Livermore Laboratory Report UCRL-51821, May 21, 1975.

[10] J. N. Brittingham, E. K. Miller, and J. T. Okada, "Bivariate interpolation approach for efficiently and accurately modelling antennas near a half-space," Electron. Lett., vol. 13, pp. 690-691, November 1977.

[11] Y. Rahmat-Samii, P. Parhami, and R. Mittra, "Transient response of a loaded horizontal antenna over lossy ground with application to EMP simulators," University of Illinois at Urbana-Champaign, Electromagnetics Laboratory Report No. 77-26, December 1977.

[12] W. C. Kuo and K. K. Mei, "Numerical approximation of the Sommerfeld integral for fast convergence," Radio Sci., vol. 13, no. 3, pp. 407-415, May 1978.

[13] J. D. McCannon, "Numerical analysis of a thin-wire antenna near lossy ground," M. S. Thesis, University of Illinois at Urbana-Champaign, Urbana, Illinois, 1972.

[14] Y. Rahmat-Samii, P. Parhami, and R. Mittra, "Loaded horizontal antenna over an imperfect ground," IEEE Trans. Antennas Propagat., vol. AP-26, no. 6, pp. 789-79-, November 1978.

[15] J. VanBladel, Electromagnetic Fields. New York: McGraw-Hill, 1967.

[16] J. A. Kong, Theory of Electromagnetic Waves. New York: Wiley, 1975.

[17] R. F. Harrington, Field Computation by Moment Methods. New York: McMillan, 1968.

[18] R. Mittra and W. L. Ko, "A finite difference approach to the wire junction problem," IEEE Trans. Antennas Propagat., vol. AP-23, pp. 435-438, May 1975.

[19] P. Parhami, Y. Rahmat-Samii, and R. Mittra, "A technique for calculating the radiation and scattering characteristics of antennas mounted on a finite ground plate," IEE Proc., vol. 124, pp. 1009-1016, November 1977.

[20] R. F. Harrington, "Matrix methods for field problems," Proc. IEEE, pp. 136-149, February 1967.

[21] E. C. Jordan and K. G. Balmain, Electromagnetic Waves and Radiating Systems. New Jersey: Prentice-Hall, 1968, pp. 566-567.

[22] M. Abramowitz and I. A. Stegum, Handbook of Mathematical Functions. New York: Dover Publications, Inc., 1970.

[23] L. B. Felsen and N. Marcuvitz, *Radiation and Scattering of Waves*. New Jersey: Prentice-Hall, 1973.